

Data assimilation and machine learning for slope stability assessment

Mohsan, M.

DOI

[10.4233/uuid:ca4aa6c4-4236-4d3c-a87f-221ac51bff26](https://doi.org/10.4233/uuid:ca4aa6c4-4236-4d3c-a87f-221ac51bff26)

Publication date

2024

Document Version

Final published version

Citation (APA)

Mohsan, M. (2024). *Data assimilation and machine learning for slope stability assessment*. [Dissertation (TU Delft), Delft University of Technology]. <https://doi.org/10.4233/uuid:ca4aa6c4-4236-4d3c-a87f-221ac51bff26>

Important note

To cite this publication, please use the final published version (if applicable).
Please check the document version above.

Copyright

Other than for strictly personal use, it is not permitted to download, forward or distribute the text or part of it, without the consent of the author(s) and/or copyright holder(s), unless the work is under an open content license such as Creative Commons.

Takedown policy

Please contact us and provide details if you believe this document breaches copyrights.
We will remove access to the work immediately and investigate your claim.

DATA ASSIMILATION AND MACHINE LEARNING FOR SLOPE STABILITY ASSESSMENT

DATA ASSIMILATION AND MACHINE LEARNING FOR SLOPE STABILITY ASSESSMENT

Dissertation

for the purpose of obtaining the degree of doctor at Delft University of Technology, by the authority of the Rector Magnificus prof. dr. ir. T.H.J.J. van der Hagen, chair of the Board for Doctorates, to be defended publicly on 25 November 2024 at 17:30.

by

Muhammad MOHSAN

Master of Science in Civil Engineering, The University of Tokyo, Japan, born in Toba Tek Singh, Pakistan.

The dissertation has been approved by the promotor(s).

promotor: Prof. dr. P.J. Vardon

promotor: Prof. dr. ir. F.C. Vossepoel

Composition of the doctoral committee:

Rector Magnificus,

Prof. dr. P.J. Vardon,

Prof. dr. ir. F.C. Vossepoel

Chairperson

Delft University of Technology, promotor

Delft University of Technology, promotor

Independent members:

Prof. dr. M.A Hicks

Dr. K. Zimmermann

Dr. ir. R. Brinkgreve

Dr. M.W.N. Buxton

Dr. I. Depina

Reserve member:

Prof. dr. K.G. Gavin

Delft University of Technology

DMT GmbH & Co. KG, Germany

Delft University of Technology

Delft University of Technology

Norwegian University of Science and Technology

Delft University of Technology



Keywords: Slope stability, data assimilation, machine learning

Printed by: Johannes Gutenberg

Copyright © 2024 by M. Mohsan

ISBN 978-94-6366-970-2

An electronic version of this dissertation is available at

<http://repository.tudelft.nl/>.

Dedicated to my
mother and maternal uncle (Munir Ahmed)

CONTENTS

Summary	ix
Samenvatting	xi
Acknowledgements	xiii
1 Introduction	1
1.1 Background	2
1.2 Current limitations	3
1.3 Motivation	4
1.4 Research Objectives	4
1.5 Slope stability for the Cottbus open-put mine.	6
1.6 Outline of the thesis.	6
2 On the use of different constitutive models in data assimilation for slope stability	15
2.1 Introduction	15
2.2 Methodology	17
2.2.1 Forward model.	17
2.2.2 Data assimilation with the recursive ensemble Kalman filter.	21
2.2.3 Implementation of the data assimilation for the slope-stability problem.	24
2.3 Synthetic twin experiment	25
2.4 Results of the data assimilation	29
2.4.1 Displacement estimates	29
2.4.2 Material parameter estimates	31
2.4.3 Factor of safety.	31
2.5 Discussion	34
2.6 Conclusion	37
3 On the use of different data assimilation schemes in a fully coupled hydro-mechanical slope stability analysis	43
3.1 Introduction	43
3.2 Methodology	46
3.2.1 Forward model.	46
3.2.2 Data assimilation schemes.	47
3.3 Synthetic example	51
3.4 Results	54
3.4.1 Parameter estimation	54
3.4.2 Displacement ensemble estimation	56

3.4.3	Factor of safety estimation	57
3.4.4	Computation time	58
3.5	Discussion	60
3.6	Conclusion	62
4	A case study of the Cottbus open pit mine: Use of data assimilation and surrogate modelling for slope stability analysis	67
4.1	Introduction	68
4.2	Available data	70
4.3	Methodology	72
4.4	Results and discussion	77
4.4.1	Data assimilation results	77
4.4.2	Surrogate model results	83
4.5	Conclusion	85
5	Conclusion And future work	91
5.1	Conclusion	92
5.2	Recommendations for the future studies	94
A	Appendix related to Chapter 3	95
A.1	Sensitivity of the displacement estimates to the data assimilation setup	95
A.1.1	Sensitivity to the number of measurements	96
A.1.2	Sensitivity to the measurement error.	97
A.1.3	Ensemble size	98
B	Appendix for Chapter 4	99
	Curriculum Vitae	103
	List of Publications	105

SUMMARY

Slope stability applications are vital assets for a country. These slope stability systems include dikes, dams, levees, embankments and enable applications such as open-pit mining. The failure of these systems pose huge impacts on society and the economy and hence the accurate stability assessment of these systems are of primary concern. Existing methods such as limit equilibrium methods, numerical methods (e.g. the finite element method, FEM), empirical methods and probabilistic methods all provide an approximate estimate of the factor of safety (FoS), and are often observed to have inaccuracies when failures occur. This lack of ability to make accurate predictions is due to many reasons, such as missing physical processes incorporated into the methods, inaccurate boundary and initial conditions, constitutive model selection, uncertainty in model parameters and limited mechanism understanding. This thesis suggests using data assimilation to combine monitoring data with a finite element model to improve the predictive capabilities of the FEM model. These days, geotechnical systems are equipped with measurement devices to monitor their response to external changes. These measurements can be in the form of surface displacements, porewater pressures, strains, etc. These measurements can be obtained from in-situ devices (such as inclinometers, strain gauges, etc.) or can be measured remotely (with Light Detection and Ranging (LIDAR), Interferometric Synthetic Aperture Radar (InSAR), etc.). These measurements can be assimilated into the popular ensemble-based well-established data assimilation methods, e.g., the ensemble Kalman filter (EnKF), ensemble smoother (ES) and ensemble smoother with multiple data assimilation (ESMDA) to improve the predictability of FEM models.

In the first stage, an FEM model of slope stability has been integrated with EnKF. Based upon the slope deformation measurements, this approach estimates the key material parameters (strength and stiffness parameters), the state (displacement), and the FoS of a slope. The effect of two different constitutive models (Mohr-Coulomb (MC) and Hardening Soil (HS) model) on the FoS was studied via a synthetic twin experiment. The HS model was able to estimate the FoS with a narrow posterior distribution, starting from a wide prior distribution of material parameters, including those not encompassing the actual parameters, demonstrating the advantage of using advanced constitutive models when combining with data assimilation.

In the second stage, the constitutive model which produced relatively more accurate results (the HS model) was selected from the first stage has been tested with three data assimilation schemes, i.e., EnKF, ES and ESMDA. Each of these schemes was integrated with the FEM to assimilate measurements of deformation of the slope and the crest of the slope stability system. The accuracy of these schemes was evaluated by comparing their FoS to the synthetic true FoS and evaluating their computation time in a synthetic twin experiment. The results of the synthetic twin experiment show that EnKF estimated an FoS that was close to the true FoS with a small standard deviation. ESMDA, when

using four iterative assimilation steps, was also able to estimate an FoS close to the truth, yet had a higher standard deviation compared to EnKF. The ES and ESMDA (with two iterative assimilation steps) were not able to reconstruct the true FoS as well as the other schemes, most likely due to the mostly linear updates of these schemes. The theoretical computation time required by the ES was the smallest, followed by ESMDA with two iterative assimilation steps, ESMDA with four assimilation steps, and finally the EnKF.

In the third stage, a data assimilation scheme was implemented on a case study of an open pit mine in Cottbus, Germany. The LIDAR measurements of the vertical displacements were assimilated into a FEM model of slope stability. Model parameters, displacement ensemble and FoS are estimated from this analysis. The posterior estimation of FoS is compared with slope failure observed in the field. The data assimilation results provide better results than only using FEM models when comparing the ground truth of slope failure. However, it was clear that not all physical processes were included in the model, resulting in a considerable mismatch of the modeled and observed deformations, although a considerable improvement was observed. This initial observation led to the choice of a data assimilation method, which is able to update the parameters to generally improve the results, as opposed to those which incrementally improved parameters.

Furthermore, as the data assimilation approach developed involved multiple FEM analyses, it is computationally expensive and therefore developing a real-time assessment system is likely to be impractical. Therefore, an effort was made to reduce the required computational resources by developing a surrogate model. The surrogate model was trained and tested based on the output of the FEM model ensemble. Specifically, it used the displacements at different locations as input and the FoS as output. The output of the surrogate model in the validation stage was compared with the observed FoS from the case study. It was found that the prediction made by the surrogate model was not reliable. This is probably due to the mismatch between the training/testing dataset (from FEM) and the validation dataset (i.e., the measurements from LIDAR). This mismatch was identified to be due to the identified missing physical processes in the model, and the fact that the on-ground measurements had a different nature than training and testing data. It is further suggested that a surrogate model can only be used provided the training testing and validation datasets are compatible - and as the FoS is rarely identifiable in reality leads to challenges using surrogate models to predict slope failure.

SAMENVATTING

De stabiliteit van hellingen is essentieel voor de veiligheid van een land, vooral wanneer het die van dijken en dammen betreft. Hellingsstabiliteit maakt ook dagmijnbouw mogelijk. Het falen van deze systemen heeft enorme gevolgen voor de samenleving en de economie en daarom is de nauwkeurige stabiliteitsbeoordeling van deze systemen van het allergrootste belang. Bestaande methoden zoals de *limit-equilibrium* methoden, andere numerieke methoden (e.g., eindige elementenmethoden, FEM), empirische methoden en probabilistische methoden geven een benadering van de veiligheidsfactor (FoS). Het onvermogen van deze modellen om nauwkeurige voorspellingen van de FoS te maken, is te wijten aan vele oorzaken, zoals ontbrekende fysische processen in de modellen, onnauwkeurige grens- en beginvoorwaarden van de modellen, constitutieve modelselectie, onzekerheid in modelparameters en beperkt begrip van mechanismen. Dit proefschrift stelt het gebruik van data-assimilatie voor om monitoringgegevens te combineren met een eindige-elementenmodel om de voorspellende mogelijkheden van het FEM-model te verbeteren. Tegenwoordig zijn geotechnische systemen uitgerust met meetapparatuur om hun reactie op externe veranderingen te monitoren. Deze metingen kunnen de vorm hebben van oppervlakteverplaatsingen, poriënwaterdrukken, spanningen, enz. Deze metingen kunnen worden verkregen met in-situ apparaten (zoals hellingsmeters, rekstrookjes, enz.) of kunnen op afstand worden gemeten (met Light Detection and Ranging (LIDAR), interferometrische synthetische apertuurradar (InSAR), enz.). Deze metingen kunnen worden geassimileerd om de voorspelbaarheid van FEM-modellen te verbeteren met populaire en gevestigde data-assimilatiemethoden die gebruik maken van een *ensemble* aan modelrealisaties, bijvoorbeeld het ensemble Kalman-filter (EnKF), de ensemble smoother (ES) en de ensemble smoother met meervoudige data-assimilatie (ESMDA).

In de eerste fase van het onderzoek in dit proefschrift is een eindige-elementenmodel van hellingsstabiliteit geïntegreerd met EnKF. Op basis van metingen van de vervorming van de helling schat deze aanpak de belangrijkste materiaalparameters (sterkte- en stijfheidsparameters), de toestand (verplaatsing) en de FoS van een helling. Het effect van twee verschillende constitutieve modellen (resp. het Mohr-Coulomb (MC) en het Hardening Soil (HS) model) op de FoS werd bestudeerd via een synthetisch tweelingexperiment. Het HS-model was in staat de FoS te schatten met een smalle a posteriori verdeling, uitgaande van een brede a-priori verdeling van materiaalparameters, inclusief a-priori verdelingen die niet de werkelijke parameters omvatten. Dit toont het voordeel aan van het gebruik van geavanceerde constitutieve modellen bij het gebruik van data-assimilatiemethoden voor de berekening van de FoS.

In de tweede fase van het onderzoek werd het constitutieve model dat relatief nauwkeurigere resultaten geeft (het HS model), geselecteerd in de eerste fase, getest met drie verschillende data-assimilatieschema's, namelijk EnKF, ES en ESMDA. Elk van deze schema's was geïntegreerd met de FEM om metingen van de vervorming van de helling en de top

van het hellingstabiliteitssysteem te assimileren. De nauwkeurigheid van deze schema's werd geëvalueerd in een synthetisch tweelingexperiment door hun FoS te vergelijken met de synthetische echte FoS en met hun rekentijd. De resultaten van dit experiment lieten zien dat EnKF een FoS schatte die dicht bij de werkelijke FoS ligt, met een kleine standaardafwijking. ESMDA was, bij gebruik van vier iteratieve assimilatiestappen, ook in staat een FoS te schatten die dicht bij de waarheid lag, maar had toch een hogere standaardafwijking vergeleken met EnKF. De ES en ESMDA (met twee iteratieve assimilatiestappen) waren niet in staat de echte FoS zo goed te reconstrueren als de andere schema's, hoogstwaarschijnlijk vanwege de veelal lineaire updates van de ES en ESMDA met twee assimilatiestappen. De theoretische rekentijd die de ES nodig heeft, is het kleinst, gevolgd door ESMDA met twee iteratieve assimilatiestappen, ESMDA met vier assimilatiestappen, en tenslotte de EnKF.

In de derde fase van het onderzoek werd een data-assimilatieschema geïmplementeerd op een case study van een dagbouwmijn in Cottbus, Duitsland. De LIDAR-metingen van de verticale verplaatsingen werden geassimileerd in een FEM-model van de hellingstabiliteit. Modelparameters, verplaatsingsensemble en FoS worden op basis van deze analyse geschat. De a posteriori schatting van FoS wordt vergeleken met hellingfalen waargenomen in het veld. De data-assimilatiere resultaten leveren betere resultaten op dan wanneer enkel FEM-modellen gebruikt zouden worden bij het vergelijken van de grondwaarheid van hellingfalen. Het was echter duidelijk dat niet alle fysieke processen in het model waren opgenomen, wat resulteerde in een aanzienlijke discrepantie tussen de gemodelleerde en waargenomen vervormingen, al werd er wel een aanzienlijke verbetering geconstateerd ten opzichte van het model zonder data-assimilatie. Deze constatering leidde tot de keuze van een data-assimilatieschema dat modelparameters schatte die over het geheel tot betere resultaten leidden, dan een schema dat incrementeel betere modelparameters gaf.

Omdat de ontwikkelde data-assimilatiebenadering meerdere FEM-analyses omvat, is deze rekentechnisch duur en daarom is het waarschijnlijk onpraktisch om een real-time beoordelingssysteem te ontwikkelen. In de laatste fase van dit onderzoek werd daarom een poging gedaan om de benodigde computertijd te verminderen door een surrogaatmodel van de geomechanica te ontwikkelen. Het surrogaatmodel werd getraind en getest op basis van de output van het FEM-modelensemble en gebruikte de verplaatsingen op verschillende locaties als input en de FoS als output. De output van het surrogaatmodel in de validatiefase werd vergeleken met de waargenomen FoS uit de casestudy. Hieruit bleek dat de voorspelling van het surrogaatmodel niet betrouwbaar is. Dit komt waarschijnlijk door de discrepantie tussen de trainings-/testdataset (van FEM) en de validatiedataset (d.w.z. de metingen van LIDAR). De mismatch die werd waargenomen werd toegewezen aan de geïdentificeerde ontbrekende fysieke processen in het model en het feit dat de echte metingen een ander karakter hadden dan de trainings- en testgegevens. Op basis van deze resultaten wordt gesuggereerd dat een surrogaatmodel alleen kan worden gebruikt op voorwaarde dat de trainingstest- en validatiedatasets compatibel zijn met de metingen die gebruikt worden in de schatting -en gezien het feit dat de FoS zelden wordt waargenomen bemoeilijkt dit het gebruik van surrogaatmodellen om de hellingstabiliteit te beoordelen.

ACKNOWLEDGEMENTS

Firstly, I am grateful to ALLAH Almighty for giving me the courage to be consistent during these years. I am also thankful to ALLAH Almighty for always rewarding me more than what I deserved.

Secondly, there are countless people I am grateful for their unconditional support. Starting from my supervisory team, I would like to thank my promoters prof. Dr. Philip J. Vardon and prof. Dr. Femke C. Vossepoel for their unwavering support and supervision. It is not possible to complete this thesis without your supervision, and guidance. My sincere gratitude to the examiners of this thesis, who spent their precious time for to read and feedback for this thesis.

I would like to thank my current and former office colleagues for their support and fun : Kishan, Willemijn, Mohsen, Kiarash, Jenny, Hamed, Samantha, Divya, Ali Glochin, Varun, Elahe, Leon.

My sincere gratitude to my Pakistani tribe, who made my stay more pleasant here in the Netherlands. I would like to thank my Pakistani friends for their emotional support, delicious food and gathering to remain alive abroad. I am highly obliged to Saad, Irfan, Aftab, Tanvir, Nauman, Qasim van der laan, Hussam dijk, Ozaif, Haris, Hassan Niazi, Husnain, Humza, Hassan, Usman, Sami, Shozab, Asif, Hateem, Abdullah, Abdul Wahab, Fouwad, Khaqan, Haider sultan, Ahmad , Ali waqas, Aitazaz, Mubariz, Minhaaj, Samad, Yasir, Junaid(s), Faisal, Irfan(s), Rizwan, Izhar, Ali and Shehryar. I am especially thankful to Aitazaz and Mubariz for listening to me and being my support. I would like to thank Nauman Raza and Kashif (Belgium) for always being my emotional backup. Furthermore, I am grateful to my friend currently staying in Pakistan Afzaal, Kashif (KK), Zeeshan Khalid, Awais and Umar.

My ultimate love and gratitude to my family for believing in me, for supporting me, and for praying for me during these years. Special thanks to my mother, maternal uncle (Munir Ahmed), mother-in-law, father-in-law, Muhammad Ahsan, Naz, Ali and Arooj for their continuous support.

Last but not least, I express my profound gratitude to my cherished wife, Zeenat, for her unwavering support, dedication and boundless love. Thank you for always trusting me, listening to me, cooking delicious food for me and smiling for me. I remember there were many ups and downs in our life and you were always there to support me. I am truly grateful to you for giving me the most beautiful gift of my life, Parisa (my angel, my anti-depressant).

1

INTRODUCTION

1.1. BACKGROUND

Slope stability applications include flood defence systems (dikes, dams, levees, embankments), transport infrastructures (embankments) and open-pit mining. These geotechnical systems are very important assets for a country. To give an impression of the extent of some of the slope stability systems, 14000 km of rural dikes contribute to the slope stability system which saves 40% of the Netherlands from inundation (Hicks et al., 2019). The failure of these systems can cause significant loss of human lives and detrimental effects on the economy. Examples of slope failures include the failure of peat dike in Wilnis, Netherlands (Van Baars, 2005), the failure of Bingham Canyon open-pit copper mine (Pankow et al., 2014) and the famous 67m high slope failure in Virginia (Berg et al., 2020). Due to the significant importance of these structures, a huge amount of government spending is being used to ensure the stability of these systems i.e. one billion euros per year are spent to upgrade and maintain the Netherlands Dutch dike network.

A variety of slope stability analysis methods are used to determine the safety of slope stability systems. These methods vary from simple analytical methods to advanced methods. A simple analytical method consists of the limit equilibrium method (LEM). LEM compute the factor of safety (FoS) of the system by dividing the stabilising forces to destabilising forces. Based on the different assumptions on the slip surface, several LEM approaches have been developed, such as Bishop (1955), Janbu (1954), Spencer (1967) and Sarma (1979) methods. Advanced methods such as the finite element method (FEM) are currently popular. In this method, there is no need to make a prior assumption of the slip surface. In FEM, the slope domain is discretised into finite elements. A suitable constitutive model is considered to define the behaviour of the slope material. The FoS is calculated either by increasing the gravity loading or by reducing the strength parameters of the soil mass. In addition, the Monte Carlo Method (MCM) has been integrated with FEM to better capture the uncertainty in the material properties of the slope stability system (Gao et al., 2019; Jiang et al., 2022; Peng et al., 2017; Phoon, 2008; Xiao et al., 2017; Y.-J. Yang et al., 2021; Z. Yang & Ching, 2020; J. Zhang et al., 2011; Z. Zhang & Ji, 2022). This allows an estimation of the probability density function of the FoS (and can be extended to the reliability-based design of geotechnical systems).

In addition to integrating FEM with MCM, there has been significant developments in FEM and constitutive models. These include the ability of the FEM for multi-physics modelling (thermo-hydro-mechanical coupling) and developments in constitutive modelling (non-linearity in elasticity, elasto-plasticity, hardening softening mechanism) (Lade, 2005). With the inclusion of these realistic soil features in the constitutive models, the prediction capabilities have improved significantly, but when compared with the field measurements model-measurement misfit is still often observed.

To obtain field measurements, geotechnical systems (including slope stability systems) can be equipped with in-situ and remote measurement devices (e.g., Light Detection and Ranging (LIDAR), Interferometric Synthetic Aperture Radar (InSAR)) which measure the response. The measured response of the can be in the form of a pore water pressure measurement, strain measurement or surface displacement measurement. For example, piezometer devices are used to measure the in-situ soil pore pressures and strain gauges measure the in-situ deformations of slope systems.

These measurements have been used in two ways for the evaluation of the model

performance. One way is to simply compare the measurements with the model predictions. The second way is to calibrate the model parameters based on these measurements. Following the former approach, several studies compare the displacement measurements produced by different constitutive models with field measurements for a range of geomechanical problems (e.g. Brinkgreve et al., 2006; Hsiung & Dao, 2014; Sekhvatian & Choobbasti, 2018). Brinkgreve et al. (2006) demonstrate the functioning of three constitutive models for a tunnel system. The authors compared field settlement and heave with FEM results which used the Mohr-Coulomb (MC) model, the hardening soil (HS) model and the hardening soil with small-strain stiffness (HSS) model. The authors conclude that the HSS model simulates the most realistic settlement and heave for this case. Hsiung and Dao (2014) studied the performance of the MC, HS and HSS models (Plaxis, 2015) for an excavation case. The authors compared the wall deflection and ground settlement with field data and concluded that the displacement produced by the HSS model was closest to the field measurements. Sekhvatian and Choobbasti (2018) compared movement prediction by FEM with field measurements in an underground excavation case. The authors compared the results produced by a number of different material models with field measurements as an indication of model performance. However, this information was not used to refine or estimate the model parameters.

In the latter approach, the authors used inverse analyses, Bayesian estimation or data assimilation to estimate the model parameters based on the measurements (e.g. Gens et al., 1996; Ledesma et al., 1996; Lee & Kim, 1999; Liu et al., 2018; Vardon et al., 2016; Wang et al., 2013; Zhou et al., 2007). Ledesma et al. (1996) and Gens et al. (1996) utilised a maximum-likelihood method to estimate Young's modulus for a tunnel excavation simulation in FEM. Lee and Kim (1999) utilised an extended Bayesian method in a simulation of a tunnel system for an inverse analysis of four parameters: elastic modulus, initial horizontal stress at rest, cohesion and friction angle. Zhou et al. (2007) proposed and implemented an extended Bayesian approach on an embankment and an excavation case. The author estimated Young's modulus for both the cases. Wang et al. (2013) conducted a probabilistic inverse analysis for a slope-failure case in Taiwan, which included soil anchors. They estimated the strength parameters and anchor force in order to better understand the slope failure mechanism. Vardon et al. (2016) and Liu et al. (2018) used an ensemble Kalman filter (EnKF) approach on a slope-stability problem. The authors combined the random finite element method (RFEM) with the EnKF to estimate the hydraulic conductivity based on pore water pressure measurements in a steady-state and transient state seepage problem in a synthetic case. The improved estimation of hydraulic conductivity led to improved pore water pressure estimation, thereby improving the prediction of slope stability. Another example of inverse analysis is provided by Kim and Finno (2020), who optimise model parameters of a hypo-plastic clay model in the case of an excavation using the measurements of lateral movements at an early stage of excavation with a gradient approach based on the Gauss-Newton method.

1.2. CURRENT LIMITATIONS

Ensemble-based methods for data assimilation are well established, e.g., the ensemble Kalman filter (EnKF), ensemble smoother (ES) and ensemble smoother with multiple data assimilation (ESMDA) and have been successfully used in different fields. For ex-

ample, the EnKF has been used in numerical weather prediction (e.g., Houtekamer & Mitchell, 2005; Szunyogh et al., 2005), oceanography (e.g., Bertino et al., 2003; Keppenne & Rienecker, 2003), hydrology (e.g., Chen & Zhang, 2006; Reichle et al., 2002), geotechnical engineering (e.g., Liu et al., 2018; Mavritsakis, 2017; Mohsan et al., 2021, 2023; Vardon et al., 2016), and petroleum reservoir history matching (e.g. Aanonsen et al., 2009; Evensen, 2009; Glegola et al., 2012; Nævdal et al., 2002; Oliver & Chen, 2011). The EnKF is currently one of the most popular data assimilation methods. ES (Van Leeuwen & Evensen, 1996) is an alternative ensemble-based formulation and is implemented in the fields of petroleum reservoir engineering (e.g., Skjervheim & Evensen, 2011) and oceanography (e.g., Van Leeuwen, 1999; Van Leeuwen & Evensen, 1996). ESMDA (Emerick & Reynolds, 2013) has been implemented in the field of petroleum engineering (e.g., Emerick, 2016; Emerick & Reynolds, 2013; Maucec et al., 2016) but has also been applied in other fields (e.g., Evensen, 2018; Evensen et al., 2021; Evensen & Eikrem, 2018).

The use of these popular well-established ensemble-based data assimilation schemes is limited in geotechnical engineering. There is a need to investigate the capabilities of these data assimilation schemes in the geotechnical engineering field for parameter and FoS estimation. Furthermore, the majority of the reported literature in the geotechnical engineering field shows the estimation of a single parameter (either the stiffness or the strength parameter) by using an inverse analysis or data assimilation scheme. The sensitivity of parameters is different at different levels of loading, e.g., the stiffness parameters are more sensitive in the early stage of loading (i.e., the elastic stage) and strength parameters are generally more sensitive in the ultimate state of loading, i.e., in the plastic stage. There is a need to further investigate techniques which estimate multiple model parameters simultaneously, considering their sensitivity at specific stress states.

1.3. MOTIVATION

It is important to predict the FoS of slope stability accurately to help stakeholders protect their assets. Current models (such as FEM) provide an approximate prediction of FoS. This can be due to the uncertainty in the constitutive model parameters, approximations in the initial and boundary conditions and missing physics in the FEM model. On the other hand, many of the geotechnical systems are equipped with in-situ or remote measurement devices such as LIDAR, InSAR, and strain gauges. These devices can measure the system response accurately, e.g., LIDAR is claimed to measure the surface (vertical and horizontal) movement to millimetre scale accuracy. These measurements can be used to improve the predictive capabilities of the FEM model by improving its parameters. An additional limitation of FEM is that it requires huge computational costs to run a probabilistic analysis. To address this, Chapter 4 of this thesis also tests a way to build a surrogate model which directly translates measurements to the FoS.

1.4. RESEARCH OBJECTIVES

The research questions of this dissertation revolve around the following lines:

Research question 1: How can the measurements be used in numerical models for slope stability? What are the effects of the different constitutive models in measurement assimilation?

With the advancement in monitoring devices, an increasing amount of slope systems are being monitored. Different slope response has been measured by using in-situ and remote devices. For example, piezometer devices are used to measure the in-situ soil pore pressures and strain gauges measure the in-situ deformations of slope systems. Remote sensing devices such as LIDAR, and InSAR claim to measure the accurate response of slope systems in the form of vertical and horizontal deformation. These measurements are useful for understanding the real-time slope behaviour but can not provide future predictions. On the other hand, FEM models are considered to be one of the most advanced slope stability prediction models which provide approximate predictions of slope stability. Their predictions are known to have errors due to their approximations in the constitutive equations, poorly known model parameters and other reasons. Currently, the majority of the studies for slope stability prediction utilise a manual calibration approach or inverse analysis (for quasi-static) to estimate mostly the single parameters (e.g. Gens et al., 1996; Ledesma et al., 1996; Lee & Kim, 1999; Wang et al., 2013; Zhou et al., 2007). There might be a benefit to investigate the use of popular data assimilation schemes such as EnKF in the slope stability system. In order to do this, it is proposed to use EnKF as the data assimilation scheme to estimate the strength and stiffness parameters based on measurements of horizontal displacements on the face of a slope. These estimated parameters can then be used to estimate the FoS. To investigate the effect of different constitutive models, two different models are used in the FEM: the Mohr-Coulomb (MC) model and the Hardening Soil (HS) model. The EnKF framework allows the investigation of the effect using the different constitutive behaviour on its ability to estimate the model parameter and FoS estimation.

Research question 2: What kind of data assimilation schemes can be used in the slope stability analysis to estimate the parameters and FoS?

There are three popular well-established data assimilation methods, namely, the ensemble Kalman filter (EnKF), ensemble smoother (ES) and ensemble smoother with multiple data assimilation (ESMDA). These schemes have been successfully used in different fields. Several researchers have compared the performance of these ensemble-based methods in different fields (e.g., Emerick, 2016; Evensen et al., 2022; Skjervheim & Evensen, 2011; Van Leeuwen & Evensen, 1996). They studied the performance of these data assimilation schemes based on both computational efficiency and the ability to estimate the physical state of a system that agrees with the measured (or synthetically generated) data thereof. The study of these data assimilation schemes is limited in the field of geotechnical engineering. In this thesis, three different data assimilation schemes have been implemented in a fully coupled hydro-mechanical slope stability model to study their performance, i.e., the EnKF, ES and ESMDA. The slope stability model in this study uses the HS model to simulate the (non-linear) material behaviour. The data assimilation schemes estimate the strength and stiffness parameters for the slope stability system. These estimated parameters have been used in the computation of the factor of safety of the slope stability system. The efficiency of these data assimilation schemes has been evaluated by comparing the results of FoS with the synthetic truth of FoS and by assessing their computation time.

Research question 3: How can we validate the data assimilation schemes and the use of surrogate models in a case study?

In the answering of research question 1 and 2, the data assimilation schemes are verified based on synthetic data. There is a need to validate these schemes for a real case study, with synthetic data that has all of the characteristics of real data. To do that, a case study has been selected, where a slope at an open pit mine in Cottbus, Germany, has been monitored. LIDAR measurements of the vertical displacements are assimilated into FEM model with missing physics. ES is implemented as the data assimilation scheme. The resulting framework aims to estimate the model parameters, displacement ensemble and factor of safety (FoS). The posterior estimation of FoS is compared with slope failure observed in the field and it provides a better estimation than when only using FEM (prior estimate). A surrogate model is then trained and tested with the prior and posterior FEM ensemble of displacements as input, and the FoS as output. The surrogate model is validated with the LIDAR measurements and the results are compared with ES results and the ground truth displacements.

1.5. SLOPE STABILITY FOR THE COTTBUS OPEN-PUT MINE

This thesis is the part of Integrated Mining Impact Monitoring (i2MON) project (<https://i2monproject.eu/about-news/>). This project is funded via the EU HORIZON 2020 programme, via the Research Fund for Coal and Steel (RFCS). The other project partners involve AIRBUS, LASERDATA, LEAG, DMT GmbH, IMG PAN, TU BAF, EFTAS GmbH, POLSKA GRUPA GÓRNICZA, and FH MAIN. The main objectives of i2MON are:

- Development of innovative monitoring tools for advanced monitoring of ground and slope deformation using geotechnical and geodetic tools such as laser technology, Sentinel, TerraSAR-X PSI, airborne and ground-based radar.
- Identification of physical processes and its numerical modelling for the ground subsidence and slope stability. Furthermore, numerical modelling is integrated with the deformation measurements. (This objective is addressed in the present thesis.)
- Development of the integrated web system which is used to quantify the risk assessments for the coal mining community.

1.6. OUTLINE OF THE THESIS

This thesis consists of the following chapters:

In Chapter 2, a specific data assimilation scheme (EnKF) is implemented on the fully coupled hydro-mechanical model of a slope stability system. In this chapter, two different constitutive models are used in the FEM model: the MC (Plaxis, 2015) and HS (Schanz et al., 1999) models. Data assimilation estimates the strength and stiffness parameters based on the measurements of slope displacements. Finally, an assessment of the FoS is made by using the improved model parameters with both constitutive models.

In Chapter 3, three different data assimilation schemes have been implemented in an FEM model of slope stability. These schemes are EnKF, ES (Van Leeuwen & Evensen,

1996) and ESMDA (Emerick & Reynolds, 2013). The strength and stiffness parameters of the HS model are estimated based on measurements of crest-slope displacements. First, an assumed synthetic truth is created by assuming the true parameter values. Then, the accuracy of each of the data assimilation schemes is evaluated based on its ability to estimate the synthetic truth of the FoS and on its computational time.

In Chapter 4, the above framework of data assimilation (ES) and the Gaussian process regression (GP) surrogate model is implemented in a case study of the Cottbus open pit mine. The LIDAR measurements of vertical displacement on the slope is used in a data assimilation experiment to estimate the strength and stiffness parameters of the HS model and ultimately to estimate the FoS. GP is also trained and tested, both on the prior and on the posterior estimates. GP is validated using the Cottbus measurements and its resulting slope deformation estimates at failure are compared with the ground truth estimates thereof.

Chapter 5 concludes the thesis with the conclusions and future recommendations.

REFERENCES

- Aanonsen, S. I., Nævdal, G., Oliver, D. S., Reynolds, A. C., & Vallès, B. (2009). The ensemble Kalman filter in reservoir engineering—a review. *SPE Journal*, 14(3), 393–412. <https://doi.org/10.2118/117274-PA>
- Berg, R. R., Collin, J. G., Taylor, T. P., & Watts, C. F. (2020). Case history on failure of a 67 m tall reinforced soil slope. *Geotextiles and Geomembranes*, 48(6), 802–811. <https://doi.org/10.1016/j.geotextmem.2020.06.003>
- Bertino, L., Evensen, G., & Wackernagel, H. (2003). Sequential data assimilation techniques in oceanography. *International Statistical Review*, 71(2), 223–241. <https://doi.org/10.1111/j.1751-5823.2003.tb00194.x>
- Bishop, A. W. (1955). The use of the slip circle in the stability analysis of slopes. *Geotechnique*, 5(1), 7–17. <https://doi.org/10.1680/geot.1955.5.1.7>
- Brinkgreve, R. B. J., Bakker, K. J., & Bonnier, P. G. (2006). The relevance of small-strain soil stiffness in numerical simulation of excavation and tunneling projects. *Proceedings of 6th European Conference in Geotechnical Engineering, Graz, Austria*, 133–139.
- Chen, Y., & Zhang, D. (2006). Data assimilation for transient flow in geologic formations via ensemble Kalman filter. *Advances in Water Resources*, 29(8), 1107–1122. <https://doi.org/10.1016/j.advwatres.2005.09.007>
- Emerick, A. A. (2016). Analysis of the performance of ensemble-based assimilation of production and seismic data. *Journal of Petroleum Science and Engineering*, 139, 219–239. <https://doi.org/10.1016/j.petrol.2016.01.029>
- Emerick, A. A., & Reynolds, A. C. (2013). Ensemble smoother with multiple data assimilation. *Computers & Geosciences*, 55, 3–15. <https://doi.org/10.1016/j.cageo.2012.03.011>
- Evensen, G. (2009). *Data assimilation: The ensemble Kalman filter*. Springer Science & Business Media.
- Evensen, G. (2018). Analysis of iterative ensemble smoothers for solving inverse problems. *Computational Geosciences*, 22(3), 885–908. <https://doi.org/10.1007/s10596-018-9731-y>
- Evensen, G., Amezcuca, J., Bocquet, M., Carrassi, A., Farchi, A., Fowler, A., Houtekamer, P. L., Jones, C. K., de Moraes, R. J., Pulido, M., et al. (2021). An international initiative of predicting the sars-cov-2 pandemic using ensemble data assimilation. *Foundations of Data Science*, 3(3). <https://doi.org/10.3934/fods.2021001>
- Evensen, G., & Eikrem, K. S. (2018). Conditioning reservoir models on rate data using ensemble smoothers. *Computational Geosciences*, 22(5), 1251–1270. <https://doi.org/10.1007/s10596-018-9750-8>
- Evensen, G., Vossepoel, F. C., & van Leeuwen, P. J. (2022). *Data assimilation fundamentals: A unified formulation of the state and parameter estimation problem*. Springer Nature. <https://doi.org/10.1007/978-3-030-96709-3>

- Gao, G.-H., Li, D.-Q., Cao, Z.-J., Wang, Y., & Zhang, L. (2019). Full probabilistic design of earth retaining structures using generalized subset simulation. *Computers and Geotechnics*, *112*, 159–172. <https://doi.org/10.1016/j.compgeo.2019.04.020>
- Gens, A., Ledesma, A., & Alonso, E. E. (1996). Estimation of parameters in geotechnical backanalysis — II. Application to a tunnel excavation problem. *Computers and Geotechnics*, *18*(1), 29–46. [https://doi.org/10.1016/0266-352X\(95\)00022-3](https://doi.org/10.1016/0266-352X(95)00022-3)
- Glegola, M. A., Ditmar, P., Hanea, R. G., Vossepoel, F. C., Arts, R., & Klees, R. (2012). Gravitometric monitoring of water influx into a gas reservoir: A numerical study based on the ensemble Kalman filter. *SPE Journal*, *17*(1), 163–176. <https://doi.org/10.2118/149578-PA>
- Hicks, M. A., Varkey, D., van den Eijnden, A. P., de Gast, T., & Vardon, P. J. (2019). On characteristic values and the reliability-based assessment of dykes. *Georisk: Assessment and Management of Risk for Engineered Systems and Geohazards*, *13*(4), 313–319. <https://doi.org/10.1080/17499518.2019.1652918>
- Houtekamer, P. L., & Mitchell, H. L. (2005). Ensemble Kalman filtering. *Quarterly Journal of the Royal Meteorological Society: A Journal of the Atmospheric Sciences, Applied Meteorology and Physical Oceanography*, *131*(613), 3269–3289. <https://doi.org/10.1256/qj.05.135>
- Hsiung, B. C., & Dao, S.-D. (2014). Evaluation of constitutive soil models for predicting movements caused by a deep excavation in sands. *Electronic Journal of Geotechnical Engineering*, *19*, 17325–17344.
- Janbu, N. (1954). Stability analysis of slopes with dimensionless parameters. *PhD thesis, Harvard University*.
- Jiang, S.-H., Liu, X., Huang, J., & Zhou, C.-B. (2022). Efficient reliability-based design of slope angles in spatially variable soils with field data. *International Journal for Numerical and Analytical Methods in Geomechanics*, *46*(13), 2461–2490.
- Keppenne, C. L., & Rienecker, M. M. (2003). Assimilation of temperature into an isopycnal ocean general circulation model using a parallel ensemble Kalman filter. *Journal of Marine Systems*, *40*, 363–380. [https://doi.org/10.1016/S0924-7963\(03\)00025-3](https://doi.org/10.1016/S0924-7963(03)00025-3)
- Kim, S., & Finno, R. J. (2020). Inverse analysis of Hypoplastic Clay model for computing deformations caused by excavations. *Computers and Geotechnics*, *122*, 103499. <https://doi.org/10.1016/j.compgeo.2020.103499>
- Lade, P. V. (2005). Overview of constitutive models for soils. *Geo-frontiers 2005: Soil constitutive models: Evaluation, selection, and calibration* (pp. 1–34). [https://doi.org/10.1061/40771\(169\)1](https://doi.org/10.1061/40771(169)1)
- Ledesma, A., Gens, A., & Alonso, E. E. (1996). Parameter and variance estimation in geotechnical backanalysis using prior information. *International Journal for Numerical and Analytical Methods in Geomechanics*, *20*(2), 119–141. [https://doi.org/10.1002/\(SICI\)1096-9853\(199602\)20:2%3C119::AID-NAG810%3E3.0.CO;2-L](https://doi.org/10.1002/(SICI)1096-9853(199602)20:2%3C119::AID-NAG810%3E3.0.CO;2-L)
- Lee, I.-M., & Kim, D.-H. (1999). Parameter estimation using extended Bayesian method in tunnelling. *Computers and Geotechnics*, *24*(2), 109–124. [https://doi.org/10.1016/S0266-352X\(98\)00031-7](https://doi.org/10.1016/S0266-352X(98)00031-7)
- Liu, K., Vardon, P. J., & Hicks, M. A. (2018). Sequential reduction of slope stability uncertainty based on temporal hydraulic measurements via the ensemble Kalman

- filter. *Computers and Geotechnics*, 95, 147–161. <https://doi.org/10.1016/j.compgeo.2017.09.019>
- Maucec, M., De Matos Ravanelli, F. M., Lyngra, S., Zhang, S. J., Alramadhan, A. A., Abdelhamid, O. A., & Al-Garni, S. A. (2016). Ensemble-based assisted history matching with rigorous uncertainty quantification applied to a naturally fractured carbonate reservoir. *SPE Annual Technical Conference and Exhibition*. <https://doi.org/10.2118/181325-MS>
- Mavritsakis, A. (2017). Evaluation of inverse analysis methods with numerical simulation of slope excavation. *MSc thesis, Delft University of Technology, Netherlands*.
- Mohsan, M., Vardon, P. J., & Vossepoel, F. C. (2021). On the use of different constitutive models in data assimilation for slope stability. *Computers and Geotechnics*, 138, 104332. <https://doi.org/10.1016/j.compgeo.2021.104332>
- Mohsan, M., Vardon, P. J., & Vossepoel, F. C. (2023). Options for the implementations of data assimilation for geotechnics. *International Conference of the International Association for Computer Methods and Advances in Geomechanics*, 255–262. https://doi.org/10.1007/978-3-031-12851-6_31
- Nævdal, G., Mannseth, T., & Vefring, E. H. (2002). Near-well reservoir monitoring through ensemble Kalman filter. *SPE/DOE Improved Oil Recovery Symposium*, (SPE 75235). <https://doi.org/10.2118/75235-MS>
- Oliver, D. S., & Chen, Y. (2011). Recent progress on reservoir history matching: A review. *Computational Geosciences*, 15(1), 185–221. <https://doi.org/10.1007/s10596-010-9194-2>
- Pankow, K. L., Moore, J. R., Hale, J. M., Koper, K. D., Kubacki, T., Whidden, K. M., & McCarter, M. K. (2014). Massive landslide at Utah copper mine generates wealth of geophysical data. *GSA Today*, 24(1), 4–9. <https://doi.org/10.1130/GSATG191A.1>
- Peng, X., Li, D.-Q., Cao, Z.-J., Gong, W., & Juang, C. H. (2017). Reliability-based robust geotechnical design using Monte Carlo simulation. *Bulletin of Engineering Geology and the Environment*, 76, 1217–1227. <https://doi.org/10.1007/s10064-016-0905-3>
- Phoon, K.-K. (2008). *Reliability-based design in geotechnical engineering: Computations and applications*. CRC Press.
- Plaxis. (2015). *PLAXIS material models manual*. Plaxis.
- Reichle, R. H., McLaughlin, D. B., & Entekhabi, D. (2002). Hydrologic data assimilation with the ensemble Kalman filter. *Monthly Weather Review*, 130(1), 103–114. [https://doi.org/10.1175/1520-0493\(2002\)130%3C0103:HDAWTE%3E2.0.CO;2](https://doi.org/10.1175/1520-0493(2002)130%3C0103:HDAWTE%3E2.0.CO;2)
- Sarma, S. K. (1979). Stability analysis of embankments and slopes. *Journal of the Geotechnical Engineering Division*, 105(12), 1511–1524. <https://doi.org/10.1061/AJGEB6.0000903>
- Schanz, T., Vermeer, P., & Bonnier, P. G. (1999). The hardening soil model: Formulation and verification. *Beyond 2000 in computational geotechnics* (pp. 281–296). Routledge.
- Sekhvatian, A., & Choobbasti, A. J. (2018). Comparison of constitutive soil models in predicting movements caused by an underground excavation. *International Journal of Soil Science*, 13(1), 18–27. <https://doi.org/ijss.2018.18.27>

- Skjervheim, J.-A., & Evensen, G. (2011). An ensemble smoother for assisted history matching. *SPE Reservoir Simulation Symposium*, (SPE-141929-MS). <https://doi.org/10.2118/141929-MS>
- Spencer, E. (1967). A method of analysis of the stability of embankments assuming parallel inter-slice forces. *Geotechnique*, 17(1), 11–26. <https://doi.org/10.1680/geot.1967.17.1.11>
- Szunyogh, I., Kostelich, E. J., Gyarmati, G., Patil, D., Hunt, B. R., Kalnay, E., Ott, E., & Yorke, J. A. (2005). Assessing a local ensemble Kalman filter: Perfect model experiments with the National Centers for Environmental Prediction global model. *Tellus A: Dynamic Meteorology and Oceanography*, 57(4), 528–545. <https://doi.org/10.3402/tellusa.v57i4.14721>
- Van Baars, S. (2005). The horizontal failure mechanism of the wilnis peat dyke. *Géotechnique*, 55(4), 319–323. <https://doi.org/10.1680/geot.2005.55.4.319>
- Van Leeuwen, P. J. (1999). The time-mean circulation in the agulhas region determined with the ensemble smoother. *Journal of Geophysical Research: Oceans*, 104(C1), 1393–1404. <https://doi.org/10.1029/1998JC900012>
- Van Leeuwen, P. J., & Evensen, G. (1996). Data assimilation and inverse methods in terms of a probabilistic formulation. *Monthly Weather Review*, 124(12), 2898–2913. [https://doi.org/10.1175/1520-0493\(1996\)124<2898:DAAIMI>2.0.CO;2](https://doi.org/10.1175/1520-0493(1996)124<2898:DAAIMI>2.0.CO;2)
- Vardon, P. J., Liu, K., & Hicks, M. A. (2016). Reduction of slope stability uncertainty based on hydraulic measurement via inverse analysis. *Georisk: Assessment and Management of Risk for Engineered Systems and Geohazards*, 10(3), 223–240. <https://doi.org/10.1080/17499518.2016.1180400>
- Wang, L., Hwang, J. H., Luo, Z., Juang, C. H., & Xiao, J. (2013). Probabilistic back analysis of slope failure – a case study in Taiwan. *Computers and Geotechnics*, 51, 12–23. <https://doi.org/10.1016/j.compgeo.2013.01.008>
- Xiao, T., Li, D.-Q., Cao, Z.-J., & Tang, X.-S. (2017). Full probabilistic design of slopes in spatially variable soils using simplified reliability analysis method. *Georisk: Assessment and Management of Risk for Engineered Systems and Geohazards*, 11(1), 146–159. <https://doi.org/10.1080/17499518.2016.1250279>
- Yang, Y.-J., Li, D.-Q., Cao, Z.-J., Gao, G.-H., & Phoon, K.-K. (2021). Geotechnical reliability-based design using generalized subset simulation with a design response vector. *Computers and Geotechnics*, 139, 104392. <https://doi.org/10.1016/j.compgeo.2021.104392>
- Yang, Z., & Ching, J. (2020). A novel reliability-based design method based on quantile-based first-order second-moment. *Applied Mathematical Modelling*, 88, 461–473. <https://doi.org/10.1016/j.apm.2020.06.038>
- Zhang, J., Zhang, L. M., & Tang, W. H. (2011). Reliability-based optimization of geotechnical systems. *Journal of Geotechnical and Geoenvironmental Engineering*, 137(12), 1211–1221. [https://doi.org/10.1061/\(ASCE\)GT.1943-5606.0000551](https://doi.org/10.1061/(ASCE)GT.1943-5606.0000551)
- Zhang, Z., & Ji, J. (2022). Geotechnical RBDO: Coupling the inverse reliability algorithm with multi-objective reliability-based design optimization of geotechnical systems. *Computers and Geotechnics*, 152, 105005. <https://doi.org/10.1016/j.compgeo.2022.105005>

- Zhou, M., Li, Y., Xiang, Z., Swoboda, G., & Cen, Z. (2007). A modified extended Bayesian method for parameter estimation. *Tsinghua Science & Technology*, 12(5), 546–553. [https://doi.org/10.1016/S1007-0214\(07\)70131-1](https://doi.org/10.1016/S1007-0214(07)70131-1)

2

ON THE USE OF DIFFERENT CONSTITUTIVE MODELS IN DATA ASSIMILATION FOR SLOPE STABILITY

A recursive ensemble Kalman filter (EnKF) is used as the data assimilation scheme to estimate strength and stiffness parameters simultaneously for a fully coupled hydro-mechanical slope stability analysis. Two different constitutive models are used in the hydro-mechanical model: the Mohr-Coulomb (MC) model and the Hardening Soil (HS) model. The data assimilation framework allows the investigation of the effect of constitutive behaviour on its ability to estimate the factor of safety using measurements of horizontal nodal displacement at the sloping face. In a synthetic study, close-to-failure and far-from-failure cases of prior property estimations illustrate the effect of initial material property distribution with different material models. The results show that both models provide a reliable factor of safety when the distribution of prior parameters is selected close-to-failure. However, the HS model results in the improved estimation of factor of safety for the far-from-failure case while this is not the case for the MC model. In addition, for the same level of accuracy the computational effort required for the HS model is comparatively less than for the MC model.

2.1. INTRODUCTION

Slope stability assessment is very important for the construction and risk assessment of infrastructure. There are a variety of methods to assess slope stability, e.g. limit equilibrium methods, numerical methods, empirical methods and probabilistic methods. With the development of numerical methods, such as the finite element method (FEM), it has

This chapter is based on Mohsan et al. (2021) and Mohsan et al. (2023).

become possible to analyse and predict the behaviour of geometrically complex slopes under hydro-mechanical non-steady-state conditions. The applicability of this type of analysis significantly depends upon the constitutive (stress-strain) behaviour of the material and the mathematical representation of the behaviour used in FEM.

In the past few decades, there have been significant developments in constitutive models. For example, the evaluation of non-linearity in elasticity, elasto-plasticity and hardening/softening are now regularly seen in more advanced constitutive models. Commercial software packages (e.g. PLAXIS) offer the possibility to include different constitutive models, for example, a formulation representing linear-elastic perfectly plastic behaviour based on Mohr-Coulomb assumptions, or a hardening soil model, which is a more advanced non-linear elasto-plastic soil model that includes hardening (Plaxis, 2015).

While numerical models have been shown to capture the hydro-mechanical processes occurring in soils, the representation of slope behaviour by numerical models often differs from what is observed in reality. This can be due to a poor representation of the physical processes (either in the governing equations or in the constitutive model), poorly known model parameters, a complex geometry, complex initial and boundary conditions, or a combination of these. To investigate or overcome these limitations, one can make use of measured behaviour of the slope. Measurements can be used in two ways: one way is to compare the numerical model output with the measurements and choose the best model formulation, and an alternative way is to assimilate the measurements in a mathematically consistent way to find the most likely state and parameters given the measurements and the uncertainty in both model and measurements.

Chapter 1 (Section 1.1) summarizes the performance evaluation of different constitutive model results based on the field measurements. Various researchers compare the displacement results from numerical models with field results for a range of geotechnical problems (e.g. Brinkgreve et al., 2006; Hsiung & Dao, 2014; Sekhvatian & Choobasti, 2018). In a number of studies, the model parameters were estimated based on field measurements by using inverse analysis or data assimilation schemes (e.g. Gens et al., 1996; Ledesma et al., 1996; Lee & Kim, 1999; Liu et al., 2018; Vardon et al., 2016; Wang et al., 2013; Zhou et al., 2007). The results of these studies have been discussed in Chapter 1 (Section 1.1).

The majority of the studies mentioned above (and discussed in Chapter 1) utilised a data assimilation approach to estimate either stiffness or strength parameters. The sole estimation of stiffness parameters does not give any information about the ultimate limit state of the system (factor of safety). On the other hand, the sole estimation of the strength parameters does not give sufficient insight into the pre-failure behaviour of the material and reduces the ability of the data to be used to estimate the strength parameters. The objective of the present study is to explore the use of data assimilation to improve estimates of slope stability by assimilating the slope deformation measurements. To this end, simultaneous estimation of the stiffness and strength parameters are conducted for two different constitutive models that incorporate material non-linearity. The evaluation of the slope-stability estimates will eventually support the development of a data assimilation framework for robust assessment of slope-failure risks.

In this chapter, the effect of constitutive models on the calculation of the factor of

safety is addressed by assimilating the measurements into the FEM simulation of a slope stability problem, under unsteady hydraulic conditions. A comparison of close-to-failure and far-from-failure prior parameter estimation cases helps to investigate the effect of material non-linearity in two different constitutive models. A recursive EnKF is implemented for two different constitutive models (HS and MC). The performance of the resulting data assimilation systems is evaluated by their ability to estimate the horizontal displacement within the model domain and to predict the Factor of Safety (FoS) of the slope. In Section 2.2, details of the forward model and the data assimilation method are presented. Section 2.3 presents an evaluation method and a synthetic example to evaluate the system's performance, with the results presented in Section 2.4. Section 2.5 presents the discussion followed by conclusions. An investigation of the system's sensitivity to various inputs is given in Appendix A.1.

2.2. METHODOLOGY

The method is made up of a forward model which simulates the physics of the problem, and a data assimilation method that combines this forward model with measurements to estimate constitutive model parameters and the corresponding state variables. A fully coupled hydro-mechanical FEM simulation is used as the forward model. In order to investigate the effect of constitutive models on the estimated state and the estimated FoS, two types of constitutive models are used, *i.e.*, the MC and the HS models. A recursive EnKF is used as the data assimilation method to estimate the constitutive model parameters (e.g. friction angle, cohesion, stiffness) based on measurements (*i.e.* surface displacements). The workflow in this study is controlled via Python, making use of the PLAXIS Python interface to control the PLAXIS analyses. The FEM equations are solved by PLAXIS and the data assimilation part is implemented and solved in Python.

2.2.1. FORWARD MODEL

FULLY COUPLED HYDRO-MECHANICAL SLOPE STABILITY MODEL

In soils under unsteady flow, both the mechanical and hydraulic behaviour must be considered. For the mechanical behaviour, equilibrium is considered, *i.e.*:

$$\nabla \cdot \boldsymbol{\sigma}' + \nabla p + \rho \mathbf{b} = \mathbf{0} \quad (2.1)$$

where ∇ is the gradient operator, $\nabla \cdot$ is the divergence, $\boldsymbol{\sigma}'$ is the effective stress tensor, p is the pore pressure, ρ is the density and \mathbf{b} are the body accelerations (e.g. from gravity). The constitutive behaviour can be expressed as:

$$\boldsymbol{\sigma}' = \mathbf{D}' \boldsymbol{\epsilon} \quad (2.2)$$

where \mathbf{D}' is the effective constitutive matrix and $\boldsymbol{\epsilon}$ is the strain tensor.

By substituting Eq. 3.2 into Eq. 3.1 and recognising that $\boldsymbol{\epsilon} = 0.5((\nabla \mathbf{u}) + (\nabla \mathbf{u})^T)$ (where \mathbf{u} is the displacement) yields the mechanical governing equation. The displacement is resolved into its x- and y-components and termed as horizontal displacements (\mathbf{u}_x) and vertical displacements (\mathbf{u}_y), respectively.

For the hydraulic behaviour, the governing equation is the conservation of mass which can be expressed as:

$$\frac{\partial(\rho_l n)}{\partial t} = -\nabla \cdot \mathbf{v} - Q \quad (2.3)$$

where ρ_l is the fluid density, n is the porosity, \mathbf{v} is the velocity vector and Q is a source term. The derivative of the fluid density with time is calculated using the compressibility of the fluid ($\partial\rho_l/\partial t = \rho_l/K_w \cdot \partial p/\partial t$, where K_w is 2183 MPa) and the change of porosity is evaluated from the change of the volumetric strain ϵ_{vol} .

The velocity of water is incorporated via Darcy's Law:

$$\mathbf{v} = -k\nabla \left(\frac{p}{\rho_l g} + z \right) \quad (2.4)$$

where k is the hydraulic conductivity matrix, g is the gravitational constant, and z is the elevation.

Both the governing equations have primary variables of displacement and fluid pressure, and are therefore a coupled system of equations. In this work, the governing equations are solved using FEM by using the software PLAXIS (Plaxis, 2015).

CONSTITUTIVE MODELS

Stress-strain (constitutive) relationships of real soils are usually non-linear. The stiffness and shear strength of soil typically depends upon the stress level, the strain level and the stress history. A variety of constitutive models exists to simulate soil behaviour. In this study, two types of constitutive models are used *i.e.* the Mohr-Coulomb (MC) model and the Hardening Soil model (HS). The MC model is commonly used in geotechnical analyses as it is simple and represents stress-dependent failure conditions reasonably well, but misses some realistic soil features, *i.e.* non-linear elasticity, stress-dependent stiffness, hardening/softening and plasticity before failure. On the other hand, the HS model takes into account these realistic features but is not as frequently used in geotechnical practice, partly due to the requirement of additional parameters.

Mohr-Coulomb model: The MC model is a simple and well known linear-elastic perfectly-plastic model, which is used widely to represent soils. The linear elastic part of the Mohr-coulomb model is based on Hooke's law, and is therefore not stress or strain dependent, and the onset of plasticity is based on the Mohr-Coulomb failure criterion, *i.e.* a stress-dependent shear strength. Plastic deformations occur without any change in stress level, *i.e.* they are perfectly plastic. A representation of the model is shown in Fig. 2.1.

A total of five model parameters are required to implement the Mohr-Coulomb model. This includes the two elastic parameters, the Young's modulus (E), Poisson's ratio (ν), and three strength parameters, cohesion (c), friction angle (ϕ) and dilatancy angle (ψ).

Hardening Soil model: The HS model is a nonlinear elasto-plastic soil model. The stress-strain relationship in a drained triaxial compression test is represented by the hyperbolic function (Fig. 2.2). The model shows a decreasing stiffness (stress-dependent stiffness) and irreversible plastic strains simultaneously when subjected to deviatoric loading. Three different stress-dependent stiffness parameters are considered to model soil behaviour. The stress-strain path due to primary loading is curved, which is mod-

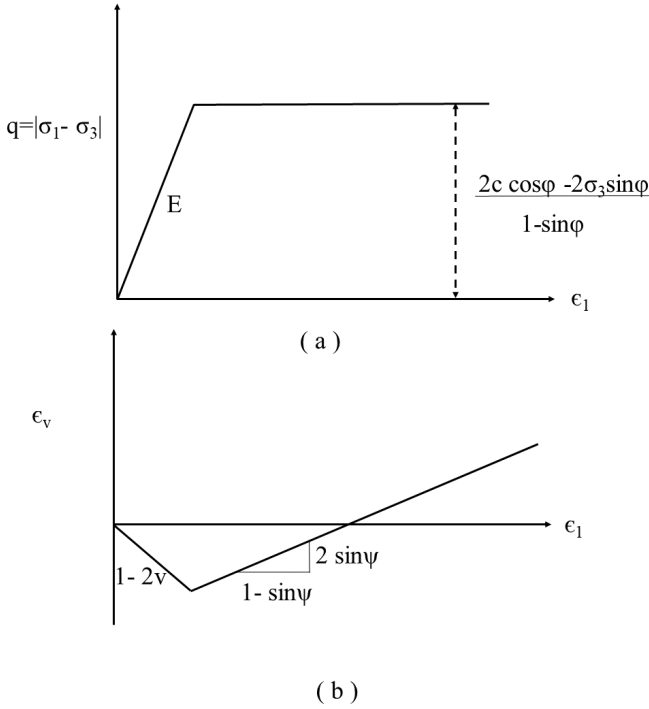


Figure 2.1: Representation of Mohr-Coulomb model

elled using E_{50} , the stress-dependent stiffness due to the primary loading.

$$E_{50} = E_{50}^{ref} \left(\frac{c \cos(\phi) - \sigma_3 \sin(\phi)}{c \cos(\phi) - p_{ref} \sin(\phi)} \right)^m, \quad (2.5)$$

where E_{50}^{ref} is the reference stiffness modulus corresponding to the reference stress p_{ref} . The actual stiffness depends upon the minor principal stress (σ_3). The amount of stress dependency is given by the power m .

The non-linear elastic part is modelled based upon the stress-dependent unloading reloading stiffness modulus:

$$E_{ur} = E_{ur}^{ref} \left(\frac{c \cos(\phi) - \sigma_3 \sin(\phi)}{c \cos(\phi) - p_{ref} \sin(\phi)} \right)^m, \quad (2.6)$$

where is E_{ur}^{ref} is the reference re/-unloading stiffness at reference pressure p_{ref} . The E_{ur} parameter is used to simulate the non-linear unloading reloading stress-strain path. The elastic components are calculated according to the Hookean elastic relationship for drained triaxial stress path:

$$\epsilon_1^e = \frac{q}{E_{ur}}. \quad (2.7)$$

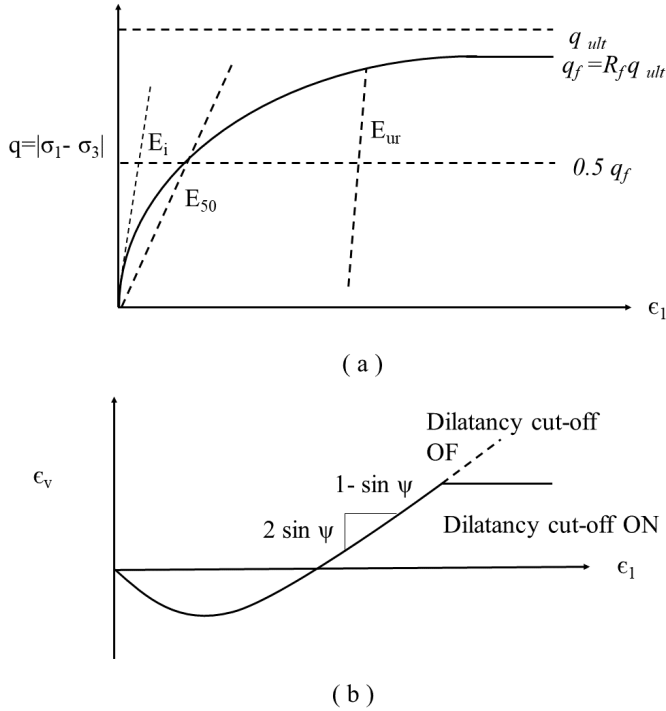


Figure 2.2: Representation of Hardening soil model

The HS model is a double-hardening plasticity model as it allows two types of hardening: shear hardening and cap hardening. The shear-hardening part controls the hyperbolic behaviour in deviatoric stress paths, and the cap-hardening part deals with irreversible compaction in primary compression. Due to the onset of loading, the material starts yielding as soon as the shear strength is mobilised. As a result, increased deviatoric plastic strain is generated as the loading increases, which apparently leads to a reduction of the stiffness. This is represented by the shear hardening yield function. At the end of shear strength mobilisation, when the Mohr-Coulomb failure criterion is reached, failure occurs. The flow rule for shear hardening is non-associated.

A cap yield surface is defined to compute the plastic volumetric strain that is measured in isotropic compression. This yield surface represents an ellipse in stress space and it is centred around the origin of the stress space. The preconsolidation pressure defines the current position of the cap. The cap parameters are evaluated from lateral pressure for normal consolidation, K_o^{nc} and E_{oed} :

$$E_{oed} = E_{oed}^{ref} \left(\frac{c \cos(\phi) - \sigma'_3 \sin(\phi)}{c \cos(\phi) - p_{ref} \sin(\phi)} \right)^m, \quad (2.8)$$

where E_{oed}^{ref} is the reference odometer stiffness at reference pressure p_{ref} .

The input parameters of the HS model are the strength parameters: cohesion (c), friction angle (ϕ) and dilatancy angle (ψ). The stiffness parameters are the secant stiffness at reference pressure in standard drained triaxial test (E_{50}^{ref}), the tangent stiffness at reference pressure for primary odometer loading (E_{oed}^{ref}), the loading unloading stiffness at reference pressure (E_{ur}^{ref}), the Poisson's ratio for unloading reloading (ν_{ur}) and a parameter m which controls the stress-level dependency for all three stiffness parameters.

FORWARD MODELLING AND STABILITY ANALYSIS

FEM simulations are used as a forward model, taking into account changes in external water loads. A hydro-mechanical FEM model computes the behaviour and state of the slope. After a defined period of time, the hydro-mechanical analysis is followed by the stability analysis, which results in an estimate of the FoS (the ratio of the original strength to the reduced strength of the material at failure). Slope stability is evaluated using Finite Element Method (FEM) with a strength reduction technique, conducted under drained conditions for relatively coarser material. The forward model calculates the results until the time when a stability analysis is required. After the stability analysis, the forward analysis resumes using the conditions immediately prior to the stability analysis. The calculated stability, therefore, can change over time reflecting the changes in hydro-mechanical conditions. In the stability analyses, the strength properties of the soil ($\tan(\phi)$ and c in both the constitutive models used here) are successively reduced until failure.

2.2.2. DATA ASSIMILATION WITH THE RECURSIVE ENSEMBLE KALMAN FILTER

Data assimilation has the objective to find the posterior distribution of a state and/or parameter given the measurements of the state. A commonly used method for data assimilation is the EnKF (Evensen, 1994) which is an ensemble-based formulation of the Kalman filter (Kalman, 1960), originally developed for state estimation in oceanography. The method uses an ensemble of model realisations to represent the error covariances. Since then, the EnKF has been implemented in diverse fields including numerical weather prediction (e.g. Houtekamer & Mitchell, 2005; Szunyogh et al., 2005), oceanography (e.g. Bertino et al., 2003; Keppenne & Rienecker, 2003), hydrology (e.g. Chen & Zhang, 2006; Reichle et al., 2002), geotechnical engineering (e.g. Liu et al., 2018; Mavritsakis, 2017; Vardon et al., 2016), and petroleum reservoir history matching (e.g. Aanonsen et al., 2009; Evensen, 2009; Glegola et al., 2012; Nævdal et al., 2002; Oliver & Chen, 2011).

The EnKF is very effective in state estimation (e.g. Evensen, 1997; Hamill et al., 2000; Houtekamer & Mitchell, 1998; Miller et al., 1999; Tamura et al., 2014) and joint parameter-state estimation (e.g. Lorentzen et al., 2001; Nævdal et al., 2003; Nævdal et al., 2002; Skjervheim & Evensen, 2011). In the case of parameter estimation, it is common to estimate the parameters first and then rerun the model with these updated estimates of the parameters to find the solution of the model state. The EnKF has been successfully applied for parameter estimation in applications in a range of fields. In the field of petroleum engineering, Nævdal et al. (2002) implemented the EnKF for history matching with a two dimensional near-well reservoir model to estimate the permeability of the

reservoir. The EnKF provided a better parameter estimation and consequently better production forecasts. In the field of atmospheric modelling, Annan et al. (2005) implemented the EnKF for estimation of parameters from radiation, convection and surface parametrisation. The authors concluded that the EnKF can handle multivariate parameter estimation comfortably and demonstrated the method to be useful in determining structural deficiencies in the model which can not be improved by tuning and can be a useful tool to guide model development. Skjervheim and Evensen (2011) applied the EnKF on a history matching problem to estimate the permeability parameter in a reservoir simulation model. It was concluded that the EnKF can be successfully used for history matching but is computationally more expensive than the Ensemble Smoother. A possible disadvantage of the EnKF is the Gaussian approximation applied in the update scheme. Furthermore, the repeated restarting of the forward model after each EnKF update needs a significant amount of computational effort, this recursive implementation of the EnKF ensures that the state is updated along with the parameters. Due to the good state, parameter and combined state-parameter estimation, relative computational efficiency and the continuous and close to Gaussian distribution (or distributions which could be transformed to Gaussian), the EnKF approach has been selected. Moreover, the approach is consistent with earlier work by Vardon et al. (2016) and the present study can be seen as an extension of that work. In the present study, the recursive EnKF is implemented to estimate poorly known parameters in a hydro-mechanical slope-stability forward model.

To formulate the principles of data assimilation, it is assumed that the model output at the measurement location \mathbf{y} is obtained by running the forward model with input model parameters $\boldsymbol{\theta}$ and mapping the outcome to measurement space. This can be represented by the operator g in the following equation:

$$\mathbf{y} = g(\mathbf{z}), \tag{2.9}$$

in which

$$\mathbf{z} = (\mathbf{x} \quad \boldsymbol{\theta})^T \tag{2.10}$$

where $\mathbf{y} \in \mathbb{R}^{N_m}$ is a vector of model output at measurement locations, $\mathbf{z} \in \mathbb{R}^{N_x+N_\theta}$ is a combined state-parameter vector, *i.e.*, a vector of model state $\mathbf{x} \in \mathbb{R}^{N_x}$ and model parameters $\boldsymbol{\theta} \in \mathbb{R}^{N_\theta}$ and g is the model operator which maps the prior state-parameter vector into measurement space. In this study, the model is considered to be perfect and model uncertainty is implicitly taken into account within the parameter uncertainty. Here, N_m is the number of measurements, N_x is the number of state points and N_θ is the number of parameters.

A forward model run provides a prediction of the model state evolution for a unique set of values of the uncertain parameters. If the model has no errors, the model output can be seen as a prediction (\mathbf{y}) of the ‘truth’. The measurements are the window to this actual state, and contain errors:

$$\mathbf{d} = \mathbf{y} + \mathbf{e}, \tag{2.11}$$

where $\mathbf{d} \in \mathbb{R}^{N_m}$ is a vector of the measurements with N_m being the number of measurements. The errors $\mathbf{e} \in \mathbb{R}^{N_m}$ include measurement errors and representation errors. In this study, measurement errors are assumed to be normally distributed with zero mean. The

distribution of the state-parameter vector \mathbf{z} is assumed to also be normally distributed around a known mean.

Bayes' theorem gives the joint probability (f) for \mathbf{z} and \mathbf{y} given the measurements \mathbf{d} as:

$$f(\mathbf{z}, \mathbf{y}|\mathbf{d}) \propto f(\mathbf{d}|\mathbf{y})f(\mathbf{y}|\mathbf{z})f(\mathbf{z}). \quad (2.12)$$

From Eq. 2.12, the posterior probability for \mathbf{z} given \mathbf{d} can be written as:

$$f(\mathbf{z}|\mathbf{d}) \propto \int f(\mathbf{d}|\mathbf{y})f(\mathbf{y}|\mathbf{z})f(\mathbf{z})d\mathbf{y} = f(\mathbf{d}|\mathbf{g}(\mathbf{z}))f(\mathbf{z}). \quad (2.13)$$

Making use of the assumption that the priors have a Gaussian distribution, Eq. 2.13 can be written as:

$$f(\mathbf{z}|\mathbf{d}) \propto \exp\{-\frac{1}{2}J\}. \quad (2.14)$$

The cost function J is defined as follows:

$$J(\mathbf{z}) = (\mathbf{z} - \mathbf{z}^f)^T \mathbf{C}_{zz}^{-1} (\mathbf{z} - \mathbf{z}^f) + (\mathbf{g}(\mathbf{z}) - \mathbf{d})^T \mathbf{C}_{dd}^{-1} (\mathbf{g}(\mathbf{z}) - \mathbf{d}), \quad (2.15)$$

where \mathbf{z}^f is the prior estimate of \mathbf{z} , $\mathbf{C}_{zz} \in \mathbb{R}^{(N_x + N_\theta) \times (N_x + N_\theta)}$ is the error covariance of \mathbf{z}^f , and $\mathbf{C}_{dd} \in \mathbb{R}^{N_m \times N_m}$ is the error covariance of measurements. It can be shown that for normally distributed variables, the maximum likelihood estimate of $f(\mathbf{z}|\mathbf{d})$ is equivalent to minimising the cost function J in Eq. 3.8. In case of an operator $\mathbf{g}(\mathbf{z})$ that can be approximated with a linear operator \mathbf{G} that relates the output to the parameters and state via $\mathbf{y} = \mathbf{G}\mathbf{z}$, minimising the cost function gives the following solution, known as the Kalman filter (Kalman, 1960):

$$\mathbf{z}^a = \mathbf{z}^f + \mathbf{K}(\mathbf{d} - \mathbf{g}(\mathbf{z})), \quad (2.16)$$

$$\mathbf{C}_{zz}^a = (\mathbf{I} - \mathbf{K}\mathbf{G})\mathbf{C}_{zz}, \quad (2.17)$$

and

$$\mathbf{K} = \mathbf{C}_{zz}\mathbf{G}(\mathbf{G}\mathbf{C}_{zz}\mathbf{G}^T - \mathbf{C}_{zz})^{-1}, \quad (2.18)$$

where \mathbf{K} is the Kalman gain, superscript "a" shows the analysis and superscript "f" represents the prior estimate.

In the EnKF, an ensemble of forward model simulations is used to approximate the error covariance \mathbf{C}_{zz} . The Kalman equation for each ensemble member $i \in N_e$ can be written as:

$$\mathbf{z}_i^a = \mathbf{z}_i^f + \mathbf{K}^e(\mathbf{d}_i - \mathbf{g}(\mathbf{z}_i^f)), \quad (2.19)$$

and

$$\mathbf{K}^e = \mathbf{C}_{zz}^e\mathbf{G}(\mathbf{G}\mathbf{C}_{zz}^e\mathbf{G}^T - \mathbf{C}_{dd})^{-1}, \quad (2.20)$$

where \mathbf{C}_{zz}^e is the combined state-parameter error covariance matrix. Here

$$\mathbf{d}_i = \mathbf{d} + \boldsymbol{\epsilon}_i \quad (2.21)$$

represents the perturbed measurements for each i th member, with $\boldsymbol{\epsilon}_i$ having the same distribution as the measurement errors $\boldsymbol{\epsilon}$ in Eq. 3.7, following the approach of (Burgers et al., 1998).

Consider the matrix $\mathbf{Z}_t^f \in \mathbb{R}^{(N_x+N_\theta) \times N_e}$ containing N_e realisations of \mathbf{z} at time t :

$$\mathbf{Z}_t^f = (\mathbf{z}_1^f, \mathbf{z}_2^f, \dots, \mathbf{z}_{N_e}^f) \quad (2.22)$$

The ensemble mean is then stored in each column of $\bar{\mathbf{Z}}_t^f \in \mathbb{R}^{(N_x+N_\theta) \times N_e}$:

$$\bar{\mathbf{Z}}_t^f = \mathbf{Z}_t^f \mathbf{I}_{N_e}, \quad (2.23)$$

where $\mathbf{I}_{N_e} \in \mathbb{R}^{N_e \times N_e}$ is a matrix with each element equal to $\frac{1}{N_e}$. The ensemble perturbation matrix $\mathbf{Z}'_t \in \mathbb{R}^{(N_x+N_\theta) \times N_e}$ is now defined as follows:

$$\mathbf{Z}'_t = \mathbf{Z}_t^f - \bar{\mathbf{Z}}_t^f \quad (2.24)$$

The combined state-parameter error covariance matrix $\mathbf{C}_{zz}^e \in \mathbb{R}^{(N_x+N_\theta) \times (N_x+N_\theta)}$ can be written as follows:

$$\mathbf{C}_{zz}^e = \frac{\mathbf{Z}'_t (\mathbf{Z}'_t)^T}{N_e - 1}, \quad (2.25)$$

where \mathbf{C}_{zz}^e consists of the state and parameter error covariances as well as the cross-covariances between state and parameters.

At assimilation time step t , the available measurements are stored in vector \mathbf{d}_t . For each ensemble member i , this measurement vector is perturbed with $\boldsymbol{\epsilon}_i$ as in Eq. 3.10. The vectors $\mathbf{d}_{i,t}$ are then stored in matrix $\mathbf{D}_t \in \mathbb{R}^{N_m \times N_e}$:

$$\mathbf{D}_t = (\mathbf{d}_{1,t}, \mathbf{d}_{2,t}, \dots, \mathbf{d}_{N_e,t}). \quad (2.26)$$

With these matrices, the analysis equation at time t becomes:

$$\mathbf{Z}_t^a = \mathbf{Z}_t^f + \mathbf{C}_{zz}^e \mathbf{G}^T (\mathbf{G} \mathbf{C}_{zz}^e \mathbf{G}^T + \mathbf{C}_{dd})^{-1} (\mathbf{D}_t - \mathbf{G} \mathbf{Z}_t^f), \quad (2.27)$$

where $\mathbf{G} \in \mathbb{R}^{N_e \times (N_x+N_\theta)}$ is the linear measurement operator which relates the state-parameter matrix to measurement space.

2.2.3. IMPLEMENTATION OF THE DATA ASSIMILATION FOR THE SLOPE-STABILITY PROBLEM

In this study, the EnKF described in Section 2.2.2 is implemented with the forward model of Section 2.2.1. The resulting model for the hydro-mechanical behaviour of given slope geometry is then used to estimate the state (\mathbf{x}), parameters ($\boldsymbol{\theta}$) and eventually the FoS. The state in the case of this setup, could be displacements of the sloping surface, or observed strain. Parameters would represent the material properties in the hydro-mechanical model simulation and could be for example the parameters of stiffness and strength, E/E_{50}^{ref} , c' and ϕ' . The selection of state and parameters to estimate this particular study will be discussed in Section 2.3. The setup of the numerical approach is illustrated in Fig. 2.3.

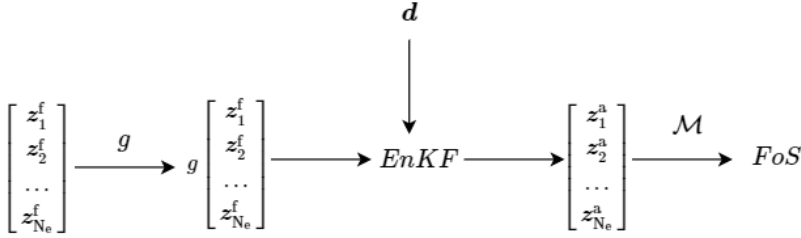


Figure 2.3: Setup of the data assimilation and forward model, where $\begin{bmatrix} z_1^f & z_2^f & \dots & z_{N_e}^f \end{bmatrix}^T$ is the ensemble of prior state-parameter estimates; g is the model operator; $EnKF$ represents the data assimilation (recursive EnKF); \mathbf{d} is the measurement vector; $\begin{bmatrix} z_1^a & z_2^a & \dots & z_{N_e}^a \end{bmatrix}^T$ is the ensemble of posterior state-parameter estimates; and \mathcal{M} is the FoS calculation

At $t = 0$, the numerical approach starts with a set of prior ensemble members which represent our prior assumption of the state (\mathbf{x}) and parameters ($\boldsymbol{\theta}$). In our case, these model parameters ($\boldsymbol{\theta}$) are sampled from a normal distribution with a prior mean and standard deviation for each of the parameters in $\boldsymbol{\theta}$:

$$f(\boldsymbol{\theta}) = \mathcal{N}(\boldsymbol{\theta}^f, \mathbf{C}_{\boldsymbol{\theta}\boldsymbol{\theta}}) \quad (2.28)$$

Based on the prior assumptions on parameters, the forward model is run from $t = 0$ to $t = t_{assim}$. The synthetic measurements at $t = t_{assim}$ are assimilated to estimate model parameters ($\hat{\boldsymbol{\theta}}$) and state variable ($\hat{\mathbf{x}}$), defined as the expected value of the posterior distribution. In the synthetic experiment, the modelled field measurements are sampled from the vector \mathbf{z} by means of the operator \mathbf{G} which maps the state-parameter space to the measurement space. As \mathbf{G} in this case combines the forward model operator with an interpolation of the model variables to the location of the measurements at the slope, the interpolation in \mathbf{G} has the form of $[\mathbf{I}|\mathbf{0}]$ which has "1" only at specified locations. $\mathbf{C}_{\mathbf{d}\mathbf{d}} \in \mathbb{R}^{N_m \times N_m}$ in Eq. 2.27 is in this case a matrix with all the diagonal elements equal to the variance of the measurement device. After each EnKF update, the forward model is rerun from $t = 0$ to next assimilation step to keep the model state consistent with the parameter estimates of the previous step. The measurements at the next assimilation step are assimilated to update the model state and parameter estimates. In this way, the data is assimilated for all the time steps. The resulting posterior ensemble of state- and parameter estimates is then used for the calculation of the FoS.

2.3. SYNTHETIC TWIN EXPERIMENT

A synthetic twin experiment is a common approach to evaluate the performance of data assimilation methods. In this experiment, synthetic measurements are generated from a synthetic "truth" data-set, which mimics the observed reality. The data assimilation should reconstruct this "truth" within the assumed accuracy of the measurements. The "truth" is the output from a specific simulation of the forward model with a certain initial state and specified model parameters, typically different from the mean of the prior distribution of the state and parameter estimates of the ensemble used in the data assimilation. By sampling measurements of the "true" state from the output of the simulation

and after adding realistic noise, synthetic measurements are obtained. The concept of a synthetic twin experiment is illustrated in Fig. 2.4. An idealised slope has been consid-

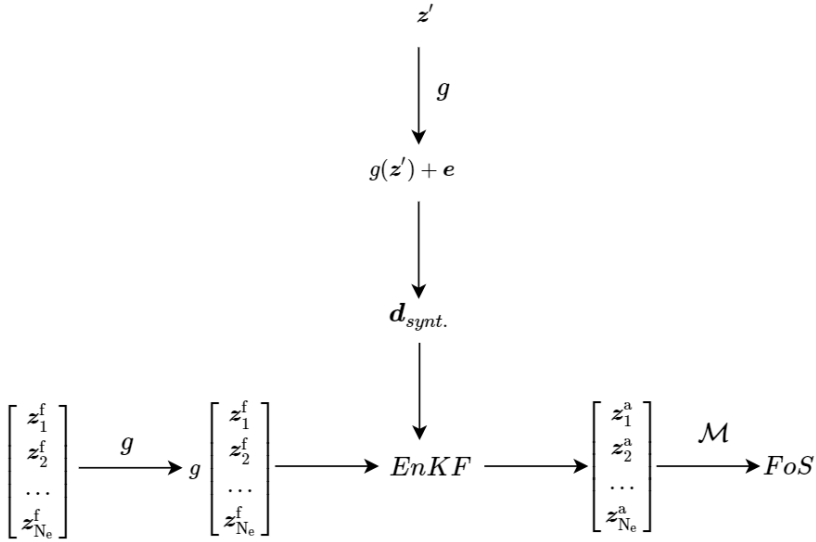


Figure 2.4: Setup of the data assimilation and forward model in a synthetic twin experiment, where z' is the state-parameter vector used to create synthetic observations; e is normally distributed measurement noise; $d_{synt.}$ is the vector containing synthetic measurements; For all other symbols, please see Fig. 2.3.

ered to illustrate and test the approach. The geometry of the slope is shown in Fig. 2.5. The initial stress state of the slope system is calculated by using gravity loading and the initial pore-water pressure distribution is calculated assuming steady-state groundwater flow considering the water level CD . Above the line CD , the degree of saturation is determined by the soil water retention curve. This hydraulic behaviour of the unsaturated soil is modelled by the model of Van Genuchten (1980). Following the initial stress state, the slope experiences a water level fluctuation of the line CD , which is included via a variable hydraulic boundary condition. The water level fluctuation has been simulated by applying $D_w = 12 - (\sin t + \sin 3t)$, where t is the time in days and D_w is the water level in meters from the bottom of the slope (see Fig. 2.6). The change of hydraulic loading are the only cause of deformations and are obtained from the fully coupled hydro-mechanical analysis. Synthetic measurements are obtained by sampling the model output of horizontal displacements (u_x) at the sloping face (along the line ACB) and adding realistic noise to mimic geodetic measurements. For this study, synthetic measurements are sampled at the peaks and troughs of D_w and at regular intervals of 200 days (see red arrows in Fig. 2.6). These synthetic measurements are assimilated after 200, 400, 600, 800, 1000, 1200, 1400, 1600, 1800 and 2000 days.

Both the MC and HS models are used in separate analyses to test their influence on the results. The stiffness and (effective) strength parameters are decided to be estimated simultaneously, as plasticity (although no full plastic mechanism) can occur prior to failure. This allows both the serviceability limit state and ultimate limit state (slope reliabil-

ity) to be investigated. To decide which parameters to estimate in the data assimilation, an average sensitivity score ($AvSS$) is calculated to study the effect of model parameters (E/E_{50}^{ref} , c' and ϕ') on the horizontal nodal displacements at the slope. First, the sensitivity score (SS) for each parameter i is calculated by:

$$SS_i = \frac{100|F(\theta_{i,max}) - F(\theta_{i,min})|}{\sum_{j=1}^n |F(\theta_{j,max}) - F(\theta_{j,min})|} \quad (2.29)$$

where θ_i is a certain parameter (E/E_{50}^{ref} , c' or ϕ'). The SS gives the parameter's sensitivity, $F(\theta_{i,max})$ is the model output (in our case horizontal nodal displacement at sloping face) when $\theta_i = \theta_{i,max}$, $F(\theta_{i,min})$ is the model output when $\theta_i = \theta_{i,min}$ and n is the total number of parameters varied to study the sensitivity. While studying the sensitivity of a specific parameters the other parameters are kept constant. The $AvSS$ is calculated by averaging the SS for all time steps. The parameter variation and $AvSS$ can be seen in Table 2.1. It can be concluded from Table 2.1 that in the case of the MC model E and ϕ' and, in the case of HS model E_{50}^{ref} and ϕ' are the parameters which have the highest sensitivity. Hence, these parameters are selected to be estimated in this study. This means that $\theta = (E \ \phi')^T$ in the MC case and $\theta = (E_{50}^{ref} \ \phi')^T$ in the HS case. As the E_{50}^{ref} is varied/updated, E_{oed}^{ref} and E_{ur}^{ref} are also varied with a specified relationship, i.e. $E_{oed}^{ref} = E_{50}^{ref}$ and $E_{ur}^{ref} = 3E_{50}^{ref}$. The state variable (\mathbf{x}) for both cases is horizontal nodal displacements (\mathbf{u}_x).

Table 2.1: Parameter variation and average sensitivity score ($AvSS$) for MC and HS

	Parameter variations			AvSS (%)	
	E/E_{50}^{ref} (kPa)	ϕ' ($^\circ$)	c' (kPa)	MC	HS
$\theta_{E/E_{50}^{ref},min} = 10000, \theta_{E/E_{50}^{ref},max} = 40000$		27	10	45.44	37.62
30000	$\theta_{\phi,min} = 20, \theta_{\phi,max} = 35$		10	42.77	48.53
30000	27	$\theta_{c,min} = 5, \theta_{c,max} = 15$		11.78	13.84

The input model parameters for the synthetic measurements are shown in Table 2.2, which result in an initial factor of safety of 1.50 for both models representing the synthetic “truth”. To evaluate the two constitutive models, two separate numerical experiments are selected for each model: a close-to-failure and a far-from-failure prior parameter estimation. The synthetic measurements in both experiments are identical, but the prior ensemble of the synthetic close-to-failure case has a mean factor of safety of close to 1.0 while the prior ensemble of the synthetic far-from-failure case has a mean factor of safety of close to 2.0. The input model parameters for prior parameter estimation are shown in Table 2.3. The model parameters to be estimated, i.e., the stiffness (E or E_{50}^{ref}) and the strength (ϕ') parameters, are sampled from their prior distributions to form the prior model ensemble.

A fully coupled hydro-mechanical analysis is conducted from $t = 0 - 200$ days for each ensemble member. The horizontal nodal displacement vector (\mathbf{u}_x) is stored in a forecast matrix (see Eq. 2.22) for each ensemble member. Then, available synthetic measurements of horizontal nodal displacement at $t = 200$ days are assimilated by using the

recursive EnKF. The output of the EnKF provides a new estimation of the E/E_{50}^{ref} and ϕ' for each ensemble member as well as the model state. The model parameters (E/E_{50}^{ref} and ϕ') are then used in the fully coupled hydro-mechanical analysis from the initial stage ($t = 0$) until the time of the next available measurements ($t = 400$ days). These measurements are then assimilated to update the estimates of model parameters. This process is repeated until all data has been assimilated.

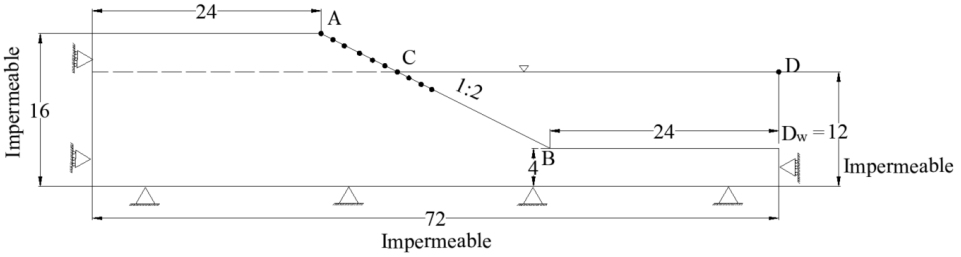


Figure 2.5: Geometry of the slope (dimensions in m) and black circles represents the measurement points

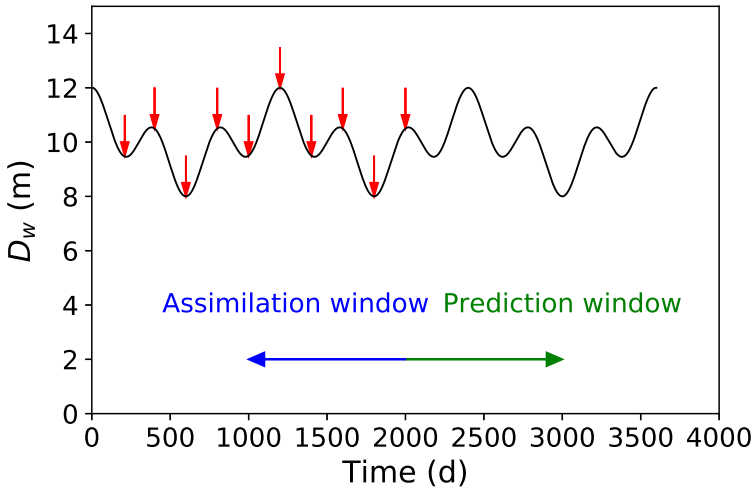


Figure 2.6: Fluctuation of the water (D_w) level in CD. The red arrows represent the assimilation points

The data is assimilated for the first 2000 days after which the forward model provides an estimate of horizontal displacement and FoS for the period from 2000 days to 3600 days. The setup uses fifty ensemble members for the comparison of the two constitutive models. The ensemble size, the number of measurements and simulated measurement error are based on sensitivity analyses (Appendices A.1.1 to A.1.3).

Table 2.2: “Truth” model parameters for MC and HS

Parameters	Truth model parameters		Unit
	MC	HS	
Effective friction angle (ϕ')	25	25	$^\circ$
Effective cohesion (c')	10	10	kPa
Dilatancy angle (ψ)	0	0	$^\circ$
Young's modulus (E)	20000	-	kPa
E_{50}^{ref}	-	20000	kPa
E_{oed}^{ref}	-	E_{50}^{ref}	kPa
E_{ur}^{ref}	-	$3E_{50}^{ref}$	kPa
Poisson's ratio (ν)	0.3	-	-
Poisson's ratio for unloading/reloading (ν_{ur})	-	0.2	-
Power (m)	-	0.5	-
Unsaturated unit weight (γ_d)	19	19	kN/m ³
Saturated unit weight (γ_s)	20	20	kN/m ³
Hydraulic conductivity ($k_x = k_y$)	1.0	1.0	m/day
VGM parameter (g_a)	3.83	3.83	m^{-1}
VGM parameter (g_n)	1.3774	1.3774	-
VGM parameter (g_l)	1.25	1.25	-
Saturated volumetric water content (θ_s)	0.403	0.403	-
Residual volumetric water content (θ_r)	0.025	0.025	-

*Note: VGM stands for Van Genuchten model and the properties are taken from Wösten et al. (1999).

Table 2.3: Initial estimation of model parameters for MC and HS

Parameters	Close-to-failure case	Far-from-failure case	Distribution	Unit
Effective friction angle(ϕ')	$\mu = 20, \sigma = 3$ (both)	$\mu = 35, \sigma = 2$ (both)	Normal	$^\circ$
Young's modulus(E)	$\mu = 25000, \sigma = 5000$ (MC)	$\mu = 25000, \sigma = 5000$ (MC)	Normal	kPa
E_{50}^{ref}	$\mu = 25000, \sigma = 5000$ (HS)	$\mu = 25000, \sigma = 5000$ (HS)	Normal	kPa

2.4. RESULTS OF THE DATA ASSIMILATION

2.4.1. DISPLACEMENT ESTIMATES

In this section, the posterior horizontal nodal displacement (\mathbf{u}_x) estimates based on the prior and estimated parameters are presented. Fig. 2.7 shows the prior and posterior ensemble of horizontal nodal displacement at point A (see Fig. 2.5) for the four different cases. This data is one of the measurements used for the data assimilation. The blue lines represent the ensemble prediction of horizontal nodal displacement at point A based on the prior ensemble of parameters (see Table 2.3), with the heavy blue line representing the mean. The red lines show the ensemble prediction based on the estimated parameters at 2000 days. The green stars are the synthetic measurements at point A for different time steps. The time period is divided into an assimilation and a prediction window. The

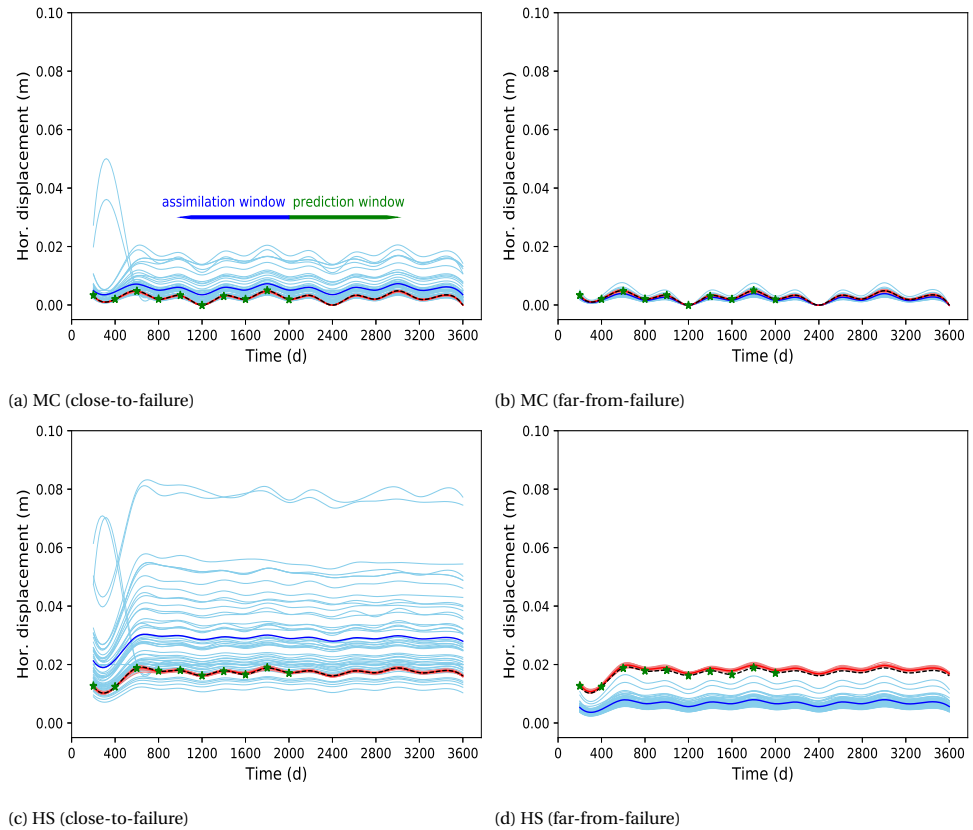


Figure 2.7: Ensemble prediction of the horizontal displacement based on (i) the prior ensemble of parameters (blue lines) and (ii) estimated parameters at 2000 days, after all data have been assimilated (red lines). Green stars represent the measurements in assimilation window and the black dashed line represents the true displacement at point A of the slope.

black dashed line represents the true displacement at point A.

The results of horizontal nodal displacement show a sinusoidal behavior, due to the variable hydraulic boundary conditions. Overall, the spread of the horizontal nodal displacement of the prior ensemble (shown in blue lines) is larger than that of the estimated ensemble parameters at 2000 days (shown in red lines) in all cases. By comparing the results of close-to-failure case for the MC and the HS models, it can be seen that displacement of the HS model analysis (Fig. 2.7c) is larger than the displacement from the MC model analysis (Fig. 2.7a). This is due to the stress-dependent stiffness in the prior HS ensemble. Due to an increase in loading, the stiffness reduces and shear strength starts mobilizing results in the larger displacements. On the other hand, this is not the case in the MC ensemble which has single stress-independent stiffness parameter and perfect plasticity develops at failure. The spread in the prior distribution of the ensemble displacement is also larger for the HS model than for the MC model.

In the far-from-failure case, the analysis shows that the model produces a smaller displacement than in the close-to-failure case (see Figs. 2.7a and 2.7b or Figs. 2.7c and 2.7d). This is because the strength properties are higher in far-from-failure, and therefore plastic deformation is very limited.

2.4.2. MATERIAL PARAMETER ESTIMATES

In this section, the estimation of poorly known parameters are presented at different time steps. Fig. 2.8 shows the true stiffness (E/E_{50}^{ref}) parameters, the initial distribution of stiffness (E/E_{50}^{ref}) parameters and the estimated stiffness (E/E_{50}^{ref}) parameters after 1000 days and 2000 days for the close-to-failure case. The mean posterior estimate of the stiffness (E/E_{50}^{ref}) approaches the true stiffness and its posterior variance reduces with each assimilation step. At 1000 days, the estimated stiffness (E) mean and standard deviation for MC case is $\mu_E = 20663$ and $\sigma_E = 1642$. In case of the HS model, the mean and standard deviation of stiffness (E_{50}^{ref}) at 1000 days is $\mu_{E_{50}^{ref}} = 19874$ and $\sigma_{E_{50}^{ref}} = 1363$. At 2000 days, the estimated mean stiffness and standard deviations for the MC and the HS model simulations are $\mu_E = 20565$ and $\sigma_E = 655$ and $\mu_{E_{50}^{ref}} = 19572$ and $\sigma_{E_{50}^{ref}} = 1053$, respectively. Fig. 2.9 shows that effective strength parameter (ϕ') for both models improves substantially during the first 1000 days, and changes less after that. The response of both models is similar for close-to-failure case.

Figs. 2.10 and 2.11 show the parameter estimation for far-from-failure case. Fig. 2.10 shows that the mean of the stiffness parameters (E/E_{50}^{ref}) also approaches towards the true stiffness and shows the similar trend as of close-to-failure case for both the MC and the HS model. Fig. 2.11 shows the initial and estimated effective strength parameter (ϕ') at 1000 days and 2000 days. The effective strength parameter (ϕ') does not improve in the case of MC model. However, the effective strength parameter (ϕ') significantly improves in estimates of the HS model and the posterior ensemble mean approaches the true solution. The effectiveness of the data assimilation is likely related to the dependence of the stiffness E_{50}^{ref} to the effective strength parameter (ϕ') as well as the dependence of horizontal nodal displacement to stiffness and strength parameters at all stages in the HS model, whereas there is no dependence between these parameters in the MC model. In HS model, as the ϕ' is varied/updated the curvature of the stress-strain curve changes which affects the stiffness response of material. In the MC model far-from-failure case, only very limited plasticity occurs in the ensemble members, leading to a negligible (or zero) cross-correlation between the effective strength parameter (ϕ') and horizontal nodal displacement (u_x) in the covariance matrix (see Eq. 2.25).

2.4.3. FACTOR OF SAFETY

The ultimate objective of this study is to improve the estimate of the FoS making use of available measurements of slope deformation. Figs. 2.12 and 2.13 show the FoS distributions for the two models at 2000 days with the prior parameters and the parameters estimated using data until 1000 and 2000 days. In the close-to-failure case (see Fig. 2.12), the FoS estimated from the model simulation with the prior parameters has a distribution with mean (μ_{FoS}) = 1.26 and standard deviation (σ_{FoS}) = 0.327. With parameters es-

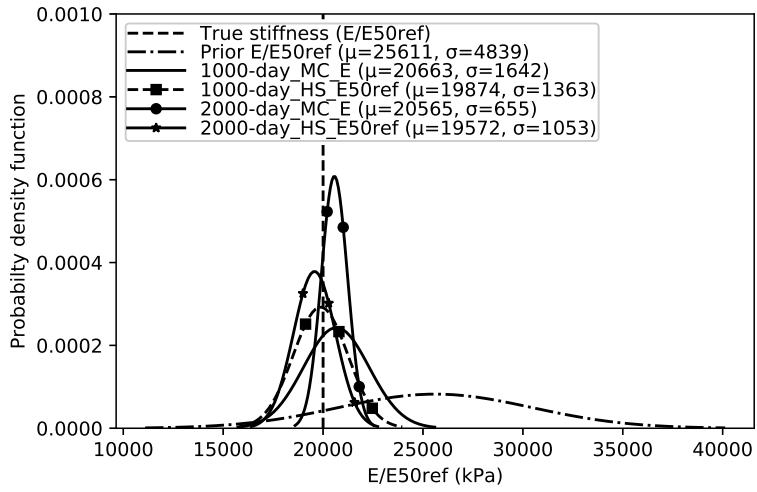


Figure 2.8: Estimation of stiffness parameter for the MC and HS soil models at $t=1000$ and $t=2000$ days (close-to-failure)

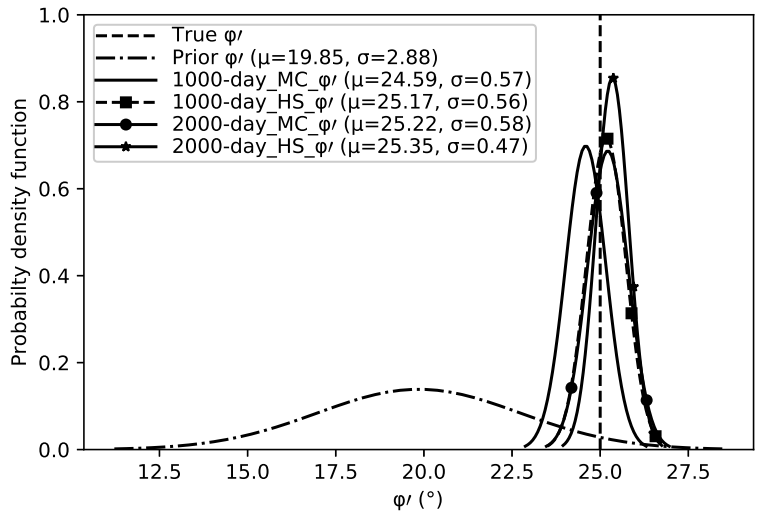


Figure 2.9: Estimation of friction angle for the MC and HS soils model at $t=1000$ and $t=2000$ days. Two curves (1000-day_HS_ ϕ' and 2000-day_MC_ ϕ') are overlapping in this figure (close-to-failure).

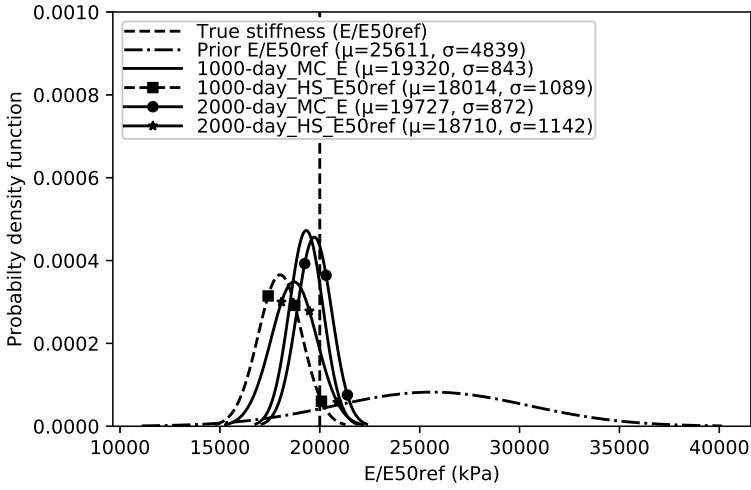


Figure 2.10: Estimation of stiffness for the MC and HS soil models at $t=1000$ and $t=2000$ days (far-from-failure).

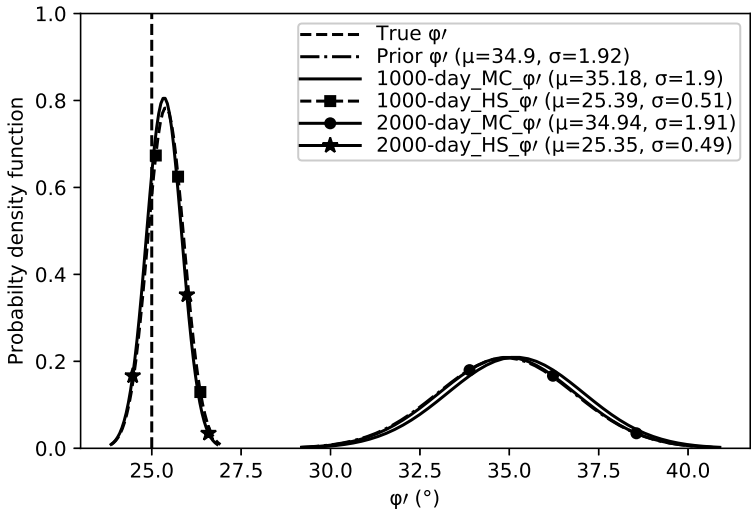


Figure 2.11: Estimation of friction angle for the MC and HS soil models at $t=1000$ and $t=2000$ days. Two curves (1000-day_HS_φ' and 2000-day_HS_φ') are overlapping on the left side and three curves (Prior φ', 1000-day_MC_φ' and 2000-day_MC_φ') are overlapping on the right side of figure (far-from-failure).

timated at 1000 days and 2000 days, only very limited differences are observed between the factors of safety as calculated using the two constitutive models. Both models show a substantial effect of the data assimilation on the FoS estimate, giving a better approximation of the true FoS, and resulting in a posterior FoS estimate with a small variance. Often slopes are required to be assessed against a target reliability, and a narrower distribution of FoS suggests a higher reliability. This will likely have a positive effect on the assessment of this FoS against a target reliability. In the far-from-failure case, similar behaviour of the FoS estimation is observed as in the case of the estimation of the strength parameter (ϕ') in Section 2.4.2, *i.e.*, the MC model results are substantially unaffected by the data assimilation, remain far from the truth and have a broader distribution of the posterior estimate of the FoS. As a consequence, in the far-from-failure case, the slope reliability of the MC model does not appear to be realistic, despite of the assimilation of measurements of displacement.

To demonstrate the behaviour of the models during the prediction window, the factor of safety is plotted at 3000 days in Fig. 2.14 for the close-to-failure case for both material models. It can be seen that the posterior estimate of the factor of safety remains stable throughout the prediction window. This is not surprising, considering the stable behaviour of the simulations during this time (Fig. 2.7) and the fact that there are no temporal material behaviour or geometry changes in the model.

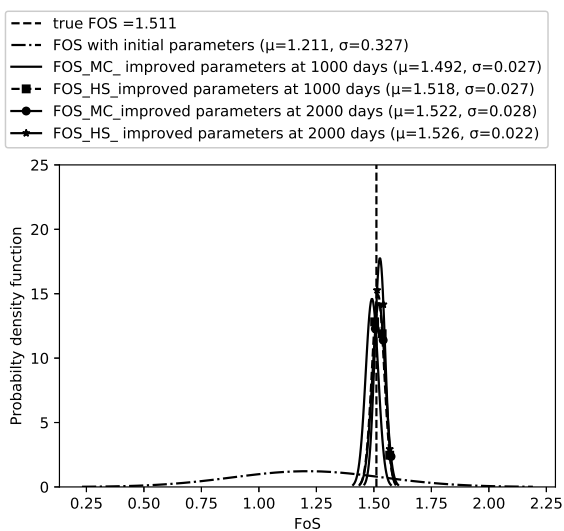


Figure 2.12: Probability distribution of factor of safety at 2000 days based on the prior and estimated parameters at 1000 and 2000 days (close-to-failure).

2.5. DISCUSSION

The above analyses reveal a number of key points regarding the use of data assimilation in geotechnical analyses. For most realistic slopes ($FoS < \approx 3$), the results suggest that

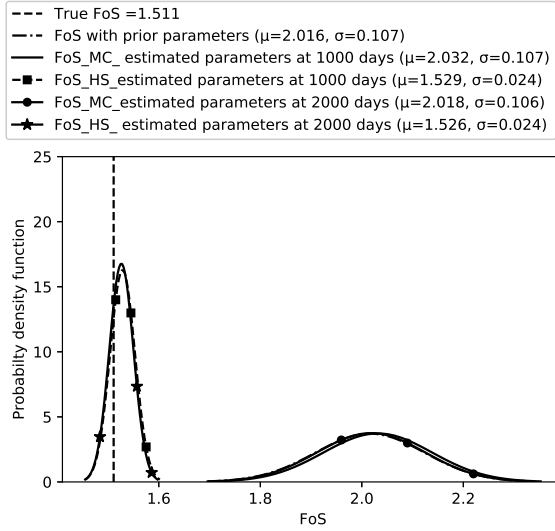


Figure 2.13: Probability distribution of factor of safety at 2000 days based on the prior and estimated parameters at 1000 and 2000 days. Two curves (FoS_HS_estimated parameters at 1000 days and FoS_HS_estimated parameters at 2000 days) are overlapping on the left side and three curves (FoS with prior parameters, FoS_MC_estimated parameters at 1000 days and FoS_MC_estimated parameters at 2000 days) are overlapping on the right side of the figure (far-from-failure).

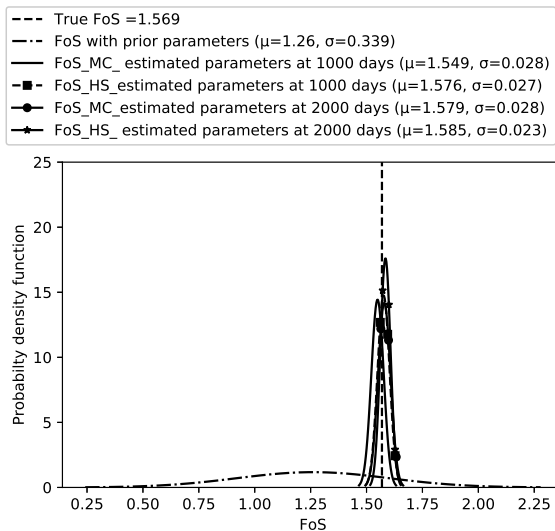


Figure 2.14: Probability distribution of factor of safety at 3000 days based on the prior and estimated parameters at 1000 and 2000 days (close-to-failure).

there is scope with relatively limited stress perturbations to improve reliability estimations using displacement measurements.

With the MC model, the most commonly used geotechnical material model, horizontal displacement has no dependence on the strength parameters in the elastic region, this means that these parameters have dependence only if sufficient plasticity is occurring, *i.e.*, in the close-to-failure case. A good estimate of the prior ensemble is needed for this material model, given that there needs to be a dependence on the displacement and the strength properties, in the representation of the model error covariance of the assimilation scheme (Eq. 2.25). In contrast, the HS model has a dependence of the elasto-plastic behaviour on the strength parameters (Eqs. 2.5, 2.6, 2.8), which means that even with a prior estimation that is less accurate, the data assimilation will be effective. Moreover, there is dependence of ϕ' on the curvature of stress-strain curve in HS model which helps to adjust the material behavior in the data assimilation update scheme. This result stresses the importance of choosing a constitutive model for data assimilation which is able to characterise the typical interplay between strength (as represented by the friction angle parameter) and stiffness.

It can also be seen that the number of measurements and number of ensemble members is able to be lower for the HS model (Appendices A.1.1 and A.1.3). This may be counter-intuitive, given that it is more complex and resembles more realistic geotechnical behaviour, however this is likely due to the stronger correlation between the strength and stiffness parameters in the HS model. Both of these effects will have the impact of reducing computational effort of the analyses, which will be significant in more complex analyses.

The notion that, especially in the case of the HS model, the assimilation of measurements of displacement leads to more realistic estimates of the strength and stiffness parameters and the associated nodal displacement in the slope, already after a small number of assimilation steps, suggests that the use of data assimilation techniques for slope-reliability estimates are promising. It should be noted though, that this study describes a synthetic case only, and assumed values of measurement errors have optimistic values. A more realistic configuration with more realistic model properties will require further study. Specifically, the spatial variability of materials within the slope has not been taken into account, and it is thought that this will have an impact, in particular on the required number of measurement points. Moreover, the temporal sampling of the measurements in this study has been regular and beneficial for the reconstruction of the temporal variations of the deformation. Additional research would be required to investigate the performance of the data assimilation setup under different measurement conditions.

Key limitations of this approach (EnKF) include (i) the Gaussian approximation in the update scheme, which means that the EnKF is difficult to implement on non-Gaussian problems; (ii) the recursive nature of the recursive EnKF, which results in restarting realizations after each parameter update step, which can be computationally expensive. It is noted that specific computation implementation characteristics, especially when using software that was not designed for this approach, can have a significant impact on computational performance.

2.6. CONCLUSION

The influence of two different constitutive models on factor of safety is studied by using data assimilation with the recursive ensemble Kalman filter in a slope stability model. In a synthetic twin experiment that mimics a slope geometry and assimilates synthetic measurements of slope deformation into a hydro-mechanical model, the use of the Mohr-Coulomb and the Hardening Soil models is tested. The HS model is seen to estimate the factor of safety with a narrow posterior distribution, starting from a wide prior distribution of material parameters, including those not encompassing the actual parameters. For this calculation, the HS model requires less computational effort than the MC model for similar or even more accurate estimates of horizontal displacement. The results suggest that constitutive models which include a smooth transition between elastic and plastic zones are more effective in data assimilation schemes than those in which the relation between stiffness and strength parameters is absent. When choosing a constitutive model that captures these relations, the results of this study suggest that the use of data assimilation techniques for slope-reliability estimates offers the opportunity to improve slope-reliability estimates with relatively limited stress perturbations.

REFERENCES

- Aanonsen, S. I., Nævdal, G., Oliver, D. S., Reynolds, A. C., & Vallès, B. (2009). The ensemble Kalman filter in reservoir engineering—a review. *SPE Journal*, 14(3), 393–412. <https://doi.org/10.2118/117274-PA>
- Annan, J., Hargreaves, J., Edwards, N., & Marsh, R. (2005). Parameter estimation in an intermediate complexity earth system model using an ensemble kalman filter. *Ocean modelling*, 8(1-2), 135–154. <https://doi.org/10.1016/j.ocemod.2003.12.004>
- Bertino, L., Evensen, G., & Wackernagel, H. (2003). Sequential data assimilation techniques in oceanography. *International Statistical Review*, 71(2), 223–241. <https://doi.org/10.1111/j.1751-5823.2003.tb00194.x>
- Brinkgreve, R. B. J., Bakker, K. J., & Bonnier, P. G. (2006). The relevance of small-strain soil stiffness in numerical simulation of excavation and tunneling projects. *Proceedings of 6th European Conference in Geotechnical Engineering, Graz, Austria*, 133–139.
- Burgers, G., van Leeuwen, P. J., & Evensen, G. (1998). Analysis scheme in the ensemble Kalman filter. *Monthly Weather Review*, 126(6), 1719–1724. [https://doi.org/10.1175/1520-0493\(1998\)126<1719:ASITEK>2.0.CO;2](https://doi.org/10.1175/1520-0493(1998)126<1719:ASITEK>2.0.CO;2)
- Chen, Y., & Zhang, D. (2006). Data assimilation for transient flow in geologic formations via ensemble Kalman filter. *Advances in Water Resources*, 29(8), 1107–1122. <https://doi.org/10.1016/j.advwatres.2005.09.007>
- Evensen, G. (1994). Sequential data assimilation with a nonlinear quasi-geostrophic model using Monte Carlo methods to forecast error statistics. *Journal of Geophysical Research: Oceans*, 99(C5), 10143–10162. <https://doi.org/10.1029/94JC00572>
- Evensen, G. (1997). Advanced data assimilation for strongly nonlinear dynamics. *Monthly Weather Review*, 125(6), 1342–1354. [https://doi.org/10.1175/1520-0493\(1997\)125%3C1342:ADAFSN%3E2.0.CO;2](https://doi.org/10.1175/1520-0493(1997)125%3C1342:ADAFSN%3E2.0.CO;2)
- Evensen, G. (2009). *Data assimilation: The ensemble Kalman filter*. Springer Science & Business Media.
- Gens, A., Ledesma, A., & Alonso, E. E. (1996). Estimation of parameters in geotechnical backanalysis — II. Application to a tunnel excavation problem. *Computers and Geotechnics*, 18(1), 29–46. [https://doi.org/10.1016/0266-352X\(95\)00022-3](https://doi.org/10.1016/0266-352X(95)00022-3)
- Glegola, M. A., Ditmar, P., Hanea, R. G., Vossepoel, F. C., Arts, R., & Klees, R. (2012). Gravitometric monitoring of water influx into a gas reservoir: A numerical study based on the ensemble Kalman filter. *SPE Journal*, 17(1), 163–176. <https://doi.org/10.2118/149578-PA>
- Hamill, T. M., Mullen, S. L., Snyder, C., Toth, Z., & Baumhefner, D. P. (2000). Ensemble forecasting in the short to medium range: Report from a workshop. *Bulletin of the American Meteorological Society*, 81(11), 2653–2664. [https://doi.org/10.1175/1520-0477\(2000\)081<2653:EFITST>2.3.CO;2](https://doi.org/10.1175/1520-0477(2000)081<2653:EFITST>2.3.CO;2)

- Houtekamer, P. L., & Mitchell, H. L. (1998). Data assimilation using an ensemble Kalman filter technique. *Monthly Weather Review*, 126(3), 796–811. [https://doi.org/10.1175/1520-0493\(1998\)126%3C0796:DAUAEK%3E2.0.CO;2](https://doi.org/10.1175/1520-0493(1998)126%3C0796:DAUAEK%3E2.0.CO;2)
- Houtekamer, P. L., & Mitchell, H. L. (2005). Ensemble Kalman filtering. *Quarterly Journal of the Royal Meteorological Society: A Journal of the Atmospheric Sciences, Applied Meteorology and Physical Oceanography*, 131(613), 3269–3289. <https://doi.org/10.1256/qj.05.135>
- Hsiung, B. C., & Dao, S.-D. (2014). Evaluation of constitutive soil models for predicting movements caused by a deep excavation in sands. *Electronic Journal of Geotechnical Engineering*, 19, 17325–17344.
- Kalman, R. E. (1960). A new approach to linear filtering and prediction problems. *Journal of Basic Engineering*, 82(1), 35–45. <https://doi.org/10.1115/1.3662552>
- Keppenne, C. L., & Rienecker, M. M. (2003). Assimilation of temperature into an isopycnal ocean general circulation model using a parallel ensemble Kalman filter. *Journal of Marine Systems*, 40, 363–380. [https://doi.org/10.1016/S0924-7963\(03\)00025-3](https://doi.org/10.1016/S0924-7963(03)00025-3)
- Ledesma, A., Gens, A., & Alonso, E. E. (1996). Parameter and variance estimation in geotechnical backanalysis using prior information. *International Journal for Numerical and Analytical Methods in Geomechanics*, 20(2), 119–141. [https://doi.org/10.1002/\(SICI\)1096-9853\(199602\)20:2%3C119::AID-NAG810%3E3.0.CO;2-L](https://doi.org/10.1002/(SICI)1096-9853(199602)20:2%3C119::AID-NAG810%3E3.0.CO;2-L)
- Lee, I.-M., & Kim, D.-H. (1999). Parameter estimation using extended Bayesian method in tunnelling. *Computers and Geotechnics*, 24(2), 109–124. [https://doi.org/10.1016/S0266-352X\(98\)00031-7](https://doi.org/10.1016/S0266-352X(98)00031-7)
- Liu, K., Vardon, P. J., & Hicks, M. A. (2018). Sequential reduction of slope stability uncertainty based on temporal hydraulic measurements via the ensemble Kalman filter. *Computers and Geotechnics*, 95, 147–161. <https://doi.org/10.1016/j.compgeo.2017.09.019>
- Lorentzen, R. J., Fjelde, K. K., Frøyen, J., Lage, A. C., Nævdal, G., & Vefring, E. H. (2001). Underbalanced and low-head drilling operations: Real time interpretation of measured data and operational support. *SPE Annual Technical Conference and Exhibition*, (SPE-71384-MS). <https://doi.org/10.2118/71384-MS>
- Mavrtsakis, A. (2017). Evaluation of inverse analysis methods with numerical simulation of slope excavation. *MSc thesis, Delft University of Technology, Netherlands*.
- Miller, R. N., Carter, E. F., & Blue, S. T. (1999). Data assimilation into nonlinear stochastic models. *Tellus A: Dynamic Meteorology and Oceanography*, 51(2), 167–194. <https://doi.org/10.3402/tellusa.v51i2.12315>
- Mohsan, M., Vardon, P. J., & Vossepoel, F. C. (2021). On the use of different constitutive models in data assimilation for slope stability. *Computers and Geotechnics*, 138, 104332. <https://doi.org/10.1016/j.compgeo.2021.104332>
- Mohsan, M., Vardon, P. J., & Vossepoel, F. C. (2023). Options for the implementations of data assimilation for geotechnics. *International Conference of the International Association for Computer Methods and Advances in Geomechanics*, 255–262. https://doi.org/10.1007/978-3-031-12851-6_31
- Nævdal, G., Johnsen, L. M., Aanonsen, S. I., & Vefring, E. H. (2003). Reservoir monitoring and continuous model updating using ensemble Kalman filter. *SPE Annual*

- Technical Conference and Exhibition*, (SPE-84372-PA). <https://doi.org/10.2118/84372-PA>
- Nævdal, G., Mannseth, T., & Vefring, E. H. (2002). Near-well reservoir monitoring through ensemble Kalman filter. *SPE/DOE Improved Oil Recovery Symposium*, (SPE 75235). <https://doi.org/10.2118/75235-MS>
- Oliver, D. S., & Chen, Y. (2011). Recent progress on reservoir history matching: A review. *Computational Geosciences*, 15(1), 185–221. <https://doi.org/10.1007/s10596-010-9194-2>
- Plaxis. (2015). *PLAXIS material models manual*. Plaxis.
- Reichle, R. H., McLaughlin, D. B., & Entekhabi, D. (2002). Hydrologic data assimilation with the ensemble Kalman filter. *Monthly Weather Review*, 130(1), 103–114. [https://doi.org/10.1175/1520-0493\(2002\)130%3C0103:HDAWTE%3E2.0.CO;2](https://doi.org/10.1175/1520-0493(2002)130%3C0103:HDAWTE%3E2.0.CO;2)
- Sekhvatian, A., & Choobasti, A. J. (2018). Comparison of constitutive soil models in predicting movements caused by an underground excavation. *International Journal of Soil Science*, 13(1), 18–27. <https://doi.org/ijss.2018.18.27>
- Skjervheim, J.-A., & Evensen, G. (2011). An ensemble smoother for assisted history matching. *SPE Reservoir Simulation Symposium*, (SPE-141929-MS). <https://doi.org/10.2118/141929-MS>
- Szunyogh, I., Kostelich, E. J., Gyarmati, G., Patil, D., Hunt, B. R., Kalnay, E., Ott, E., & Yorke, J. A. (2005). Assessing a local ensemble Kalman filter: Perfect model experiments with the National Centers for Environmental Prediction global model. *Tellus A: Dynamic Meteorology and Oceanography*, 57(4), 528–545. <https://doi.org/10.3402/tellusa.v57i4.14721>
- Tamura, H., Bacopoulos, P., Wang, D., Hagen, S. C., & Kubatko, E. J. (2014). State estimation of tidal hydrodynamics using ensemble Kalman filter. *Advances in Water Resources*, 63, 45–56. <https://doi.org/10.1016/j.advwatres.2013.11.002>
- Van Genuchten, M. T. (1980). A closed-form equation for predicting the hydraulic conductivity of unsaturated soils. *Soil Science Society of America Journal*, 44(5), 892–898. <https://doi.org/10.1139/t66-009>
- Vardon, P. J., Liu, K., & Hicks, M. A. (2016). Reduction of slope stability uncertainty based on hydraulic measurement via inverse analysis. *Georisk: Assessment and Management of Risk for Engineered Systems and Geohazards*, 10(3), 223–240. <https://doi.org/10.1080/17499518.2016.1180400>
- Wang, L., Hwang, J. H., Luo, Z., Juang, C. H., & Xiao, J. (2013). Probabilistic back analysis of slope failure – a case study in Taiwan. *Computers and Geotechnics*, 51, 12–23. <https://doi.org/10.1016/j.compgeo.2013.01.008>
- Wösten, J., Lilly, A., Nemes, A., & Le Bas, C. (1999). Development and use of a database of hydraulic properties of european soils. *Geoderma*, 90(3-4), 169–185. [https://doi.org/10.1016/S0016-7061\(98\)00132-3](https://doi.org/10.1016/S0016-7061(98)00132-3)
- Zhou, M., Li, Y., Xiang, Z., Swoboda, G., & Cen, Z. (2007). A modified extended Bayesian method for parameter estimation. *Tsinghua Science & Technology*, 12(5), 546–553. [https://doi.org/10.1016/S1007-0214\(07\)70131-1](https://doi.org/10.1016/S1007-0214(07)70131-1)

3

ON THE USE OF DIFFERENT DATA ASSIMILATION SCHEMES IN A FULLY COUPLED HYDRO-MECHANICAL SLOPE STABILITY ANALYSIS

Different data assimilation schemes such as the ensemble Kalman filter (EnKF), ensemble smoother (ES) and ensemble smoother with multiple data assimilation (ESMDA) are implemented in a hydro-mechanical slope stability analysis. For a synthetic case, these schemes assimilate displacements at the crest and the slope to estimate strength and stiffness parameters. These estimated parameters are then used to estimate the system's state and factor of safety (FoS). The results show that EnKF provides an FoS estimation with a mean close to the truth and with the smallest standard deviation, with the ESMDA using the largest amount of assimilation steps also providing a mean close to the truth but with less confidence. The ES and ESMDA with fewer assimilation steps underestimate the FoS approximation and have low confidence. Assimilating measurements over a longer period provides a more accurate parameter, state and FoS estimation. ES has the best computational performance, with ESMDA performing worse, with its performance dependent on the number of assimilation steps. The computational performance of the EnKF is better than the ESMDA but around 50% worse than the ES. Non-linearity of the underlying problem is a key cause of the multi-step assimilation processes having a better performance.

3.1. INTRODUCTION

Data assimilation provides an estimate of the state and parameters based on numerical models and measurements, considering uncertainties in both (Evensen et al., 2022).

This chapter is based on Mohsan et al. (2023) and Mohsan et al. (2024).

Ensemble-based methods use multiple (statistically equivalent) models (so-called realisations) in order to calculate a prior distribution of a given variable. This distribution can be combined with measurements to update the state or parameters and as such calculate a posterior distribution or so-called analysis. Such a process can be computationally expensive, and therefore computational performance is important. Ensemble-based methods for data assimilation are well established, e.g., the ensemble Kalman filter (EnKF), ensemble smoother (ES) and ensemble smoother with multiple data assimilation (ESMDA).

The EnKF (Evensen, 1994) is an ensemble-based method based on the Kalman filter (Kalman, 1960), which assimilates measurements sequentially in time. The EnKF has been widely implemented in different fields and is currently one of the most popular data assimilation methods. This method has been used in numerical weather prediction (e.g., Houtekamer & Mitchell, 2005; Szunyogh et al., 2005), oceanography (e.g., Bertino et al., 2003; Keppenne & Rienecker, 2003), hydrology (e.g., Chen & Zhang, 2006; Reichle et al., 2002), geotechnical engineering (e.g., Liu et al., 2018; Mavritsakis, 2017; Mohsan et al., 2021, 2023; Vardon et al., 2016), and petroleum reservoir history matching (e.g. Aanonsen et al., 2009; Evensen, 2009; Glegola et al., 2012; Nævdal et al., 2002; Oliver & Chen, 2011). The EnKF has a sequential scheme, where states or parameters are updated every time measurements are available, which has the disadvantage of potentially leading to inconsistencies in previous steps. Another possible disadvantage of the EnKF is the Gaussian approximation of error covariances in the update scheme. Because of this, the EnKF may not give optimal results for problems with non-Gaussian parameter distributions. Furthermore, when applying EnKF for parameter estimation, repeated restarting after each update step can lead to a significant use of computation time.

ES (Van Leeuwen & Evensen, 1996) is an alternative ensemble-based formulation, which assimilates all measurements simultaneously and outputs a global update. ES has been implemented in the fields of petroleum reservoir engineering (e.g., Skjervheim & Evensen, 2011) and oceanography (e.g., Van Leeuwen, 1999; Van Leeuwen & Evensen, 1996). In ES, the recursion in time is not needed, making this scheme generally computationally more efficient in comparison with the EnKF (Skjervheim & Evensen, 2011). However, for non-linear dynamic models, particularly models with strongly nonlinear dynamics, the EnKF has shown better results than ES, because the recursive nature of EnKF steers the ensemble such that the resulting estimate gets close to the true solution. In addition to that, the EnKF deals the weakly non-linear model better than ES. With ES, on the other hand, a single global correction is made by assimilating all data to update all ensemble members. Given that a limited number of ensemble members are used and hence the limited part of the solution space sampled, ES may not be able to find a reasonable data match.

ESMDA (Emerick & Reynolds, 2013) is an improved form of ensemble methods such as ES, which assimilates measurements in an iterative procedure and has been implemented in the field of petroleum engineering (e.g., Emerick, 2016; Emerick & Reynolds, 2013; Maucec et al., 2016) but has also been applied in other fields (e.g., Evensen, 2018; Evensen et al., 2021; Evensen & Eikrem, 2018).

Several publications have compared the performance of these ensemble based methods in different fields (e.g., Emerick, 2016; Evensen et al., 2022; Skjervheim & Evensen,

2011; Van Leeuwen & Evensen, 1996). The performance has been studied based on both computational effort and the ability to steer the analyses towards the measured (or synthetically generated) data. Van Leeuwen and Evensen (1996) tested both the EnKF and ES on ocean circulation models. They concluded that the EnKF gives better results than ES in an ocean circular model. The better accuracy of the EnKF can be explained by the manner in which it deals with nonlinear behaviour of the system. The sequential nature of this scheme as implemented here brings the numerical model state closer to the data at each assimilation point. In contrast, ES takes all measurements over a time period into consideration at once, which makes it more difficult to find a close match of the model state and the data over the entire time period.

Skjervheim and Evensen (2011) implemented the sequential EnKF and ES for the reservoir models. They concluded that these two methodologies output similar results, but ES took approximately 10% of the computational time of that of the EnKF. Emerick (2016) implemented the EnKF, ES and ESM DA in a reservoir engineering problem. It was concluded that ES did not provide a reasonable data match and that ESM DA provided a better data match than EnKF with a comparable computational cost. It seems, therefore, that the performance of the schemes depends on the problem at hand.

Geotechnical structures (such as slope structures) are now increasingly equipped with measurement devices to monitor their response to external changes. These measurements can be surface displacements, porewater pressures, strains, etc. These measurements can be obtained from in-situ devices (such as inclinometers, strain gauges, etc.) or can be measured remotely (with Light Detection and Ranging (LIDAR), Interferometric Synthetic Aperture Radar (InSAR), etc.). In Chapter 2, it was shown that such measurements can be used in one specific data assimilation scheme to estimate uncertain material model parameters in an FEM model of slope stability. An uncertainty in model parameters exists because of many reasons, such as errors caused by the equipment or procedure, transformation errors (Ching & Phoon, 2015; Van der Krogt et al., 2019; Wang et al., 2017), the inherent spatial variability (Phoon & Kulhawy, 1999a, 1999b) or a combination of these. To ensure safety of the system, the proximity to failure (e.g., FoS) is important to know, however it cannot be directly measured. Therefore, related measurements must be used in a system to predict or evaluate the FoS.

Vardon et al. (2016) and Liu et al. (2018) implemented an ensemble Kalman filter (EnKF) in a slope stability problem. They integrated the EnKF with the random finite element method (RFEM) for the estimation of hydraulic conductivity based on measurements of pore water pressure. They implemented data assimilation for slopes in steady state and transient conditions. The authors concluded that the improved estimation of hydraulic conductivity led to improved pore water pressure estimation, and ultimately provided an improved factor of safety estimation. In Chapter 2, the EnKF was used on a fully coupled hydro-mechanical slope stability system to study the performance of two constitutive models: the Mohr-Coulomb (MC) model and the hardening soil (HS) model. It was concluded that the HS model can more generally be used to get reliable results (FoS estimation) while assimilating the horizontal slope deformations into the model.

In this chapter, three different data assimilation methodologies have been implemented in a fully coupled hydro-mechanical slope stability model to study the performance of these schemes, i.e. the EnKF, ES and ESM DA. The slope stability model uses

the HS model to simulate the (non-linear) material behaviour. In Section 3.2, details of the overall methodology for stability analysis, including the forward model and the data assimilation schemes are presented. Section 3.3 presents a synthetic example to evaluate the performance of the data assimilation schemes, with the results presented in Section 3.4. These results are followed by a discussion in Section 3.5 and conclusions in Section 3.6.

3.2. METHODOLOGY

The data assimilation framework considered in this study consists of a forward model that simulates the geomechanical behaviour of a slope and a specified data assimilation scheme that assimilates measurements of surface deformation into this forward model to estimate the geomechanical parameters. The forward model is a fully coupled hydro-mechanical slope stability model with a changing external water level, simulated using the commercial code PLAXIS (Plaxis, 2015). Unsteady flow generates a simulation from which synthetic deformation measurements can be sampled that reflect a changing stress state in the slope. We will explore to what extent different data assimilation schemes can relate these measurements to model parameters, and consequently the FoS. A constitutive model called the hardening soil (HS) model (Plaxis, 2015) is used to define the material behaviour, following previous work (Mohsan et al., 2021) which demonstrated the benefits of the model over more commonly used models such as the Mohr-Coulomb model. The forward model is integrated with a specific data assimilation scheme (the EnKF, ES or ESMDA) to investigate the performance of the data assimilation scheme with synthetic twin experiments. The synthetic measurements for these experiments are sampled from a realisation of the forward model referred to as the ‘truth’. The performance of the data assimilation schemes is evaluated based on the comparison between the synthetic (‘true’) and estimated model parameters, the model-data misfit (deformation), the distribution of the estimated FoS and the computation time. The FoS estimation is the target metric, but the other metrics give important insight into the performance of the scheme and therefore its further applicability.

3.2.1. FORWARD MODEL

The forward model consists of a coupled system of mechanical and hydraulic equations. For the mechanical behaviour, equilibrium is considered, i.e.:

$$\nabla \cdot \boldsymbol{\sigma}' + \nabla p + \rho \mathbf{b} = \mathbf{0}, \quad (3.1)$$

where ∇ is the gradient operator, $\nabla \cdot$ is the divergence, $\boldsymbol{\sigma}'$ is the effective stress tensor, p is the pore pressure, ρ is the density and \mathbf{b} are the body accelerations (e.g., from gravity). The constitutive behaviour can be expressed as:

$$\boldsymbol{\sigma}' = \mathbf{D}' \boldsymbol{\epsilon} \quad (3.2)$$

where \mathbf{D}' is the effective constitutive matrix and $\boldsymbol{\epsilon}$ is the strain tensor. Substitution of Eq. 3.2 into Eq. 3.1, recognising that $\boldsymbol{\epsilon} = 0.5((\nabla \mathbf{u}) + (\nabla \mathbf{u})^T)$, where \mathbf{u} is the displacement, yields the mechanical governing equation. The HS model, used as the constitutive model in this study, is a non-linear elastoplastic model, which includes several realistic soil features such as non-linear elasticity, stress-dependent stiffness, irreversible

non-linear plastic strain and hardening/softening mechanisms. For more details of the HS model, see Schanz et al. (1999). The HS model uses the following parameters: cohesion (c'), friction angle (ϕ'), dilatancy angle (ψ), the secant stiffness at reference pressure in a standard drained triaxial test (E_{50}^{ref}), the tangent stiffness at reference pressure for primary odometer loading (E_{oed}^{ref}), the loading-unloading stiffness at reference pressure (E_{ur}^{ref}), the Poisson's ratio for unloading reloading (ν_{ur}) and a parameter m which controls the stress-level dependency for the stiffness parameters.

To model the hydraulic behaviour, the conservation of mass is considered which can be expressed as:

$$\frac{\partial(\epsilon_{vol})}{\partial t} = -\nabla \cdot \mathbf{v} - Q, \quad (3.3)$$

where ϵ_{vol} is the volumetric strain (which can be determined from the displacement), \mathbf{v} is the velocity vector and Q is a source term. The velocity of water is incorporated via Darcy's Law:

$$\mathbf{v} = -k\nabla \left(\frac{p}{\rho_l g} + z \right), \quad (3.4)$$

where k is the hydraulic conductivity matrix, g is the gravitational constant, and z is the elevation.

Both mechanical and hydraulic equations have primary variables of displacement and fluid pressure, and are therefore a coupled system of equations.

The equations are discretised in space and time using standard FEM procedures, and compute the behaviour of the slope due to the gravity and hydraulic loading. The horizontal slope deformations are extracted from this hydro-mechanical analysis. The model calculates the results until the time when a stability analysis is required and a number of measurements are available. Then a stability analysis is carried out (using the strength reduction method, where $\tan(\phi')$ and c' are successively reduced until failure), which results in an estimate of the factor of safety (FoS) which is the ratio of the original strength to the reduced strength of the material at failure.

3.2.2. DATA ASSIMILATION SCHEMES

EnKF, ES and ESM DA are all ensemble-based data assimilation schemes used to estimate the parameters of the system. In all cases, an initial set of realisations (i.e., an ensemble) is generated by randomly selecting parameters from a prior distribution that is based on what is known about the system. Then the model parameters are estimated based on available measurements.

The EnKF assimilates the measurements sequentially in time. In the scheme as applied, the ensemble is run from the start to a time when the measurements (\mathbf{d}_1) are available (see Fig. 3.1a for a schematic of the process). These measurements are assimilated into the model which results in the posterior distribution. To make the model state consistent with the posterior parameters, the posterior model parameters are used to rerun the model from the start of the simulation to the next time when the new measurements (\mathbf{d}_2) are available. This new set of measurements is then assimilated into the numerical model to again update parameter estimates and so on. Thus, after each EnKF update step, the forward model restarts from the beginning of the analysis.

ES is an alternative ensemble-based data assimilation scheme. ES does not assimilate the data sequentially in time, but performs a single estimation assimilating all available measurements ($\mathbf{d}_1 - \mathbf{d}_n$) in the space-time domain. In this scheme, the model prediction is first computed for all ensemble members at all time steps. Then all available measurements are assimilated to find the global parameter update. Finally, the model is re-run with the updated parameters to find the final output of the data assimilation framework (see Fig. 3.1b for the illustration). Both the EnKF and the ES use the same equations for the posterior, but in the case of the ES it is applied once for all measurements, whereas for the EnKF it is applied every time when measurements are available.

Emerick and Reynolds (2012) proposed ESM DA as an improvement of ES. In ESM DA, the same data is assimilated iteratively. To account for the fact that the scheme assimilates the same data multiple times, it uses an inflation factor for the error covariance matrix of measurements. This means that instead of making a single linear, potentially large update, multiple smaller linear updates are performed. These iterations can partly resolve reported problems with non-linearity and generally lead to more accurate reconstruction of the ‘truth’ than ES.

FORMULATION OF THE DATA ASSIMILATION SCHEMES

In order to formulate the data assimilation principles, suppose we have the model prediction \mathbf{y} which is obtained by running the perfect forward model with pre-defined input model parameters. In order to map this model output to the measurement space for comparison with the measurements, we use the measurement operator g , i.e.

$$\mathbf{y} = g(m(\mathbf{z})), \quad (3.5)$$

in which

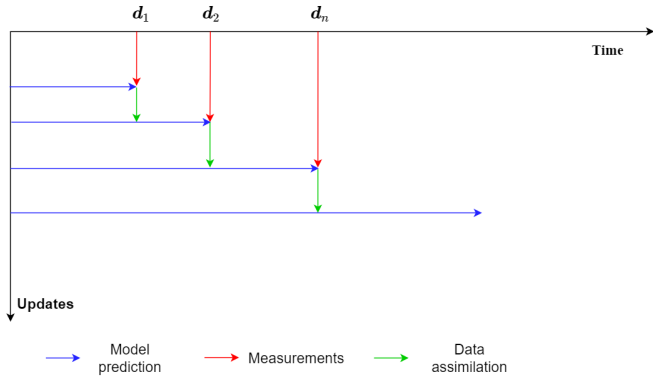
$$\mathbf{z} = (\mathbf{x} \quad \boldsymbol{\theta})^T \quad (3.6)$$

Here $\mathbf{y} \in \mathbb{R}^{N_m}$ is the model forecast mapped to the measurement locations with N_m is the number of measurements, m is model operator which relate input parameters to output, g is the measurement operator which maps the output to measurement space. Furthermore, in Eq. 3.6, $\mathbf{z} \in \mathbb{R}^{N_x + N_\theta}$ is a control or state vector consisting of the state ($\mathbf{x} \in \mathbb{R}^{N_x}$) and ($\boldsymbol{\theta} \in \mathbb{R}^{N_\theta}$) represents the parameters with N_x the number of state points and N_θ the number of model parameters.

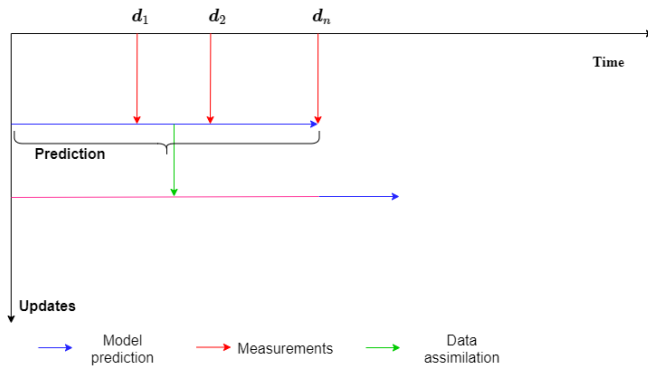
For a unique given set of parameters, we consider a single simulation of the model and assume this to be the ‘truth’ (\mathbf{y}). The synthetic measurements are created from the ‘truth’ and perturbed with randomly selected measurement errors and hence can be represented as:

$$\mathbf{d} = \mathbf{y} + \mathbf{e}, \quad (3.7)$$

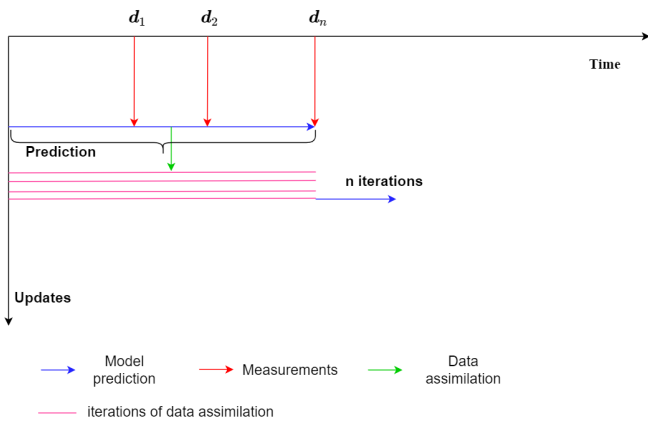
where $\mathbf{d} \in \mathbb{R}^{N_m}$ is the measurement vector and $\mathbf{e} \in \mathbb{R}^{N_m}$ is the measurement error vector. Measurement errors are assumed to include instrument errors and representation errors and are normally distributed with zero mean and variance defined by the inaccuracies inherent to the measurement device and the representation error (for a discussion on representation error see Janjić et al. (2018)).



(a) EnKF



(b) ES



(c) ESM DA

Figure 3.1: Illustration of the data assimilation schemes. (a) EnKF (b) ES (c) ESM DA ((a) and (b) after Evensen (2009)).

By using Bayes' theorem and following the derivation steps from Sec. 2.2.2, the cost function J can be achieved as:

$$J(\mathbf{z}) = (\mathbf{z} - \mathbf{z}^f)^T \mathbf{C}_{zz}^{-1} (\mathbf{z} - \mathbf{z}^f) + (\mathbf{g}(\mathbf{z}) - \mathbf{d})^T \mathbf{C}_{dd}^{-1} (\mathbf{g}(\mathbf{z}) - \mathbf{d}), \quad (3.8)$$

In Eq. 3.8, \mathbf{z}^f is the prior estimate of \mathbf{z} , $\mathbf{C}_{zz} \in \mathbb{R}^{(N_x+N_\theta) \times (N_x+N_\theta)}$ is the error covariance of \mathbf{z}^f , and $\mathbf{C}_{dd} \in \mathbb{R}^{N_m \times N_m}$ is the error covariance of measurements. The Kalman filter formulation can be derived by assuming the linear operator and minimization of the cost function (Eq. 3.8). For further details, see Evensen et al. (2022). Below, the main features of the different assimilation schemes are presented, the algorithms are presented in more detail in the Appendix.

EnKF: In the case of EnKF, multiple realisations of the forward model are being performed. The Kalman equation for each of the ensemble member $i \in N_e$ can be written as:

$$\mathbf{z}_i^a = \mathbf{z}_i^f + \mathbf{C}_{zz}^e \mathbf{G}^T (\mathbf{G} \mathbf{C}_{zz}^e \mathbf{G}^T - \mathbf{C}_{dd})^{-1} (\mathbf{d}_i - \mathbf{G}(\mathbf{z}_i^f)), \quad (3.9)$$

where \mathbf{z}^a represents the analysis estimate and \mathbf{z}^f represents the prior estimate and \mathbf{C}_{zz}^e is termed as the model covariance matrix. Here

$$\mathbf{d}_i = \mathbf{d} + \boldsymbol{\epsilon}_i \quad (3.10)$$

represents the perturbed measurements for each i th member, with $\boldsymbol{\epsilon}_i$ having the same distribution as the measurement errors \boldsymbol{e} in Eq. 3.7, following the approach of Burgers et al. (1998).

In the implementation of the EnKF in this study, the update equation (Eq. 3.9) is applied whenever the measurements are available. At each update step, elements of Eq. 3.9 consist of the available information at that specific assimilation step in which $\mathbf{z}_i^a, \mathbf{z}_i^f \in \mathbb{R}^{N_x+N_\theta}$ represent the analysis and forecast vector, respectively, at that specific data assimilation time for i^{th} ensemble member, $\mathbf{C}_{zz} \in \mathbb{R}^{(N_x+N_\theta) \times (N_x+N_\theta)}$ is the error covariance of \mathbf{z}_i^f at that specific data assimilation time and $\mathbf{C}_{dd} \in \mathbb{R}^{N_m \times N_m}$ is the error covariance of measurements for that specific data assimilation time.

Ensemble smoother (ES): The ES equations are essentially the same equations as those of the EnKF. Just like the equations for the EnKF, Eq. 3.9, they are found by equating the cost function gradient equal to zero to find its minimum and defining the covariances around its mean (Evensen, 2018).

In the case of ES, all measurements are assimilated in a single step to find a global update which means the measurement vector (\mathbf{d}_i) in Eq. 3.9 consists of all information at all data assimilation steps. This implies that $\mathbf{z}_i^a, \mathbf{z}_i^f \in \mathbb{R}^{(N_x+N_\theta) * t}$, the analysis and forecast vectors, consist of the state-parameter vector for all time steps until the end of data assimilation window for a specific, i^{th} , ensemble member, where $\mathbf{C}_{zz} \in \mathbb{R}^{(N_x+N_\theta) * t \times (N_x+N_\theta) * t}$ is the spatio-temporal error covariance of \mathbf{z}_i^f , and $\mathbf{C}_{dd} \in \mathbb{R}^{(N_m \times N_m) * t}$ is the error covariance of measurements for all data assimilation steps.

ESMDA: ESDMA can also be derived from Bayes theory and has the same theoretical basis as ES. However, rather than computing the analysis in a single iteration, it is obtained in a number of steps, where the posterior ($f(\mathbf{z}|\mathbf{d})$) is made up of a combination of

tempered likelihood functions ($\prod_{j=1}^{N_{\text{mda}}} f(\mathbf{d}|\mathbf{g}(\mathbf{z}_{j-1}))^{\frac{1}{\alpha_j}}$) and prior ($f(\mathbf{z})$). This implies:

$$f(\mathbf{z}|\mathbf{d}) = f(\mathbf{z}) \prod_{j=1}^{N_{\text{mda}}} f(\mathbf{d}|\mathbf{g}(\mathbf{z}_{j-1}))^{\frac{1}{\alpha_j}}. \quad (3.11)$$

where,

$$\sum_{j=1}^{N_{\text{mda}}} \frac{1}{\alpha_j} = 1. \quad (3.12)$$

In these equations, α_j is the tempering parameter for the j^{th} recursive step to inflate the measurement error to damp the model update. With this formulation, the cost function can be written as:

$$J(\mathbf{z}_{i,j+1}) = (\mathbf{z}_{i,j+1} - \mathbf{z}_{i,j}^f)^T \mathbf{C}_{zz}^{-1} (\mathbf{z}_{i,j+1} - \mathbf{z}_{i,j}^f) + (\mathbf{g}(\mathbf{z}_{i,j+1}) - \mathbf{d}_i - \sqrt{\alpha_j} \boldsymbol{\epsilon})^T \alpha_j \mathbf{C}_{dd}^{-1} (\mathbf{g}(\mathbf{z}_{i,j+1}) - \mathbf{d}_i - \sqrt{\alpha_j} \boldsymbol{\epsilon}), \quad (3.13)$$

where $J(\mathbf{z}_{i,j+1})$ is the cost function for ensemble i and $j+1$ recursive update step. Minimization of cost function corresponds to maximization of the each recursion, that is:

$$\mathbf{z}_{i,j+1}^a = \mathbf{z}_{i,j}^f + \mathbf{C}_{zz}^{e,j} \mathbf{G}^T (\mathbf{G} \mathbf{C}_{zz}^{e,j} \mathbf{G}^T - \alpha_j \mathbf{C}_{dd})^{-1} (\mathbf{d}_i + \sqrt{\alpha_j} \boldsymbol{\epsilon} - \mathbf{g}(\mathbf{z}_{i,j}^f)). \quad (3.14)$$

In each step, the measurement error matrix is inflated with α_j and measurements are perturbed with $\sqrt{\alpha_j} \boldsymbol{\epsilon}$. The error covariance matrix is updated for each of the recursive update steps with a new value of α_j . The α_j parameters should satisfy the Eq. 3.12 condition assimilate the observations in multiple steps, i.e., with multiple smaller corrections, and at the same time to ensure the measurements do not obtain too much weight. As the same data is assimilated in N_{mda} iterations, a practical difficulty of the implementation of ESM DA is that N_{mda} and its coefficients need to be selected prior to the data assimilation. (Emerick & Reynolds, 2013) suggests choosing α values in decreasing order to ensure that the initial updates are smaller.

3.3. SYNTHETIC EXAMPLE

An idealised 2D slope geometry is considered to test and illustrate the performance of the data assimilation schemes described in Section 3.2.2. The geometry of the slope with mechanical and hydraulic boundary conditions are shown in Fig. 3.2. The black circles on the crest and slope represent the measurement locations. The slope undergoes gravity and hydraulic loading (variable hydraulic boundary conditions). To setup the initial stress state of the slope system, gravity loading with steady-state groundwater flow calculations are performed by considering the water level at line CE in Fig. 3.2. In this study, the Van Genuchten (1980) model is used to simulate the behaviour of unsaturated soil with the properties mentioned in Table 3.1. After the initial stress state, the slope is subjected to the generally-rising fluctuation (D_w) of the water level. The fluctuation of (D_w) is shown on the top-right of the Fig. 3.2. The changes in hydraulic boundaries associated with this water level fluctuation cause vertical and lateral slope deformations and changes in the factor of safety that are computed with the forward model.

A so-called truth is defined by selecting a unique simulation of the forward model by specifying 'true' parameters (Table 3.1) and the initial state. True model evolution

in the form of horizontal displacements at point G (see Fig. 3.2) and the resulting FoS can be seen in Fig 3.3. The displacements are seen to increase as the water level rises, in conjunction with the effective stress decrease. The FoS is seen to first decrease, most likely due to the reduction in effective stress and the consequential reduction in shear strength due to the friction component, and then increase, most likely due to the reduction in buoyant weight of the material. Both the reduction in shear strength and buoyant weight are due to the increase in the water level, with the details of the geometry and material parameters governing which impact is dominant. The horizontal deformations on the crest-slope are sampled from this forward simulation during a time interval of 150-200 days (with the sample times indicated in the top right sub-figure of Fig. 3.2 by red-stars). Considering the millimetre scale accuracy of measurements devices (such as INSAR, and laser scanners), we have added realistic measurement noise (with zero mean and 10^{-7} m variance) to the data, and then these synthetic measurements are assimilated into an FEM model with the same initial conditions and water level fluctuations as the truth simulation, but with different parameter distributions for strength and stiffness as shown in Table 3.2. EnKF, ES and ESMDA are tested in this setup to estimate the two

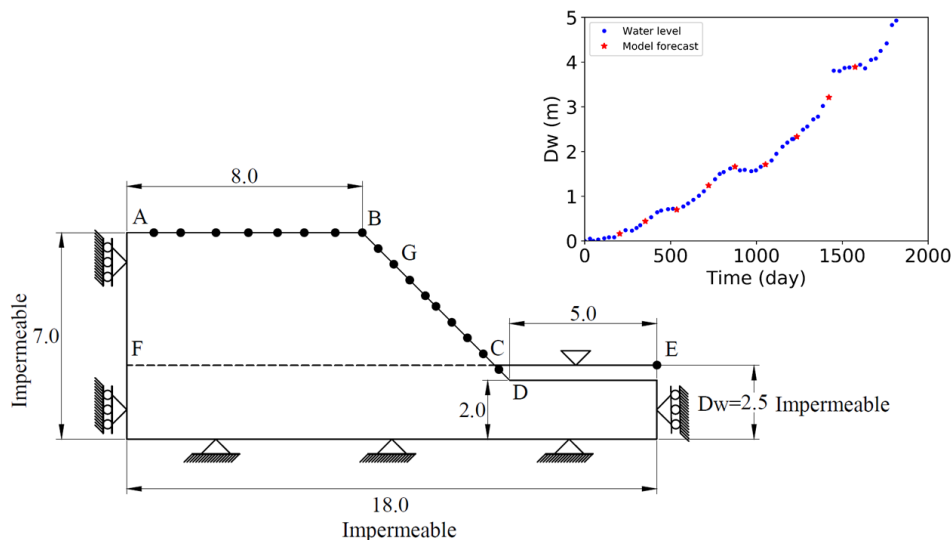


Figure 3.2: Geometry of the slope (dimensions in m) and black circles represent the measurement points. On the top right, water level fluctuation is shown. The model forecast at the red stars are computed to perform the data assimilation.

most sensitive parameters, the friction angle (ϕ') and secant stiffness at reference pressure (E_{50}^{ref}) parameters, and then finally the FoS estimation. For each of the schemes, the ensemble has 50 members. The performance of the data assimilation schemes is evaluated by comparing their ability to reconstruct the truth within the assumed accuracy of the measurements and by comparing computational performance. *Note: VGM stands for Van Genuchten model

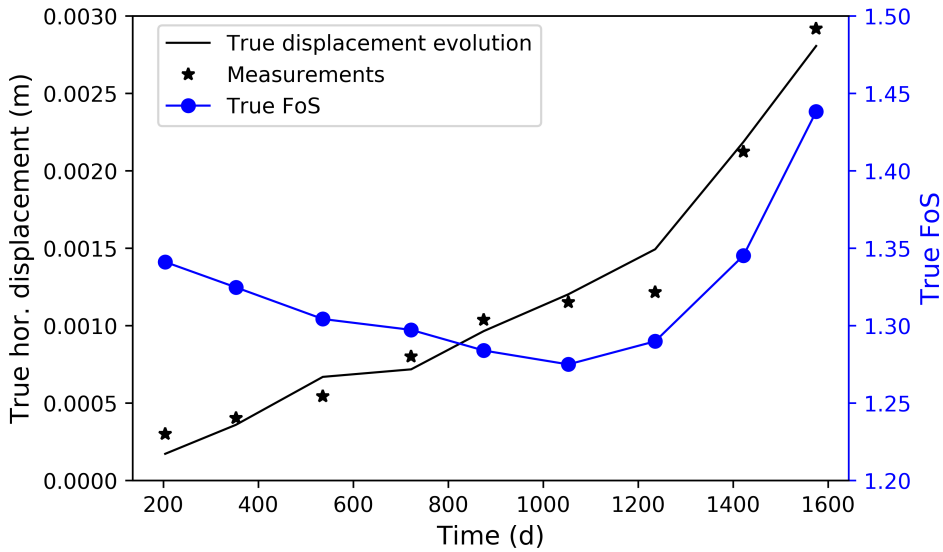


Figure 3.3: Evolution of horizontal displacement (m) at point G on the slope and FoS evolution based on the true model parameters (see in Table 3.1) and water level fluctuation (see in Fig 3.2)

Table 3.1: ‘Truth’ model parameters for EnKF, ES, ESM DA

Parameters	values	Unit
Effective friction angle (ϕ')	25	$^{\circ}$
Effective cohesion (c')	5	kPa
Dilatancy angle (ψ)	0	$^{\circ}$
E_{50}^{ref}	20000	kPa
E_{oed}^{ref}	E_{50}^{ref}	kPa
E_{ur}^{ref}	$2.5E_{50}^{ref}$	kPa
Poisson's ratio for unloading/reloading (ν_{ur})	0.2	-
Stress-level dependency (m)	0.5	-
Unsaturated unit weight (γ_d)	17	kN/m ³
Saturated unit weight (γ_s)	18.5	kN/m ³
Hydraulic conductivity ($k_x = k_y$)	0.12	m/day
VGM parameter (g_a)	3.83	m^{-1}
VGM parameter (g_n)	1.3774	-
VGM parameter (g_l)	1.25	-
Saturated volumetric water content (θ_s)	1.0	-
Residual volumetric water content (θ_r)	0.062	-

Table 3.2: Initial estimation of model parameters

Parameters	Parameter values	Distribution	Unit
Effective friction angle (ϕ')	$\mu = 30, \sigma = 3$	Normal	$^{\circ}$
E_{50}^{ref}	$\mu = 25000, \sigma = 2500$	Normal	kPa

The setup of the experiments is shown in Table 3.3. In the first experiment, EnKF is implemented as the data assimilation scheme, and the measurements are assimilated sequentially in time. For this setup, estimates of parameter values, displacement and FoS are available at each assimilation step. There are two variants of the test case, with a shorter and longer availability of measurements. For a shorter period (indicated by -s), measurements are assimilated until 1053 days and for a longer period (indicated by -l) measurements are assimilated until 1575 days. In the second test case, two independent experiments are performed with ES: ES-s and ES-l, with the same data availability as for the EnKF test cases. Then, ESMDA is applied in three different cases (named as ESMDA(x2e), ESMDA(x4e) and ESMDA(x4d)) to see the effect of choosing the number of update steps and the effect of α values. For ESMDA(x2e), there are two iterations by taking equal α values, while in ESMDA(x4e), there are four iterations with equal α values. For ESMDA(x4d), the measurements are assimilated in four iterations using decreasing α values. Furthermore, each of these experiments (ESMDA(x2e), ESMDA(x4e) and ESMDA(x4d)) are subdivided into two in the same way as for EnKF and ES with shorter and longer measurement availabilities.

Table 3.3: Experimental plan for different data assimilation schemes

Test case name	Data assimilation scheme	α values
EnKF-s, EnKF-l	EnKF	[-]
ES-s, ES-l	ES	[-]
ESMDA(x2e)-s, ESMDA(x2e)-l	ESMDA(x2e)	[2,2]
ESMDA(x4e)-s, ESMDA(x4e)-l	ESMDA(x4e)	[4,4,4,4]
ESMDA(x4d)-s, ESMDA(x4d)-l	ESMDA(x4d)	[9.3,7.0,4.0,2.0]

3.4. RESULTS

The data assimilation performance is evaluated with the estimation of the selected parameters (E_{50}^{ref} and ϕ'), displacement, FoS estimation and by the computation time. While FoS estimation is the primary target, the parameter and displacement estimation are prerequisites for the FoS to be reliably predicted.

3.4.1. PARAMETER ESTIMATION

Fig. 3.4 presents the parameter estimation (E_{50}^{ref} and ϕ') after assimilating the measurement for the shorter period. The true parameters, prior parameter distribution, and the posterior estimate using EnKF-s, ES-s, ESMDA(x2e)-s, ESMDA(x4e)-s and ESMDA(x4d)-s are presented for both parameters. By construction, the distribution of the true pa-

parameters and the prior parameter distribution are the same for all test cases. After the assimilation of measurements, the posterior parameter mean (μ) and standard deviation (σ) are computed from the ensemble, and the resulting normal distributions with these statistical moments are shown in Fig. 3.4. The mean (μ) obtained from the posterior distribution of E_{50}^{ref} is closer to the true value of E_{50}^{ref} than the prior mean for all the data assimilation schemes. But in most cases, the width of the posterior distribution of E_{50}^{ref} has not changed significantly by assimilating the measurements for this (shorter) time period. The limited amount of information from the measurements has thus resulted in a shift of the distribution relative to the prior, but has not narrowed the ensemble spread. In the estimation of ϕ' , a significant change from the prior to the posterior distribution can be seen in all cases. In the cases of EnKF-s, ESMDA(x4e)-s and ESMDA(x4d)-s: the posterior mean moves towards the true value and the standard deviations are smaller than that of the prior distribution. The parameter estimates of the ES-s and ES(x2e)-s move in the direction of the mean, but overshoot significantly the true ϕ' , with the standard deviation only reducing slightly.

To study the effect of measurement assimilation for a longer period, Fig. 3.5 presents

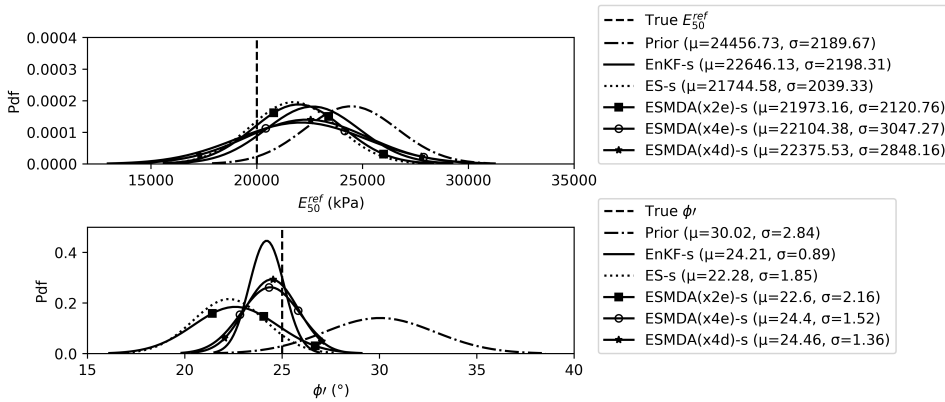


Figure 3.4: Estimation of parameters (E_{50}^{ref} and ϕ') by EnKF-s, ES-s, ESMDA(x2e)-s, ESMDA(x4e)-s, and ESMDA(x4d)-s.

the parameter estimation results after using the measurements available until 1575 days. The posterior improves substantially for the estimation of E_{50}^{ref} for all the data assimilation schemes as compared to the results in Fig. 3.4, most notably for ES; the mean estimates of E_{50}^{ref} are closer to the true value and their standard deviation is reduced, although the distribution is still relatively broad. This gives the impression that when data are assimilated over a longer period, a more accurate estimate is achieved. On the other hand, the estimate of ϕ' changes very little compared to the results of the shorter period of assimilation as presented in Fig. 3.4. This suggests that the estimates of ϕ' in the earlier assimilation steps are as close to the truth as they can possibly get by assimilation of measurements of deformation.

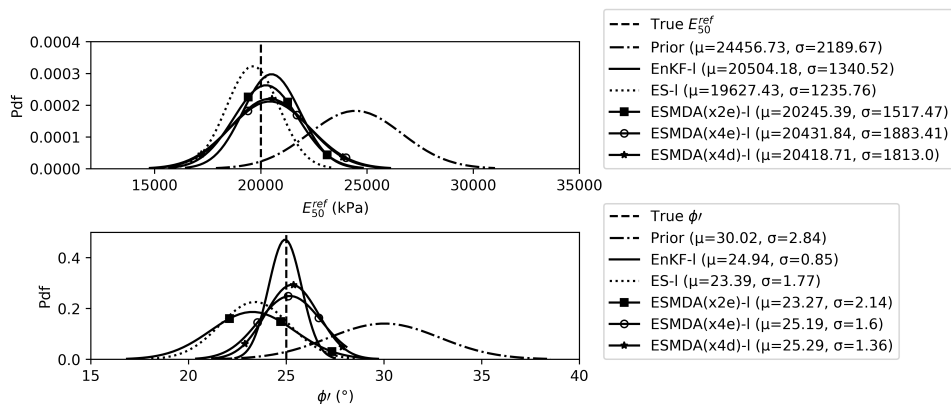


Figure 3.5: Estimation of parameters (E_{50}^{ref} and ϕ') by EnKF-I, ES-I, ESMDA(x2e)-I, ESMDA(x4e)-I, and ESMDA(x4d)-I.

3.4.2. DISPLACEMENT ENSEMBLE ESTIMATION

This section presents the displacement evolution based on the true, prior and estimated parameters. The displacement evaluation is studied in the form of horizontal displacement of a point G (see Fig. 3.2) on the slope, which is towards the top of the slope, to capture the largest displacements. Fig. 3.6 and Fig. 3.7 illustrate the displacements computed using estimated parameters by assimilating the measurements for shorter and longer periods, respectively. The black line represents the true model evolution based on true model parameters, and the synthetic measurements are represented by black stars. The prior horizontal displacement ensemble (in green) is computed using the prior parameter distribution and as a direct result of initially poorly selected parameter values, it has lower horizontal displacements than the truth. It should be noted that with another initial selection this could be different. Detailed results in the form of the ensemble mean and spread only from EnKF and ES are presented to keep the figures readable - and these represent the best and worst performing methods in Section 3.4.1. For the other experiments (ESMDA(x2e), ESMDA(x4e) and ESMDA(x4d)), only the mean of the displacement ensemble is plotted.

It can be seen from Fig. 3.6 that the mean obtained with EnKF-s, ESMDA(x4e)-s and ESMDA(x4d)-s experiments are very close to the true value. This is because a significant update of the parameters (especially ϕ') is obtained by assimilating the measurements for a shorter period. In the case of ES-s (and ES(x2e)-s), ϕ' overshoots the true value and the posterior of the ES-s (and ESMDA(x2e)-s) estimation has a wider spread than that of the EnKF-s estimation (see Fig. 3.4). The posterior distributions of E_{50}^{ref} are similar for all the assimilation methods and cannot be the main cause of the differences. Due to the difference in ϕ' estimation, the displacement ensembles produced by the ES-s (and ESMDA(x2e)-s) estimated parameters have a wider spread and compare not as favourably to the true displacement as the other posterior distributions. Furthermore, ES-s and ESMDA(x2e)-s show a larger displacement magnitude than the truth and EnKF-s because they underestimate the strength (ϕ') as compared to the EnKF-s estimation.

Fig. 3.7 presents the displacement ensemble with estimated parameters after assim-

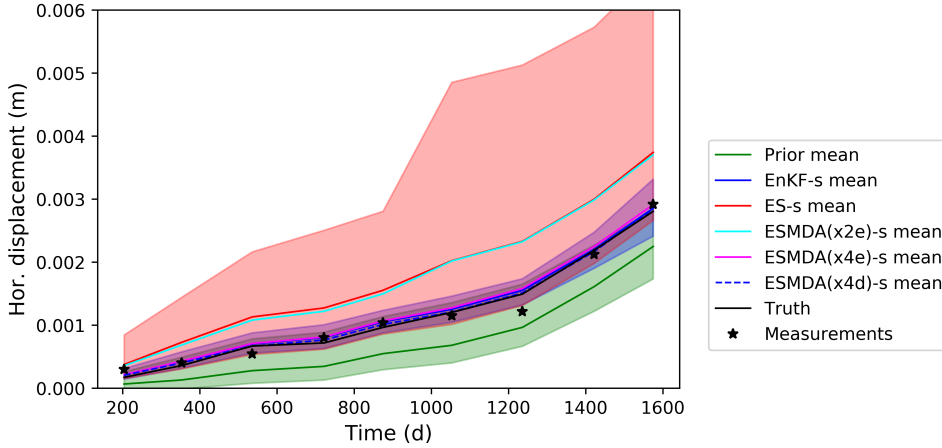


Figure 3.6: Data assimilation estimate of the horizontal displacement at point G on the slope based on true, prior and estimated parameters with EnKF-s, ES-s, ESMDA(x2e)-s, ESMDA(x4e)-s and ESMDA(x4d)-s. The EnKF-s, ESMDA(x4e)-s and ESMDA(x4d)-s means are overlapping. Furthermore, the mean of ES-s and ESMDA(x2e)-s are also overlapping.

ilating measurements for a longer period. It can be seen that for the ES-l (ESMDA(x2e)-l) case the posterior ensemble spread of the displacements is slightly reduced as compared to its posterior as illustrated in Fig. 3.6. As measurements are assimilated for a longer period, the ensemble means of ES-l and ESMDA(x2e)-l move towards the true model evolution. The reason for this can be that further data assimilation resulted in a notable improvement of E_{50}^{ref} and a furthermore minor improvement in ϕ' . This improvement is not easily observed for the EnKF-l, ESMDA(x4e)-l and ESMDA(x4d)-l ensemble prediction of deformation, which have already experienced relatively large updates in the first few assimilation steps.

3.4.3. FACTOR OF SAFETY ESTIMATION

Obtaining an accurate estimate of the FoS is the ultimate goal of this study. As the true distribution of the FoS is not defined, a narrow distribution, i.e., a precise estimate, of the FoS is not necessarily the best result. The FoS estimation is computed by using true parameters, prior parameters and estimated posterior parameters by EnKF, ES, ESMDA, ESMDA(x2e), ESMDA(x4e) and ESMDA(x4d). Again, the estimated parameters from shorter and longer assimilation periods are used, with the FoS evaluated in both cases at the end time, after 1575 days.

Fig. 3.8 shows the FoS at the end of the simulation time, based on the estimated parameters obtained by assimilating the measurement for the shorter period. It can be seen from Fig. 3.8 that the FoS with prior parameters results in a distribution with mean ($\mu_{f_{os}} = 1.48$) and standard deviation ($\sigma_{f_{os}} = 0.11$). The true FoS falls within this distribution, yet is significantly lower than the mean FoS calculated using the prior distri-

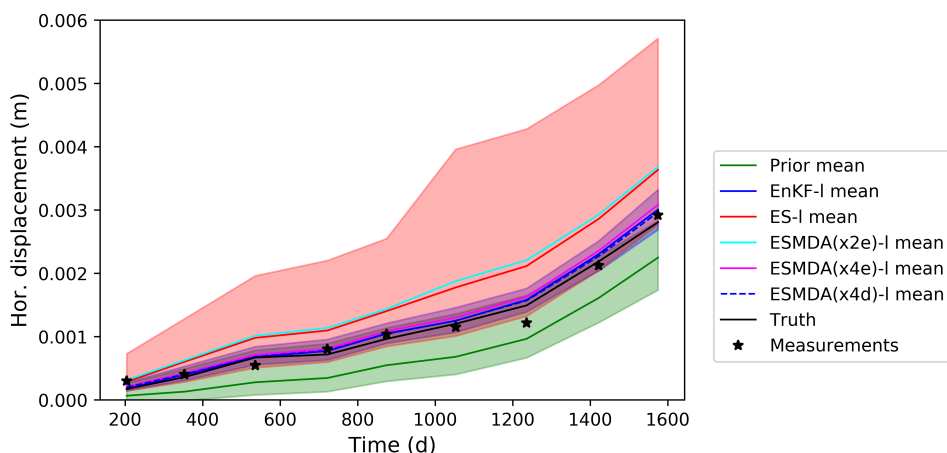


Figure 3.7: Data assimilation estimate of the horizontal displacement at point G on the slope based on true, prior and estimated parameters with EnKF-I, ES-I, ESMDA(x2e)-I, ESMDA(x4e)-I and ESMDA(x4d)-I. The EnKF-I, ESMDA(x4e)-I and ESMDA(x4d)-I means are overlapping. Furthermore, the mean of ES-I and ESMDA(x2e)-I are also overlapping.

tribution. The true FoS and prior FoS are computed with true and prior parameters by using the strength reduction method. The FoS estimation is considered to be best if it is close to true FoS (accurate). The FoS obtained with EnKF-s is both more accurate and has a smaller standard deviation than ESMDA(x4e)-s, ESMDA(x4d)-s, ESMDA(x2e)-s and ES-s. ES-s and ESMDA(x2e)-s give approximations that are less accurate than the other methodologies. This FoS estimation can be explained by the estimation of parameters, especially ϕ' , as the FoS is calculated by the strength reduction method in which ϕ' has a significant contribution.

Fig 3.9 illustrates FoS at the end of the simulation time, based on the estimated parameters obtained by assimilating the measurement for the longer period. The result is very similar to the one presented in Fig. 3.8. This is because the FoS depends mostly on the shear strength parameters and has only a slight dependence on stiffness parameters. There is not a significant improvement in the estimation of ϕ' by assimilating measurements after a shorter period.

3.4.4. COMPUTATION TIME

For a practical application of the workflow presented in this study, the computation time of the data assimilation is important, i.e., the computation time of both the forward analyses and the data assimilation steps. So, we divide the framework into two parts i.e. (i) forward model runs (ii) data assimilation steps. In this research, the forward model (FEM analysis) is more computationally expensive than the data assimilation part. EnKF is a sequential data assimilation method in which measurements are assimilated whenever they are available and the forward model is re-run with the resulting estimated parameters. In ES, the forward model is run only two times: once with prior parameters and once more with estimated parameters. In ESMDA, the forward model is run for N_{mda}

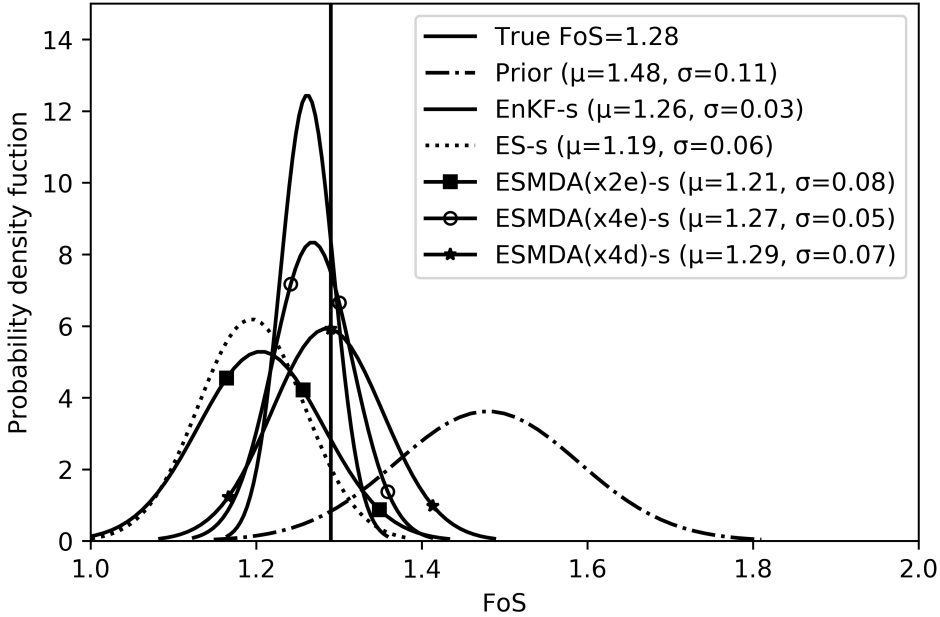


Figure 3.8: Probability distribution of the FoS at the end time (after 1575 days) based on true parameters, prior parameters and estimated parameters with EnKF-s, ES-s, ESM DA(x2e)-s, ESM DA(x4e)-s and ESM DA(x4d)-s.

times during the assimilation and lastly with the estimated parameters. Table 3.4 shows that the EnKF needs more forward runs ($N_{da} + 1 = 10$) than ESM DA(x4) ($N_{mda} + 1 = 5$) and ES ($=2$). The forward runs in EnKF have variable simulation times (they run until the next measurement is available), but this has a limited impact as the initial solution of the equations takes the majority of the simulation time. On top of that, the number of data assimilation steps is also higher for the EnKF, followed by ESM DA(x4) and ES. Based on this, the EnKF is theoretically the most computationally expensive followed by ESM DA(x4d and e) and then ES.

Table 3.4: Breakdown of computation time for different schemes for one ensemble member (N_{da} = data assimilation steps, N_{mda} =multiple data assimilation)

Methodology	forward model runs	data assimilation steps
EnKF	$N_{da} + 1$	N_{da}
ES	2	1
ESMDA	$N_{mda} + 1$	N_{mda}

A complicating factor is that the FEM software used in this study delivers output at intermediate steps but is not able to do so at predefined data assimilation steps, without re-initialising a calculation, i.e., resolving a linear system of equations. (Note, this is

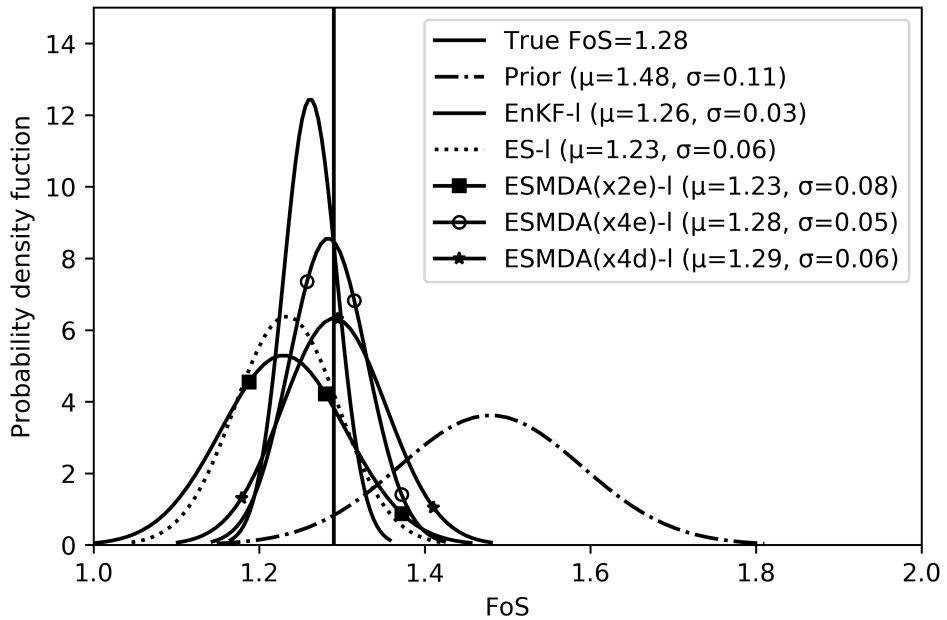


Figure 3.9: Probability distribution of the FoS at the end time (after 1575 days) based on true parameters, prior parameters and estimated parameters with EnKF-I, ES-I, ESMDA(x2e)-I, ESMDA(x4e)-I and ESMDA(x4d)-I

not the same as restarting the whole analysis, as a staged construction approach is available where results from a previous step can be used in a subsequent one). Therefore, the smoothers are more computationally expensive in practice than in theory. In Fig. 3.10, the total simulation time for each of the methods considered, normalised to the ES simulation time. The results show that in our implementation EnKF is 1.43 times more computationally expensive than ES. The other methods take ≈ 1.6 times (ESMDA(x2e)), ≈ 2.9 times (ESMDA(x4e)) and ≈ 2.6 times (ESMDA(x4d)) more simulation time than ES.

3.5. DISCUSSION

There are four important points that can be discussed based on this study and its future directions. Firstly, the data assimilation methods (especially EnKF, ESMDA(x4e) and ESMDA(x4d)) give promising results for reliable parameter estimation, displacement estimation and FoS estimation. The EnKF provides better estimates of parameters, state and FoS than the other schemes. This can be due to the reason that the EnKF deals relatively well with weakly non-linear models and/or its recursive nature of sequential assimilation. In the EnKF as implemented in this study, we are sequentially updating the parameters at each assimilation step and re-rerun the model with estimated parameters. Sequential parameter estimation in a realistic case, i.e., in a case of an imperfect model where model and observations may not be fully consistent, may however cause inconsistency between the analysis and the observations in the intermediate steps of

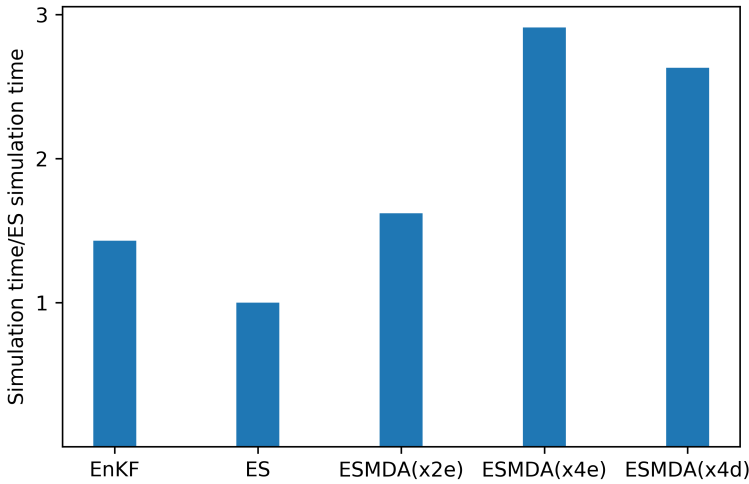


Figure 3.10: Computation performance for different data assimilation methods in the present setup of data assimilation.

the model, where the early data may match the prediction less well than at the end of the simulation. In the case where a model is not perfect, for example because it does not include all processes (e.g., creep), this imperfect match would probably not hamper the forecast of the model into the immediate future. Building on this observation, poorly matching initial data may eventually be used to detect and analyse model error. The ES and ESMDA(x2e) are shown to perform less well than the EnKF and ESMDA(x4e). For the longer assimilation window, ES estimated the model parameters better than for the shorter assimilation window, with the added advantage of using the least computation time compared to the other schemes investigated here. This can be due to the reason that the ES is not designed to perform with a non-linear model. The other methods such as ESMDA(x4e) and ESMDA(x4d) give good results, using all of the measurements at the same time. The resulting evolution of deformation can be considered more physically representative and consistent with the slope having the same material (behaviour) throughout. The results suggest that in comparison to ES, the MDA steps in ESMDA provide corrections for the linear approximation of ES when applied to a non-linear model. The ESMDA performance can be enhanced by choosing more iterations (MDA steps) as we have seen in our experiments by comparing ESMDA(x2e) and ESMDA(x4e). It can be seen further that the choice of α values (in ESMDA) does not make a significant difference in our study perhaps due to the nature of the perfect model experiment (synthetic twin). Furthermore, better approximations of parameter, state and FoS can be achieved by assimilating the measurements for a longer period compared to a shorter period.

Secondly, it is difficult to assimilate the measurements in an imperfect model. By doing so, one may get unrealistic estimates of parameters. Such unrealistic parameter estimates will not be able to provide improved estimations of the state of the system. Therefore, it is advised to consider the important physical processes in the numerical

model simulations (or consider the representation errors in the model) so that the numerical model prediction qualitatively matches that of the measurement trend before the assimilation. This may also affect the choice of assimilation method. The smoothers attempt to match the data throughout the simulation time, whereas the EnKF assimilates the data sequentially and therefore allows the simulation -especially when the model is imperfect- to progressively drift away from the measurements at early times as the simulation continues. This implies that to use smoothers there is a higher requirement for the model to well represent all processes, or to explicitly account for model error in the data assimilation formulation. Naturally, a better representation of all processes will lead to a higher confidence in the model forecast, especially at longer terms.

Thirdly, having a forward model software which can calculate solutions at prescribed timesteps and extract results at specified intermediate steps can improve the computation performance of smoothers. It could be further investigated how interpolation would allow the performance to be improved while resulting in effective assimilation.

Fourthly, this study is limited to a homogeneous slope. One may test these data assimilation methodologies by considering the spatial variability in the slope domain, frequency of measurements, and the period with available measurements.

3.6. CONCLUSION

In this chapter, different data assimilation schemes namely EnKF, ES, and ESMDA are implemented to estimate selective constitutive model parameters (i.e., E_{50}^{ref} and ϕ') in a slope stability system. These estimated parameters are then used to estimate the state and FoS of the system. The results of a synthetic twin experiment show that the EnKF estimates an FoS that is close to the true FoS with a small standard deviation. ES provides a physically consistent displacement state estimation at relatively low computational costs. It provides reasonably realistic parameter values, especially for longer assimilation periods (see in Fig. 3.5). However, the displacement and FoS estimates of ES are less accurate than those of the other schemes, regardless of the length of the period (Figs. 3.6 and 3.7). ESMDA, a smoother with four iterative assimilation steps, also estimates an FoS close to the truth with a distribution that has a higher standard deviation. ES and ESMDA (with two iterative assimilations) are not able to reconstruct the true FoS very well but they provide a physical consistent estimate. The theoretical computation time required by the ES is the smallest, followed by ESMDA with two iterative assimilation steps, ESMDA with four assimilation steps, and the EnKF. Due to some forward model limitations in the commercial software used (i.e., PLAXIS cannot output the results at specific data assimilation steps without additional computations to resolve the system of equations), ESMDA needs relatively more computation time than the EnKF and ES.

REFERENCES

- Aanonsen, S. I., Nævdal, G., Oliver, D. S., Reynolds, A. C., & Vallès, B. (2009). The ensemble Kalman filter in reservoir engineering—a review. *SPE Journal*, 14(3), 393–412. <https://doi.org/10.2118/117274-PA>
- Bertino, L., Evensen, G., & Wackernagel, H. (2003). Sequential data assimilation techniques in oceanography. *International Statistical Review*, 71(2), 223–241. <https://doi.org/10.1111/j.1751-5823.2003.tb00194.x>
- Burgers, G., van Leeuwen, P. J., & Evensen, G. (1998). Analysis scheme in the ensemble Kalman filter. *Monthly Weather Review*, 126(6), 1719–1724. [https://doi.org/10.1175/1520-0493\(1998\)126<1719:ASITEK>2.0.CO;2](https://doi.org/10.1175/1520-0493(1998)126<1719:ASITEK>2.0.CO;2)
- Chen, Y., & Zhang, D. (2006). Data assimilation for transient flow in geologic formations via ensemble Kalman filter. *Advances in Water Resources*, 29(8), 1107–1122. <https://doi.org/10.1016/j.advwatres.2005.09.007>
- Ching, J., & Phoon, K.-K. (2015). Reducing the transformation uncertainty for the mobilized undrained shear strength of clays. *Journal of Geotechnical and Geoenvironmental Engineering*, 141(2), 04014103. [https://doi.org/10.1061/\(ASCE\)GT.1943-5606.0001236](https://doi.org/10.1061/(ASCE)GT.1943-5606.0001236)
- Emerick, A. A. (2016). Analysis of the performance of ensemble-based assimilation of production and seismic data. *Journal of Petroleum Science and Engineering*, 139, 219–239. <https://doi.org/10.1016/j.petrol.2016.01.029>
- Emerick, A. A., & Reynolds, A. C. (2012). History matching time-lapse seismic data using the ensemble kalman filter with multiple data assimilations. *Computational Geosciences*, 16(3), 639–659. <https://doi.org/10.1016/j.petrol.2016.01.029>
- Emerick, A. A., & Reynolds, A. C. (2013). Ensemble smoother with multiple data assimilation. *Computers & Geosciences*, 55, 3–15. <https://doi.org/10.1016/j.cageo.2012.03.011>
- Evensen, G. (1994). Sequential data assimilation with a nonlinear quasi-geostrophic model using Monte Carlo methods to forecast error statistics. *Journal of Geophysical Research: Oceans*, 99(C5), 10143–10162. <https://doi.org/10.1029/94JC00572>
- Evensen, G. (2009). *Data assimilation: The ensemble Kalman filter*. Springer Science & Business Media.
- Evensen, G. (2018). Analysis of iterative ensemble smoothers for solving inverse problems. *Computational Geosciences*, 22(3), 885–908. <https://doi.org/10.1007/s10596-018-9731-y>
- Evensen, G., Amezcuca, J., Bocquet, M., Carrassi, A., Farchi, A., Fowler, A., Houtekamer, P. L., Jones, C. K., de Moraes, R. J., Pulido, M., et al. (2021). An international initiative of predicting the sars-cov-2 pandemic using ensemble data assimilation. *Foundations of Data Science*, 3(3). <https://doi.org/10.3934/fods.2021001>

- 3
- Evensen, G., & Eikrem, K. S. (2018). Conditioning reservoir models on rate data using ensemble smoothers. *Computational Geosciences*, 22(5), 1251–1270. <https://doi.org/10.1007/s10596-018-9750-8>
- Evensen, G., Vossepoel, F. C., & van Leeuwen, P. J. (2022). *Data assimilation fundamentals: A unified formulation of the state and parameter estimation problem*. Springer Nature. <https://doi.org/10.1007/978-3-030-96709-3>
- Glegola, M. A., Ditmar, P., Hanea, R. G., Vossepoel, F. C., Arts, R., & Klees, R. (2012). Gravitometric monitoring of water influx into a gas reservoir: A numerical study based on the ensemble Kalman filter. *SPE Journal*, 17(1), 163–176. <https://doi.org/10.2118/149578-PA>
- Houtekamer, P. L., & Mitchell, H. L. (2005). Ensemble Kalman filtering. *Quarterly Journal of the Royal Meteorological Society: A Journal of the Atmospheric Sciences, Applied Meteorology and Physical Oceanography*, 131(613), 3269–3289. <https://doi.org/10.1256/qj.05.135>
- Janjić, T., Bormann, N., Bocquet, M., Carton, J., Cohn, S., Dance, S. L., Losa, S., Nichols, N. K., Potthast, R., Waller, J. A., et al. (2018). On the representation error in data assimilation. *Quarterly Journal of the Royal Meteorological Society*, 144(713), 1257–1278. <https://doi.org/10.1002/qj.3130>
- Kalman, R. E. (1960). A new approach to linear filtering and prediction problems. *Journal of Basic Engineering*, 82(1), 35–45. <https://doi.org/10.1115/1.3662552>
- Keppenne, C. L., & Rienecker, M. M. (2003). Assimilation of temperature into an isopycnal ocean general circulation model using a parallel ensemble Kalman filter. *Journal of Marine Systems*, 40, 363–380. [https://doi.org/10.1016/S0924-7963\(03\)00025-3](https://doi.org/10.1016/S0924-7963(03)00025-3)
- Liu, K., Vardon, P. J., & Hicks, M. A. (2018). Sequential reduction of slope stability uncertainty based on temporal hydraulic measurements via the ensemble Kalman filter. *Computers and Geotechnics*, 95, 147–161. <https://doi.org/10.1016/j.compgeo.2017.09.019>
- Maucec, M., De Matos Ravanelli, F. M., Lyngra, S., Zhang, S. J., Alramadhan, A. A., Abdelhamid, O. A., & Al-Garni, S. A. (2016). Ensemble-based assisted history matching with rigorous uncertainty quantification applied to a naturally fractured carbonate reservoir. *SPE Annual Technical Conference and Exhibition*. <https://doi.org/10.2118/181325-MS>
- Mavritsakis, A. (2017). Evaluation of inverse analysis methods with numerical simulation of slope excavation. *MSc thesis, Delft University of Technology, Netherlands*.
- Mohsan, M., Vardon, P. J., & Vossepoel, F. C. (2021). On the use of different constitutive models in data assimilation for slope stability. *Computers and Geotechnics*, 138, 104332. <https://doi.org/10.1016/j.compgeo.2021.104332>
- Mohsan, M., Vardon, P. J., & Vossepoel, F. C. (2023). Options for the implementations of data assimilation for geotechnics. *International Conference of the International Association for Computer Methods and Advances in Geomechanics*, 255–262. https://doi.org/10.1007/978-3-031-12851-6_31
- Mohsan, M., Vossepoel, F. C., & Vardon, P. J. (2024). On the use of different data assimilation schemes in a fully coupled hydro-mechanical slope stability analysis.

- Georisk: Assessment and Management of Risk for Engineered Systems and Geohazards*, 18(1), 121–137. <https://doi.org/10.1080/17499518.2023.2258607>
- Nævdal, G., Mannseth, T., & Vefring, E. H. (2002). Near-well reservoir monitoring through ensemble Kalman filter. *SPE/DOE Improved Oil Recovery Symposium*, (SPE 75235). <https://doi.org/10.2118/75235-MS>
- Oliver, D. S., & Chen, Y. (2011). Recent progress on reservoir history matching: A review. *Computational Geosciences*, 15(1), 185–221. <https://doi.org/10.1007/s10596-010-9194-2>
- Phoon, K.-K., & Kulhawy, F. H. (1999a). Characterization of geotechnical variability. *Canadian geotechnical journal*, 36(4), 612–624. <https://doi.org/10.1139/t99-038>
- Phoon, K.-K., & Kulhawy, F. H. (1999b). Evaluation of geotechnical property variability. *Canadian Geotechnical Journal*, 36(4), 625–639. <https://doi.org/10.1139/t99-039>
- Plaxis. (2015). *PLAXIS material models manual*. Plaxis.
- Reichle, R. H., McLaughlin, D. B., & Entekhabi, D. (2002). Hydrologic data assimilation with the ensemble Kalman filter. *Monthly Weather Review*, 130(1), 103–114. [https://doi.org/10.1175/1520-0493\(2002\)130%3C0103:HDAWTE%3E2.0.CO;2](https://doi.org/10.1175/1520-0493(2002)130%3C0103:HDAWTE%3E2.0.CO;2)
- Schanz, T., Vermeer, P., & Bonnier, P. G. (1999). The hardening soil model: Formulation and verification. *Beyond 2000 in computational geotechnics* (pp. 281–296). Routledge.
- Skjervheim, J.-A., & Evensen, G. (2011). An ensemble smoother for assisted history matching. *SPE Reservoir Simulation Symposium*, (SPE-141929-MS). <https://doi.org/10.2118/141929-MS>
- Szunyogh, I., Kostelich, E. J., Gyarmati, G., Patil, D., Hunt, B. R., Kalnay, E., Ott, E., & Yorke, J. A. (2005). Assessing a local ensemble Kalman filter: Perfect model experiments with the National Centers for Environmental Prediction global model. *Tellus A: Dynamic Meteorology and Oceanography*, 57(4), 528–545. <https://doi.org/10.3402/tellusa.v57i4.14721>
- Van der Krogt, M., Schweckendiek, T., & Kok, M. (2019). Uncertainty in spatial average undrained shear strength with a site-specific transformation model. *Georisk: Assessment and Management of Risk for Engineered Systems and Geohazards*, 13(3), 226–236. <https://doi.org/10.1080/17499518.2018.1554820>
- Van Genuchten, M. T. (1980). A closed-form equation for predicting the hydraulic conductivity of unsaturated soils. *Soil Science Society of America Journal*, 44(5), 892–898. <https://doi.org/10.1139/t66-009>
- Van Leeuwen, P. J. (1999). The time-mean circulation in the agulhas region determined with the ensemble smoother. *Journal of Geophysical Research: Oceans*, 104(C1), 1393–1404. <https://doi.org/10.1029/1998JC900012>
- Van Leeuwen, P. J., & Evensen, G. (1996). Data assimilation and inverse methods in terms of a probabilistic formulation. *Monthly Weather Review*, 124(12), 2898–2913. [https://doi.org/10.1175/1520-0493\(1996\)124<2898:DAAIMI>2.0.CO;2](https://doi.org/10.1175/1520-0493(1996)124<2898:DAAIMI>2.0.CO;2)
- Vardon, P. J., Liu, K., & Hicks, M. A. (2016). Reduction of slope stability uncertainty based on hydraulic measurement via inverse analysis. *Georisk: Assessment and Management of Risk for Engineered Systems and Geohazards*, 10(3), 223–240. <https://doi.org/10.1080/17499518.2016.1180400>

- Wang, C., Osorio-Murillo, C. A., Zhu, H., & Rubin, Y. (2017). Bayesian approach for calibrating transformation model from spatially varied CPT data to regular geotechnical parameter. *Computers and Geotechnics*, 85, 262–273. <https://doi.org/10.1016/j.compgeo.2017.01.002>

4

A CASE STUDY OF THE COTTBUS OPEN PIT MINE: USE OF DATA ASSIMILATION AND SURROGATE MODELLING FOR SLOPE STABILITY ANALYSIS

An ensemble smoother (ES) is implemented as a data assimilation scheme for slope stability assessment for an open pit mine in Cottbus, Germany. The LIDAR measurements of the vertical displacements are assimilated into a finite element method (FEM) model with missing physics. The aim of the assimilation is to estimate the model parameters, displacement ensemble and the factor of safety (FoS). The posterior estimation of the FoS is compared with slope failure observed in the field, and ES provides a better estimation than when only using the FEM model (prior estimate). Two surrogate models (named surrogate model-I and II) are then trained and tested with the prior and posterior FEM ensemble of displacements and the FoS, respectively. Both surrogate models are attempted to be validated with the LIDAR measurements and compared with the ground truth of the slope deformation (at failure). The results show that the ES provides a better estimation of the FoS when compared with the field observations, and that the surrogate models perform worse than the data assimilation.

4.1. INTRODUCTION

Cottbus Ostsee (situated in eastern Germany) is an artificial lake that is under development at the location of a decommissioned open pit mine. The decommissioned open pit is the outcome of past lignite mining. This lake is one of the largest artificial lakes in Germany with a surface area of 19 km^2 (see the aerial photo in Fig. 4.1 for an overview of the site). The average depth of the lake is proposed to be 2.5-3 m with a maximum depth of 30 m when it is completely filled.



Figure 4.1: Site overview of the case study. Cottbus Ostsee plan view: with the selected slope (section A-A) for modelling.

The pit is being slowly flooded with river water to create the lake, with water level measurements taken in 20-day intervals from mid-2016 to mid-2020. The displacement of the slopes surrounding the lake has been continuously monitored between mid-2018 to mid-2019 by partners within the i2MON project (<https://i2monproject.eu>), using different remote sensing devices such as LIDAR, InSAR and terrestrial laser scanning (TLS). In this study, the measurements (at locations from 1 to 12 in Fig. 4.2) of vertical displacements are used.

An initial site investigation and slope stability analysis have informed the design. The flooding of the lake (and other possible mechanisms, i.e. meteorological cycle) provides an effective stress change in the system, which leads to a mechanical response, and it is hypothesized that this response can be used to carry out data assimilation (integrating the monitoring observations with the FEM) to calculate the stability of the slopes better. However, the detailed FEM models used to simulate the full physics can be computationally expensive and, therefore, may not be able to provide real-time predictions.

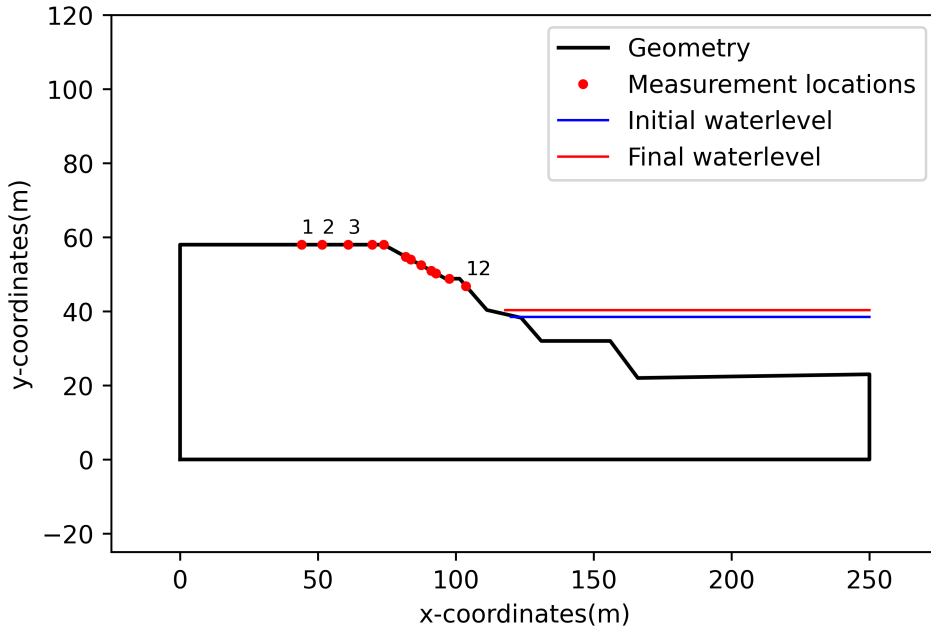


Figure 4.2: Slope geometry of the case study at section A-A (in Fig. 4.1) with measurement locations (1 to 12). The initial and final water levels are also mentioned for the duration of our study.

Thus, this study has been divided into two parts. In the first part, the measurements are utilised in an FEM analysis by using a popular ensemble data assimilation, i.e., the ensemble smoother. ES has been selected as the data assimilation scheme because it offers a physically consistent estimate (using all the data at once) with minimal computational time. In this scheme, the measurements for all time steps have been assimilated in a single step. Through an in-house investigation, it has been seen that the recursive parameter estimation approaches (such as the EnKF) may lead to an unrealistic parameter estimation so ES has been preferred over the other ensemble-based schemes, despite the better performance seen in Chapter 3 where it was shown that the scheme had the ability to reproduce the measured results. This is further discussed in Section 4.4.1. The details of this method have been presented in Chapter 3. In the second part of this study, two surrogate models have also been developed based on the synthetic data (prior and posterior). These two surrogate models have been validated with the actual measurements. Then a comparison has been made between with the ground truth to evaluate the efficacy of both of these techniques (data assimilation and surrogate model).

Due to the high computational cost of physics-based methods (e.g., FEM) in the geotechnical engineering field, many researchers built surrogate models through the use of machine-learning techniques (e.g. Ada & San, 2018; Al-Bittar et al., 2018; Chakraborty & Goswami, 2017; Jamalnia, Tehrani, et al., 2021a; Kang et al., 2015; Mentani et al., 2023; Qi & Tang, 2018; Soubra et al., 2019; Toe et al., 2018; Van den Eijnden et al., 2022; Wang et al., 2023; Wei et al., 2021). Surrogate models relate the model parameters (input) to the

FoS of the slope stability system (output). A range of surrogate modeling techniques are available (e.g., decision tree model, random forest, support vector machine, Gaussian process (GP) regression model, artificial neural network) for geotechnical applications to relate the model parameters with the FoS. Given the relatively good performance of the GP (e.g., Mahmoodzadeh, Mohammadi, Daraei, Ali, et al., 2020; Mahmoodzadeh, Mohammadi, Daraei, Faraj, et al., 2020; Mahmoodzadeh et al., 2021; Van den Eijnden et al., 2022) with limited data, this technique has been used in this research.

GP is a non-parametric machine learning technique which relates the inputs to a target variable and assumes that the target variable follows the Gaussian probability density function. It provides the mean and variance of the predicted target variable. GP can be represented as:

$$f(x) \sim \text{GP}(\mu(x), k(x_1, x_2)) \quad (4.1)$$

where $f(x)$ is the target function, GP denotes the Gaussian process, $\mu(x)$ is the mean of the function and $k(x_1, x_2)$ is the covariance function (the kernel). The kernel defines the correlation between two points (x_1, x_2) .

Assuming a training set $D = (\mathbf{x}_i, f_i), i = 1 : N$ in which $f_i = f(\mathbf{x}_i)$ and a test set \mathbf{X}_* to predict the f_* , the GP can be written as:

$$\begin{pmatrix} \mathbf{f} \\ \mathbf{f}_* \end{pmatrix} \sim \mathcal{N}\left(\begin{pmatrix} \boldsymbol{\mu} \\ \boldsymbol{\mu}_* \end{pmatrix}, \begin{pmatrix} \mathbf{K} & \mathbf{K}_* \\ \mathbf{K}_*^T & \mathbf{K}_{**} \end{pmatrix}\right) \quad (4.2)$$

where $\boldsymbol{\mu}$ and $\boldsymbol{\mu}_*$ are the vectors consisting of the mean of the training and testing data respectively, \mathbf{K} is part of the covariance matrix which represents the covariance of the training data, \mathbf{K}_* represents the covariance of the training and testing data and \mathbf{K}_{**} represents the covariance of the testing data. GP aims to optimize the kernel hyper-parameter to improve the accuracy of model prediction. There are many types of kernels that exist and the Radial Basis Function (RBF) is the most commonly used:

$$k(x, x') = \sigma^2 \exp\left(-\frac{|x - x'|^2}{2l^2}\right), \quad (4.3)$$

where σ^2 and ' l ' are the hyper-parameters which control the amplitude and smoothness of the kernel, respectively.

In this chapter, first the case study and available data are detailed. Then the methodology is detailed showing first the use of a detailed FEM model to make a prior prediction of behaviour, then the development of a surrogate model based on the results of the FEM model (prior and posterior). Following that, the site monitoring data is used to both carry-out data assimilation and validate the surrogate model. The ability to predict the slope Factor of Safety (FoS) is then validated for both methods. A discussion and concluding remarks finish the chapter.

4.2. AVAILABLE DATA

A two-dimensional slope stability system is considered to test the performance of the data assimilation scheme and surrogate model. The geometry of the slope is shown in Fig. 4.2 with a maximum slope height of around 40m. On the slope side, the pit is flooded

with river water to create the lake. Water level measurements were taken in 20-day intervals from mid-2016 to mid-2020. Due to flooding, the effective stress of the slope is changed and hence the slope mass deforms. For the flooding, the water level rise between mid-2018 to mid-2019 is considered and shown in Fig. 4.3. The water level before mid-2018 is assumed as the initial water level (Fig. 4.2). This is because measurements of vertical displacements are available between mid-2018 to mid-2019 and hence can be assimilated consistently with the water level.

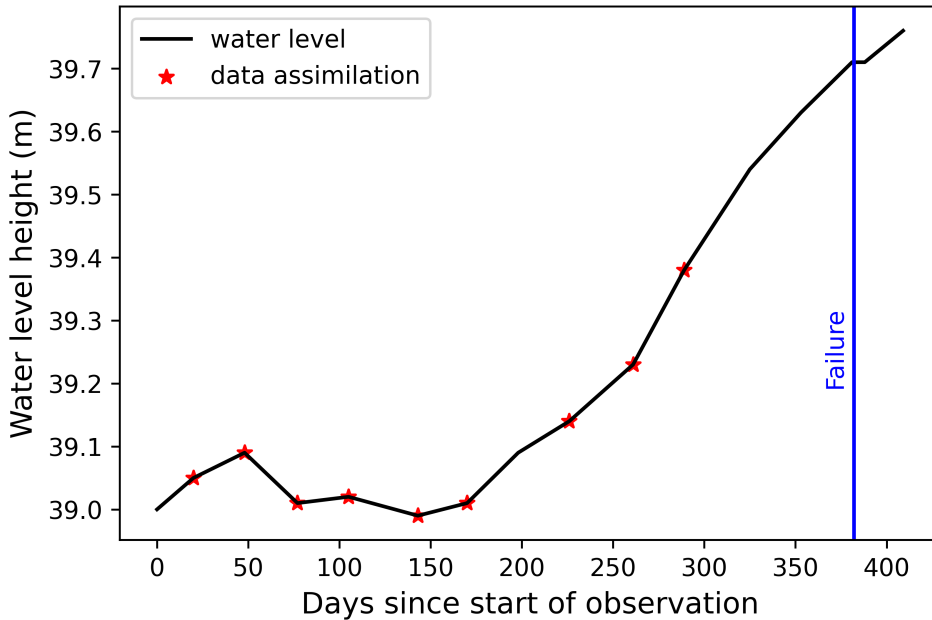


Figure 4.3: Water level rise in the lake. The red stars are dates when the data assimilation is performed.

The slope response in the form of vertical deformation at the crest and slope is measured with LIDAR, with the vertical deformation measurements shown in Fig. 4.4, with the deformation being the incremental deformation after time zero (20th March 2018). The vertical deformation is due to the water level rise and other meteorological processes. It can be seen from Fig. 4.4 that the slope shows settlement and heave at different times. It can be presumed further from these measurements that settlement and heave might be due to the typical seasonal meteorological processes. Since these weather related soil processes are not explicitly represented in the FEM model, the estimation will not capture the effects of these processes. In this chapter, these processes will be referred to as "missing physics" or "missing physical processes". Unfortunately, detailed meteorological data was not available and hence it was decided to attempt to see whether data assimilation could cope with the missing physical processes in the FEM model. To incorporate the missing physics in data assimilation, it can be formulated as follows:

$$\mathbf{y} = g(\mathbf{z}) + \mathbf{q}, \quad (4.4)$$

where y is a vector of model output at measurement locations, z is a combined state-parameter vector, g is the model operator which maps the prior state-parameter vector into measurement space. q is the model error which represents the unresolved processes or missing physics in the forward model. For our forward model, the meteorological processes, time-dependent soil behaviour (creep and viscosity) and consolidation processes are missing physics that have not been considered.

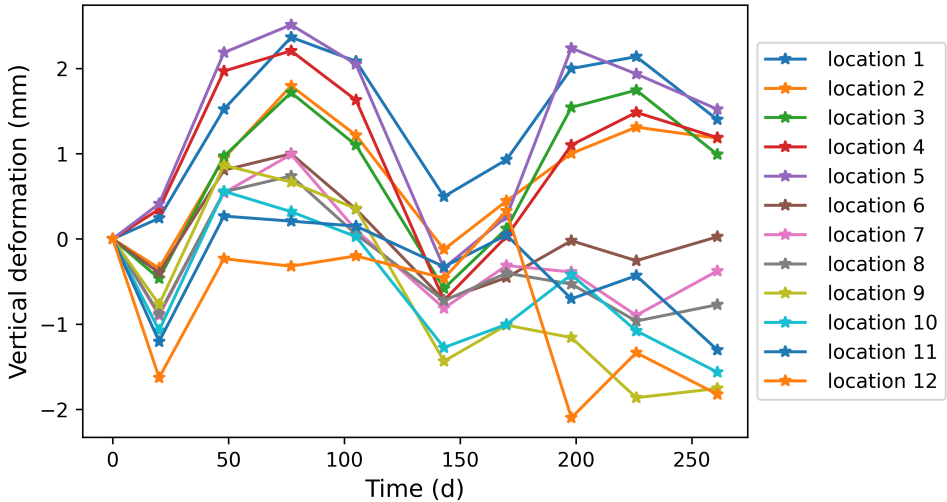


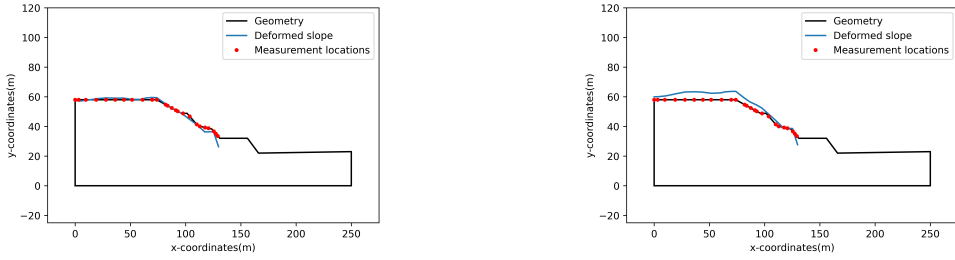
Figure 4.4: Measurements of the vertical displacement at locations 1 to 12

To determine the slope failure, deformed profiles of the slope at different times have been investigated (as shown in Fig. 4.5). The figure illustrates the progressive deformation and allow a determination of the slope failure point. From the animations, it can be concluded that the slope is progressively deforming and local failure is observed when the water level is raised to 39.7 m after 381 days. At this moment, the FoS is known to be equal to one. Initially, the slope is stable ($FoS > 1$) and by raising the water level the FoS reduces ($FoS \rightarrow 1$) and ultimately shows failure ($FoS \approx 1$) at a water level of 39.7 m. The $FoS \approx 1$ value indicates slope failure and can be used as ground truth to validate the results of the FEM model, data assimilation and surrogate model.

4.3. METHODOLOGY

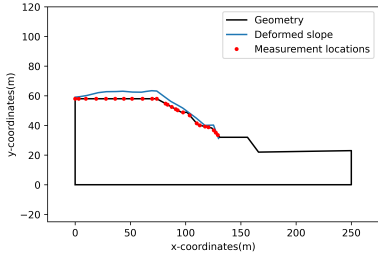
The overall methodology is divided into three main parts, as show in Figs. 4.6 and 4.7: (i) data assimilation workflow using the displacement measurements, (ii) surrogate model development and (iii) surrogate model validation.

In the data assimilation workflow, initially, a set of thirty HS model prior parameters (E_{50}^{ref}, ϕ') form the basis for the randomly generated ensemble (Table 4.1). For each ensemble member, hydro-mechanical and stability FEM analyses are conducted to compute the prior estimates. This prior estimate includes the displacements (at the same 12 locations as measurements as in Fig. 4.2) and FoS for all timesteps from mid-2018 to



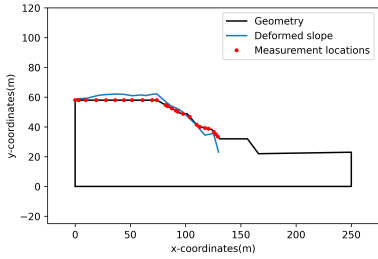
(a) At 48 days

(b) At 105 days



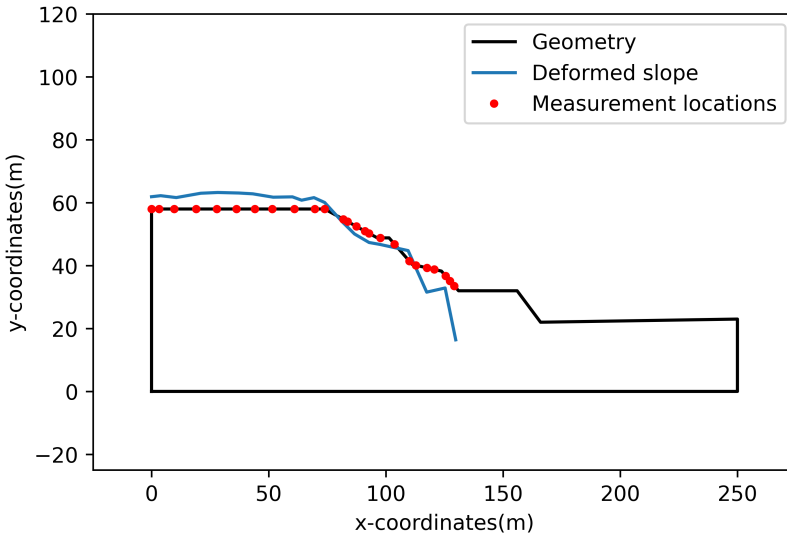
(c) At 198 days

(d) At 261 days



(e) at 325 days

(f) At 353 days



(g) At 381 day (local failure)

Figure 4.5: Progressive failure of the slope, the deformed slope geometry shows deformations exaggerated 1000 times.

Table 4.1: Model parameters from CPT

Parameters	Values	Units
Friction angle (ϕ)	$\mu=34.63, \sigma=1.66$	$^{\circ}$
Cohesion (c)	0-5	kPa
Dilatancy angle (ψ)	0	$^{\circ}$
Young's modulus (E)	$\mu=26366, \sigma=5823$	kPa
E_{50}^{ref}	$0.6 * E$	kPa
E_{oed}^{ref}	$\approx E_{50}^{ref}$	kPa
E_{ur}^{ref}	$\approx 3E_{50}^{ref}$	kPa
Poisson's ratio for unloading/reloading (ν_{ur})	0.2	-
Power (m)	0.5	-
Unsaturated unit weight (γ_d)	16.5-18.0	kN/m ³
Saturated unit weight (γ_s)	18.0-19.5	kN/m ³
Hydraulic conductivity ($k_x = k_y$)	0.12	m/day

mid-2019. For the FEM analysis, variable hydraulic boundaries have been chosen according to Fig. 4.3, with a steady state analysis forming the start point at day zero. Other parameters of the HS model (as shown in Table 4.1) are fixed given the lower sensitivity of the displacement for these parameters. Displacement measurements are assimilated by using ES to estimate the parameters of the ensemble members. The FoS is not a measurable parameter, unless it is 1 (i.e. the slope is failing), and therefore cannot be used in the data assimilation. It is however, the key required output of the data assimilation process. Based on the updated set of parameters for each ensemble member, FEM analysis is again conducted to estimate the posterior. This posterior consists of the displacement and the FoS for each ensemble member. The details of the FEM analysis including the HS model and the ES have been presented in Sections 2.2.1 and 3.2.2, respectively.

In the surrogate model development step, the GP-based surrogate model is trained and tested based on the prior and posterior estimates of the above data assimilation experiment. This model trained on the prior estimates is referred to as surrogate model I and the one trained on the posterior estimates as surrogate model II. These surrogate models relate the vertical displacements (at the 12 locations as measurements as in Fig. 4.2) and the FoS for each realisation.

The third and final step includes validating the surrogate models against the original measurements. In this step, LIDAR measurements of vertical displacements at twelve locations are considered the input and their corresponding FoS the output of these surrogate models.

The predicted FoS from the surrogate model is compared with the FoS computed by ES to determine the efficiency of the surrogate model. The accuracy of the surrogate model during the training, testing, and validation stage was studied with the squared error indicator (R^2)

$$R^2 = 1 - \frac{\sum_{i=1}^n (FoS_i - \hat{FoS}_i)^2}{\sum_{i=1}^n (FoS_i - \bar{FoS})^2}, \quad (4.5)$$

where n is the total number of data points presented in the dataset, FoS_i is the i^{th} value

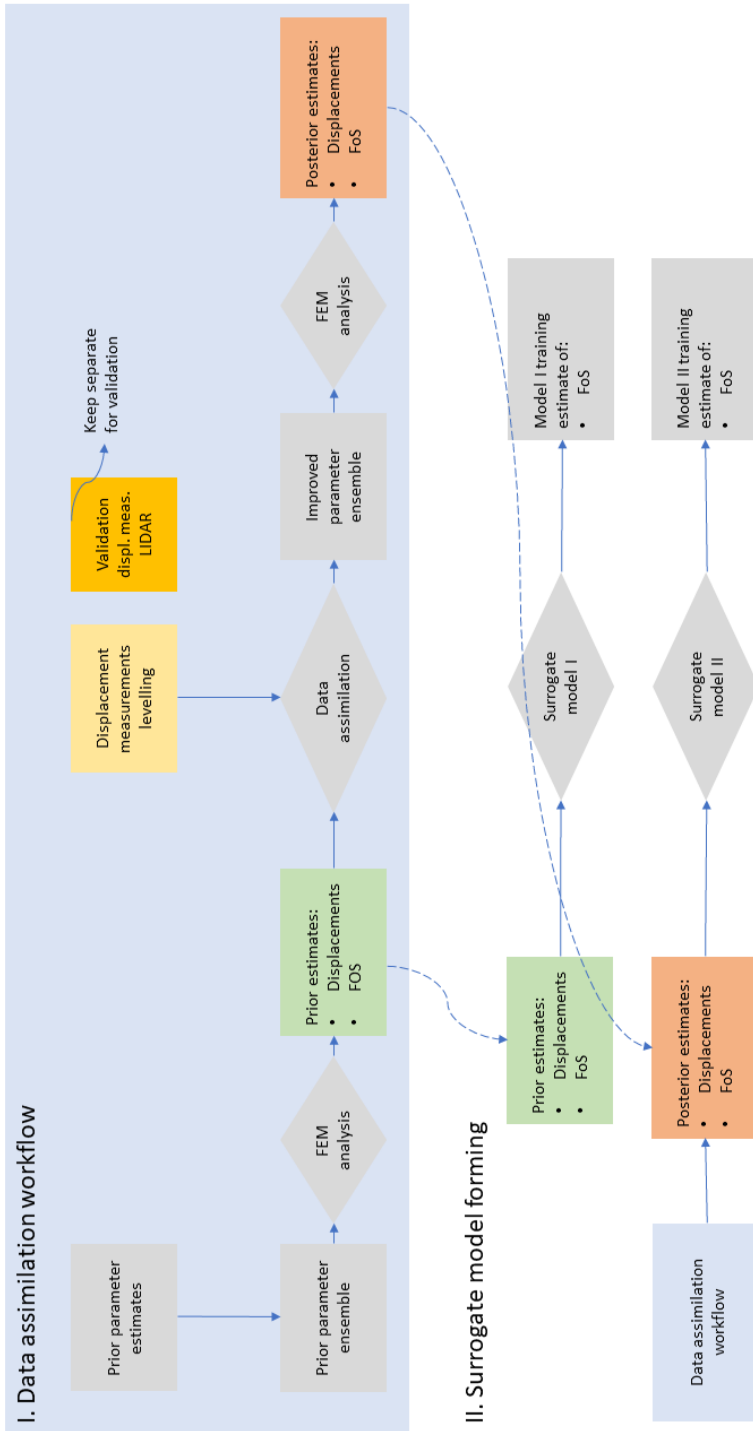


Figure 4.6: Framework of the methodology

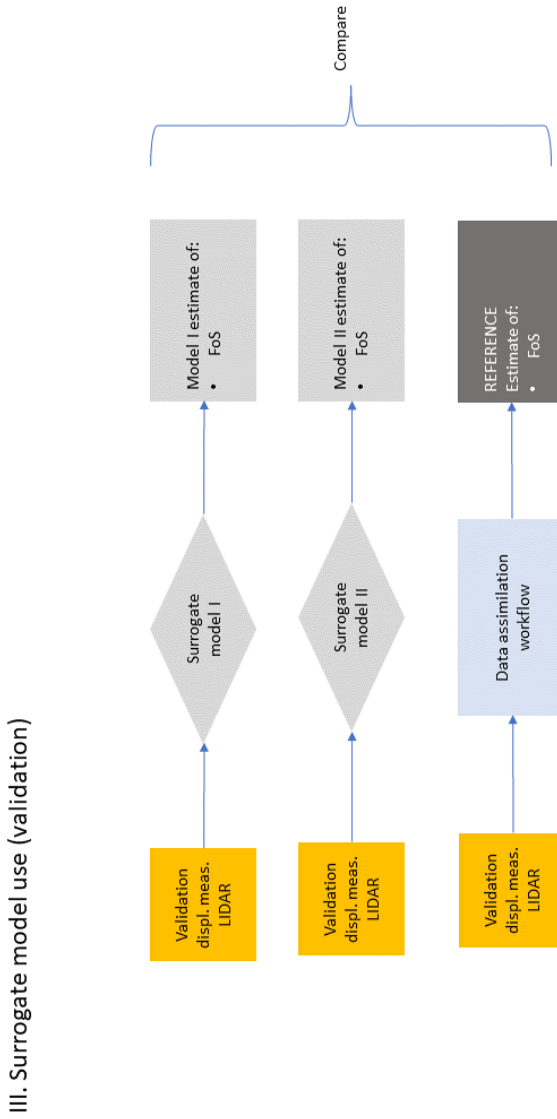


Figure 4.7: Framework of the methodology

of the FoS computed by FEM, $F\hat{o}S_i$ is the GP predicted value of FoS, $F\bar{o}S$ is the mean of the FEM estimated FoS for the given dataset. An R^2 of 1 indicates that the model is perfect and an R^2 of 0 indicates that it has no performance.

4.4. RESULTS AND DISCUSSION

In this section, the results of ES for parameter estimation, displacement ensemble estimation and FoS estimation are first shown. Following that, the results for the surrogate models are presented.

4.4.1. DATA ASSIMILATION RESULTS

The data assimilation results are evaluated based on the parameter estimation (E_{50}^{ref} , ϕ'), the vertical displacement estimation, and finally the FoS estimation. The displacements have field data that can be compared throughout time, which provides the ability to check how the model performs throughout the simulation and is the data used for the assimilation, therefore can provide a comparison as to whether the model is able to simulate the field behaviour. The parameters can be assessed in order to assess whether they are reasonable and whether the data assimilation is performing as expected and finally, the FoS has a single point in time whether the value is known (i.e., when the slope collapses) and provides another opportunity to investigate the model outcome.

Fig. 4.8 shows the prior and posterior estimation of E_{50}^{ref} . It can be seen that the prior ensemble has a wider distribution than the posterior ensemble. This is due to the reason that the ES assimilates measurements and hence finds the updated estimation E_{50}^{ref} with reduced variance. While some data points fall outside the resulting distribution, the majority were also already outside the distribution, and it is therefore likely that the sensitivity of the parameter to those points is low, i.e. the DA cannot improve them. This is most likely a consequence of using ES, where a physically consistent set a parameters considering all data is used. Fig. 4.9 shows the prior and posterior distribution of ϕ' . It can be seen that the posterior shows a lower mean of ϕ' than the prior due to assimilation. Both of these results suggest that the ES algorithm gives updated parameters that are more likely to reproduce the measurements.

The ensemble of displacement results at the measurement locations at the measurement times are shown in in Fig. 4.10. The displacements at day zero are all zero and therefore are not displayed. It can be noted from Fig. 4.10 that the measurements at the different locations show different characteristics. At a few locations (locations 1, 2, 3, 4, 5, 6, 7, which are at the slope crest and the top of the slope) they lie away from the prior ensemble, and the assimilation removes the realisations furthest away from the measurements, but does not significantly move the mean towards the measurements. For the remaining locations (locations 8, 9, 10, 11, 12, which are at the lower parts of the slope), the measurements are generally within the prior realisations, and the assimilation mean moves towards the measurements and reduces in spread.

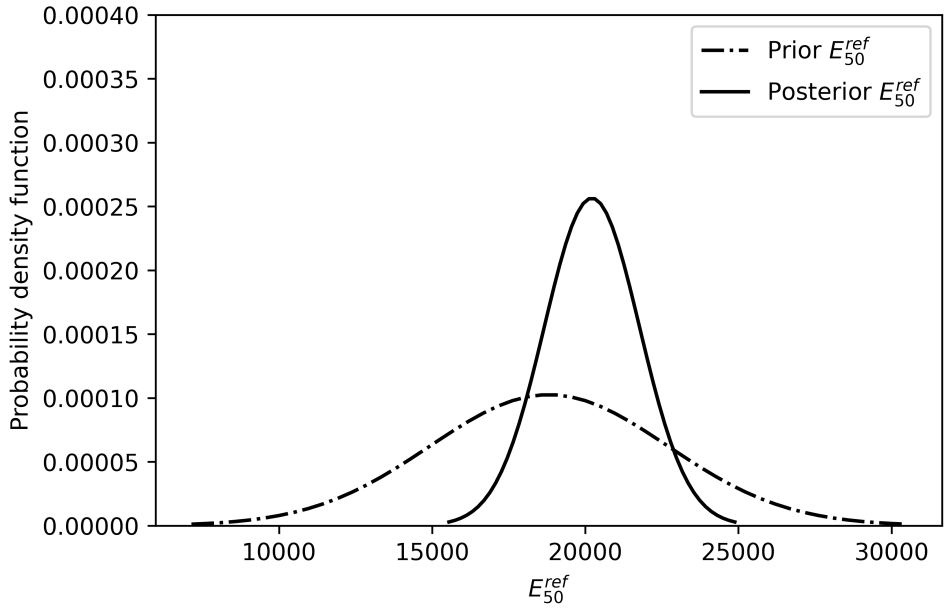


Figure 4.8: Estimation of E_{50}^{ref} by ES

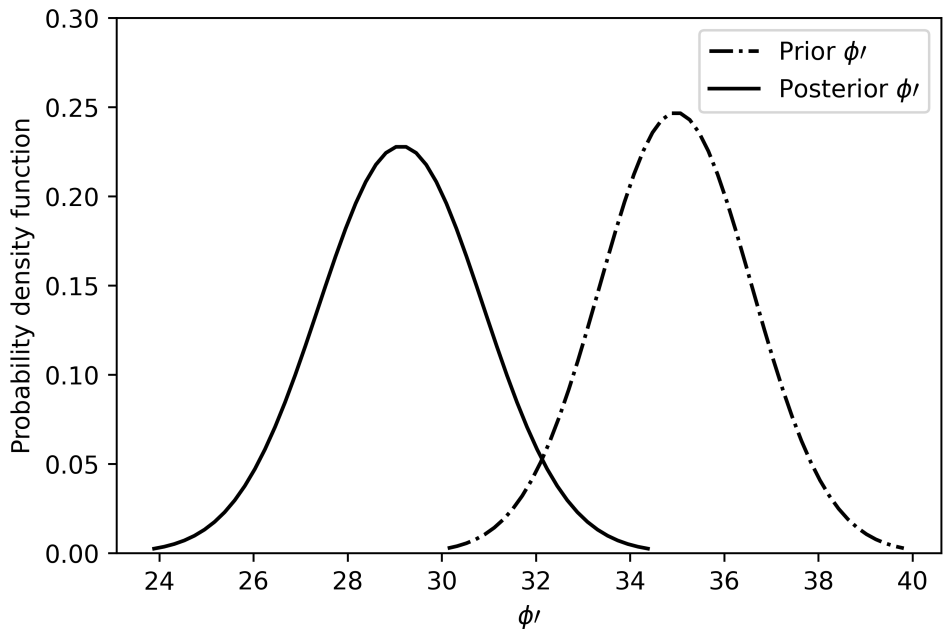


Figure 4.9: Estimation of ϕ' by ES

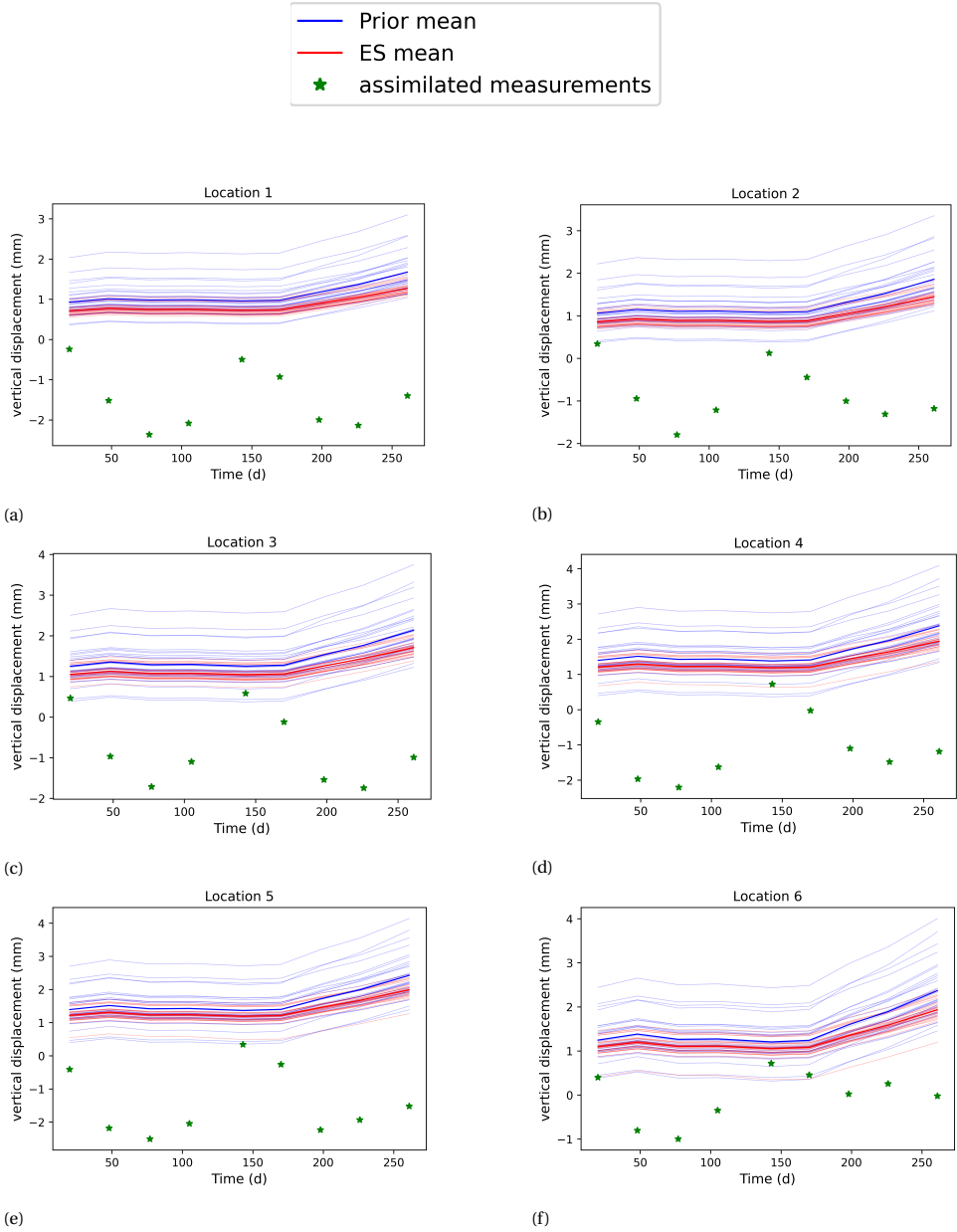


Figure 4.10: Displacement ensemble estimation at the slope locations

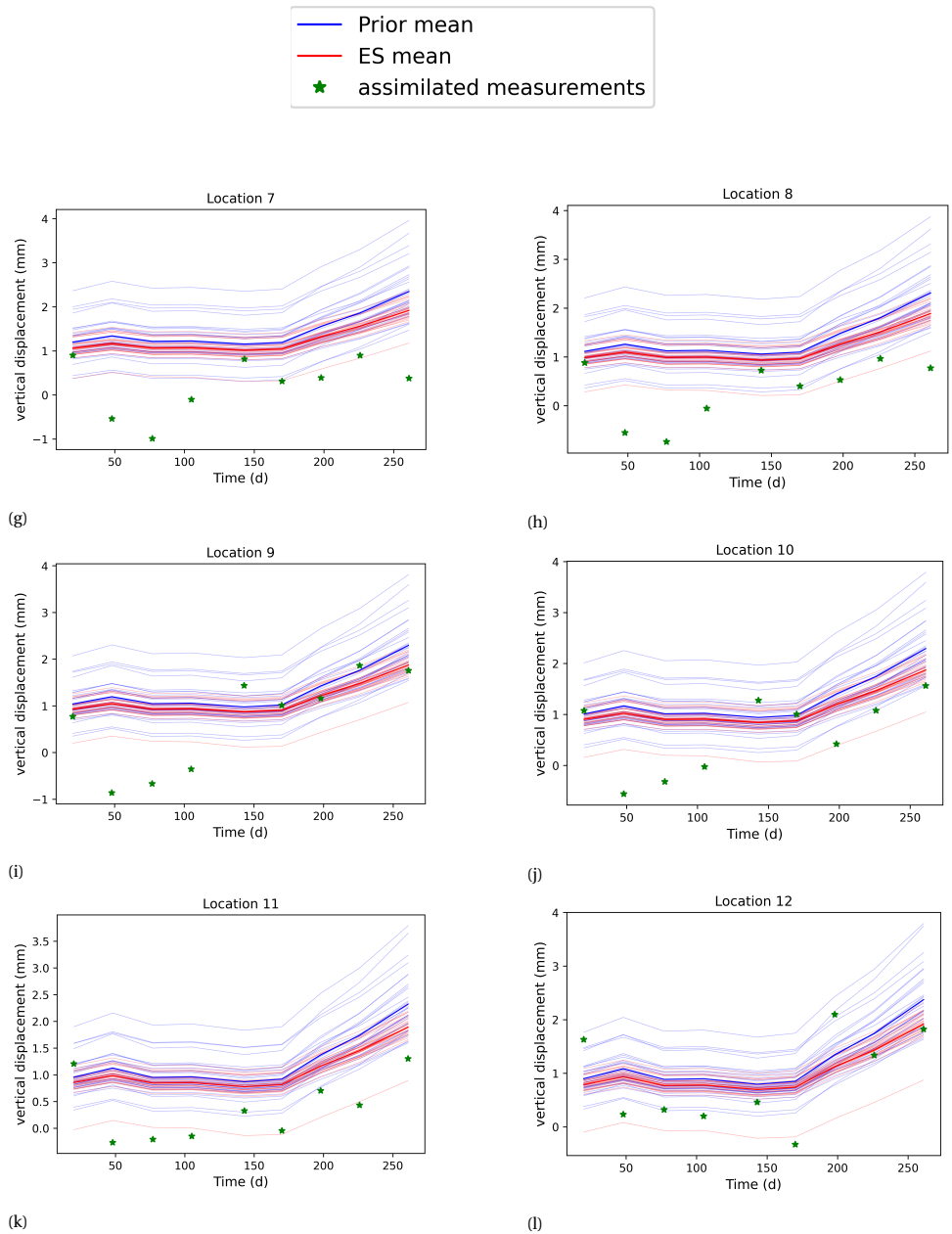


Figure 4.10: (Cont.) Displacement ensemble estimation at the slope locations

Two different locations (location 5 shown in Fig. 4.10 (e) and location 12 shown in Fig. 4.10 (l)) are selected to further discuss the ensemble and measurement quality. At location 5, it can be seen that the prior shows an increasing trend of displacement with the given parameter set and increasing water level. On the other hand, the LIDAR measurements show a cyclic trend, with potentially an underlying slight increase that is not entirely conclusive. This suggests that there are physical processes missing from the numerical model that do not lead to a cyclic behaviour. These cyclic fluctuations in the measurements are hypothesised to be due to annual meteorological processes. Furthermore, while the first and mid-time points lie within the prior ensemble, the remaining measurements are far from the prior - with the spread of the data larger than the spread of the prior ensemble. On the other hand, the measurements show a similar cyclic trend (with a lower magnitude) at location 12 but are overlaying the prior ensemble - albeit with more scatter. At the other locations, measurements show a similar cyclic trend as these two locations, with the data on the slope overlaying more the prior ensemble, and those on the crest and the upper part of the slope being further away (as location 5).

The cyclic nature of the displacement data, which appears to be driven by processes not included in numerical model, has driven the choice for a smoother, in this case ES. ES utilises all data in the data assimilation scheme, with a global set of parameters estimated. With the assimilation of measurements, the variance of the posterior displacement ensemble has been reduced. This is due to the reason that the posterior parameter ensemble has a lower variance and hence the displacement ensemble also does. At location 5, the posterior displacement ensemble moves towards the measurements, and its spread is significantly reduced. Here it can be noted that ES partially takes into account the missing physics and provides the estimation which is between the measurements and prior estimation. This does not mean that data assimilation implicitly adds the missing physics into the model, but that it modifies the parameters such that the impact of the missing physics is included. This implies that care must be taken in utilising the assimilated model, and also partially explains why laboratory or in situ measurements of the parameters may differ from those which best estimate field performance. In addition, the cyclic nature of the data is not reproduced, as the numerical model does not including forcing that can achieve this. At location 12, the displacement ensemble variance is reduced and is deemed to be acceptable as the posterior estimation lies between the prior and measurements.

Fig. 4.11 shows the prior and posterior estimation of the FoS at the end of 380 days. The slope failure observations suggest that the slope failed at 380 days. The prior FoS has a distribution with a higher mean than the posterior, i.e. the stability calculated by the posterior is lower, driven mostly by the posterior distribution of the friction angle. This is consistent with what is observed from the real measurements. This means that ES estimates the FoS better (close to realistic value) than only using the prior ensemble parameters in FEM.

It can be concluded from the ES estimation that even with the missing physical processes within the model, the data assimilation estimates the better factor of safety which is in better agreement with field observations than prior estimation. It is shown that even with the mismatch in observations and model output, the use of ES can significantly improve the estimate of FoS. This is probably due to a number of reasons: (i) the use of an

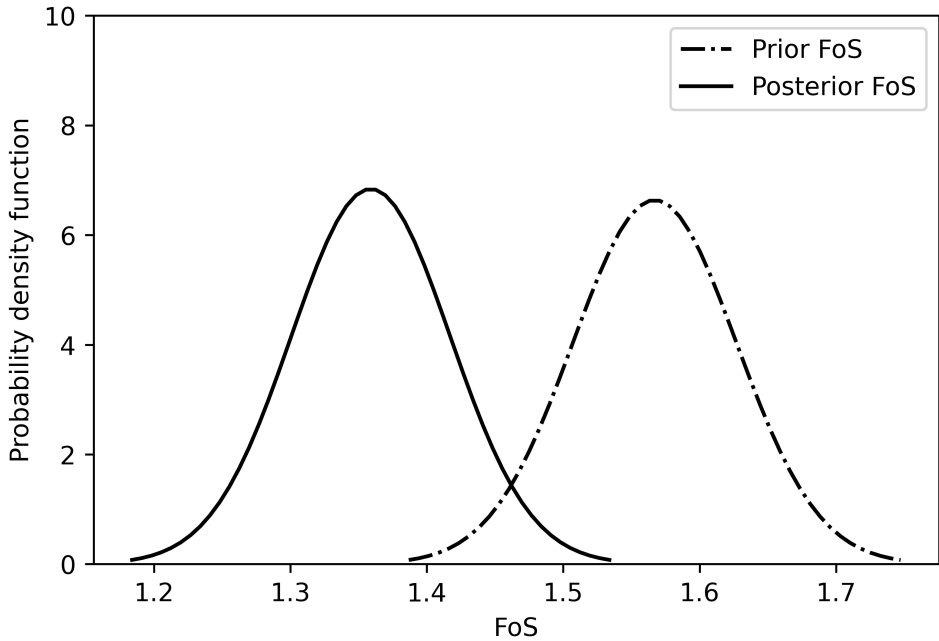


Figure 4.11: Estimation of FoS by using prior and posterior parameters (E_{50}^{ref} and ϕ') at the time of failure (380 days)

advanced non-linear material model. Here the non-linear changes in model output (displacements) compared to changes in input (water level) have an indication of how close to failure the slope is. This follows the results seen in Chapter 2. (ii) The cyclic nature of the missing physical process and use of a smoother in the data assimilation. This implies that by using a global update of all parameters with all data concurrently, greater non-structural differences (i.e. differences between the measured and simulated which are not constant) can be used and a single set of (realistic) parameters can be found. This is different from the recursive data assimilation techniques, where data is used each time new data is available and parameters can be updated at each assimilation step. In those cases, parameters are not constant throughout the analysis and can be strongly affected by the latest data, which can mean FoS results also change strongly. (iii) the cyclic forcing aspects do not either create the failure and the parts that are most impacted remain in the elastic region. The meteorological forcing that is hypothesised to create the cyclic response most strongly impacts the surface where shear stresses are not as significant as on the slope.

Furthermore, it is important to realise that data assimilation is not able to add the missing physics in the model but it estimates the parameters which produce the equivalent model of approximately the same factor of safety. This further suggests that it is not possible to estimate the trend of displacement response correctly (originally it has cyclic fluctuation but posterior estimation does not have any cyclic fluctuation), but it can be

used to estimate the better factor of safety (i.e., can produce the equivalent model with the same factor of safety). It should be noted that this conclusion and the ability of the technique to realistically determine a realistic FoS depends on details of the simulated system. The slope modelled in this case is quite large, which means that effective stress changes due to changes are likely to be small.

Despite that it is seen that the data assimilation aided in producing an improved estimate of the factor of safety, it is recommended where possible to take as many known physical processes in the model. This will help to further improve the estimate of the system's state and factor of safety. Missing physics may significantly impact the data assimilation results, and eliminates the possible use of alternative data assimilation techniques which are seen to offer improved outcomes as illustrated in Chapter 3.

If processes are not included, there is a risk of bias in the outcome. For example, if the meteorological mechanism is not properly taken into account, the predicted pore water pressures are inaccurate which further leads to incorrect system response. This can make prior bias which leads to error propagation resulting in skewing the data assimilation results. There it is recommended to incorporate all known processes and use the data assimilation scheme which can achieve the highest accuracy.

4.4.2. SURROGATE MODEL RESULTS

The surrogate model aims to relate the measurements (vertical displacements and water level) to the FoS. Two surrogate models (surrogate model-I and surrogate model-II) have been developed based on the prior and posterior estimation.

Surrogate model-I is trained and tested based on the dataset produced from the prior parameters. The input data for the surrogate model consists of vertical displacements (prior from all twelve monitored points shown in Fig. 4.10 for the full-time period) and the water level rise (Fig. 4.3) in the lake. The output attribute of the surrogate model is FoS (prior FoS data in Fig. 4.11). The GP model is trained to relate the input attributes to the output attribute. The prior dataset has been divided into two parts: 90% of the data is used for training and 10% is used for the testing. The dataset is randomly divided into training and testing sets based on above mentioned specified ratio. During the training process, the hyperparameters of the GP model ($\sigma^2=3734266$ and $l=31.46$) are optimised by using gradient-based optimization to best describe the correlation between input and output attributes.

Fig 4.12 shows the training results. The mean FoS from the numerical ensemble is plotted against the surrogate model prediction. It can be seen that the accuracy for the training data is $R^2=0.99$ with the optimised hyperparameters. Subsequently, the model's accuracy has been computed for the testing dataset. This is crucial to know that the model adequately learns patterns correctly and prevents overfitting. Fig. 4.13 shows $R^2=0.98$ which indicates that the GP model is performing well and is not overfitted in the training phase. It can be further concluded that with synthetic data, the surrogate model is performing well. Fig. 4.14 shows the validation results. The validation step has been achieved by using the field measurements. The prediction made by the surrogate model predicts FoS values between 5 and -22, clearly being unrealistic as negative FoS values are impossible, and the maximum of these values is significantly higher than could realistically be expected for a slope with reasonable parameters. This suggests that this

surrogate model cannot be used with real data. This is likely due to the reason that the field data is not well represented by the prior ensemble on which this surrogate model is trained and tested, including the identified limitations in the model to reproduce the weather related cyclic nature of the field data. It is a well-known and typical limitation of machine-learning models that they show poor performance for extrapolation.

Surrogate model-II is trained and tested on the dataset produced from the posterior estimation of the displacement (posterior from all twelve monitored points shown in Fig. 4.10 for the full-time period) and FoS (posterior FoS data in Fig. 4.11). This posterior estimation already considered the Cottbus measurements through the data assimilation process. This means that the surrogate model-II includes indirect information from the actual data that were assimilated into the FEM model. Therefore, it was hypothesised that the surrogate model-II would be able to give a better estimation of the FoS as compared to surrogate model-I. Fig. 4.15 shows that the FoS estimation range shrinks considerably and is better centred on the red line. Unfortunately, these results still show a highly unrealistic range and impossible values. This is likely to be due to the persisting considerable mismatch between some of the training and testing data and the validation data (as shown in Fig. 4.10), and it might in particular be due to the large scatter in the data.

The FoS predictions with the data assimilation methods used in this thesis is seen to be better than GP models used in this thesis. In data assimilation, the physics-based FEM model is consistently updated by adjusting its parameters continuously. This characteristic of the data assimilation generally improves the FEM fidelity over time. Furthermore, the physics-based nature of the numerical model has reasonable extrapolative prediction capabilities. These can be the reasons that ES provides better results than GP. Unlike ES, the GP model is trained and tested based on the synthetic dataset and develops the specific patterns for that specific dataset. Later, when the GP model is used with a validation dataset, with different (and realistic) data characteristics (cyclic fluctuations) and in particular where the input data is out of the upper and lower bounds of those predicted by the FEM model, it fails to make a reasonable estimation of FoS output. Though the kernel in the GP model can estimate a weakly non-linear model, there is the possibility that it struggles to capture the high non-linearity of the validation dataset.

The methodology used in this chapter, i.e., using an FEM model to train and test the GP model, is a key cause of the challenge faced by the GP model. This was necessitated by the lack of observability of FoS. FoS is only directly observable at a value of 1, i.e. when a structure is failing. Therefore, a step in between the data and the prediction of FoS is needed, and if this step does not reliably reproduce all data, this problem is likely to reoccur.

The overall limitation of the work in this chapter is that there are likely some key physical processes not included in the numerical model. These processes are typically ignored in stability analyses, with the exception of some novel works focusing on the impacts of those processes (e.g. Jamalnia, Tehrani, et al., 2021a, 2021b; Jamalnia et al., 2020, 2021). The data assimilation in a numerical model with missing physics can likely lead to unrealistic parameter estimation, which means that the resulting model could be used in this particular circumstances, but its application would not be general. If the complete physical processes were better captured in the numerical model before per-

forming the data assimilation, the resulting estimation of displacements would be more realistic and the overall result would be improved. The inclusion of additional meteorological observations and the appropriate physical processes into the numerical model could address this shortcoming of the present data-assimilation framework and lessen the risk of estimating unrealistic combinations of parameter values, at the cost of additional parameterisation and computational effort.

For GP, it is well known that most of the surrogate models/machine learning models have good interpolation predictive capabilities. In the current study, the surrogate model was tested against data produced in the same method as it was trained, with good results. It was then validated for a dataset which was observed to have a different nature, leading to an inability to produce accurate estimates of FoS. So, it can be concluded that the surrogate models must be trained, tested and validated on data with similar characteristics. However, when the output parameter cannot be directly observed, as is the case with FoS, this leads to a key challenge.

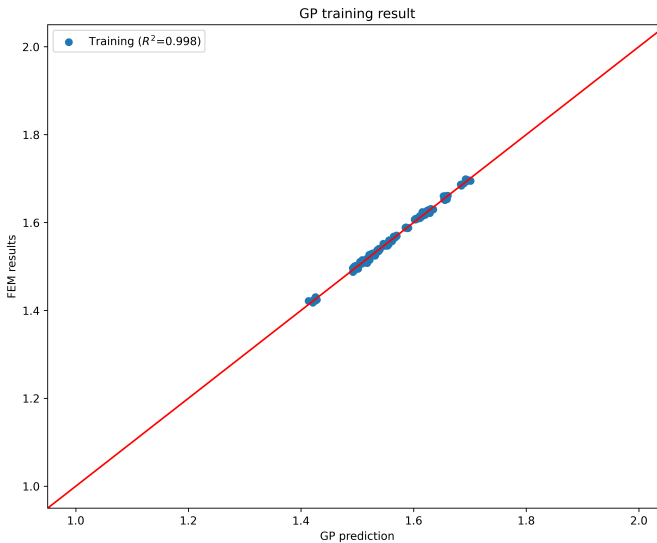


Figure 4.12: Surrogate model-I: Estimation of FoS by FEM and GP prediction in the training phase. The red line is a one-to-one line.

4.5. CONCLUSION

In this chapter, a data assimilation scheme (ES) and two GP surrogate models (surrogate-I and surrogate-II) are used to estimate the FoS of a slope stability system. A FEM model with missing physics is used to produce the prior ensemble of vertical displacements at the crest and slope and the associated FoS. In the data assimilation, the measurements of LIDAR at a field site were assimilated into the FEM model to improve the estimates of displacement, model parameters and the FoS. For the surrogate models, two GP models were trained and tested based on the prior and posterior ensemble of displacements

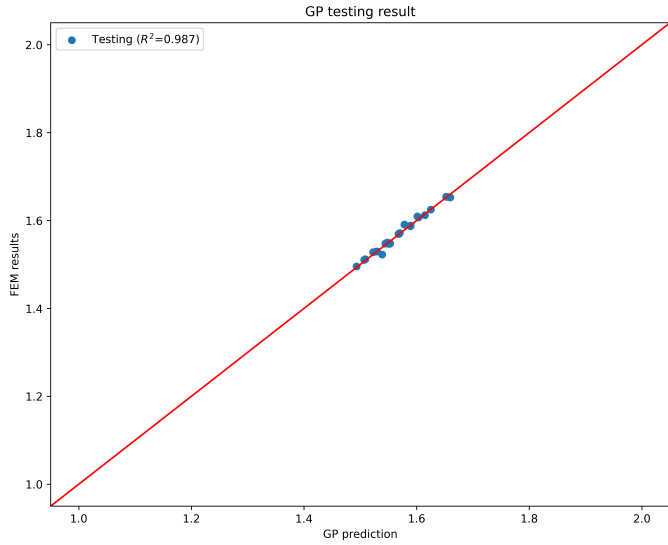


Figure 4.13: Surrogate model-I: Estimation of FoS by FEM and GP prediction in the testing phase. The red line is a one-to-one line.

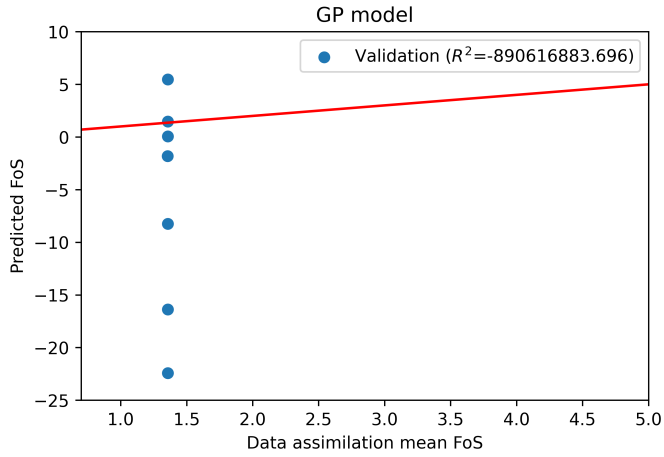


Figure 4.14: Surrogate model-I: Estimation of FoS by FEM and GP prediction in the validation phase. The red line is a one-to-one line.

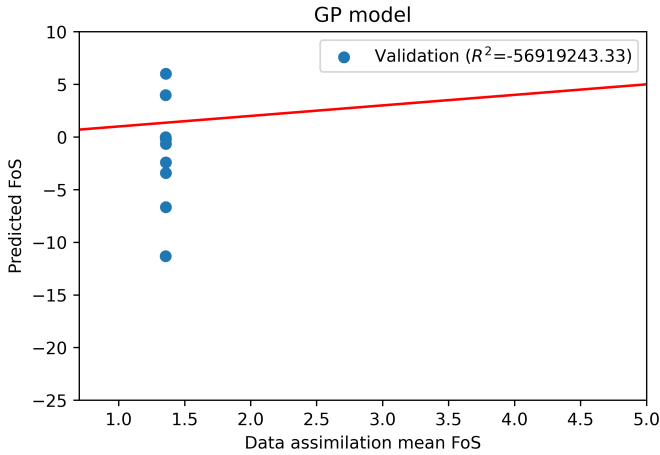


Figure 4.15: Surrogate model-II: Estimation of FoS by FEM and GP prediction in the validation phase. The red line is a one-to-one line.

and FoS and then a validation process is attempted using field LIDAR measurements to estimate the FoS. The estimation of FoS by data assimilation is compared with the FoS estimation of the surrogate models. It is concluded that the data assimilation estimates a FoS (and material parameters) that is consistent with the field observations of the slope failure. On the other hand, the surrogate models do not provide reasonable estimates, despite success in the testing phase. It is probably due to the reasons that the GP model is trained and tested based on datasets which were produced differently and therefore have different characteristics than the validation data. Furthermore, due to the hard Gaussian assumption in the GP, it is prone to predict uncertain extreme values. Unlike GP, ES is a well established data assimilation technique for dynamical models which consistently estimates the model parameters of physics based numerical models. For this reason, the use of ES is recommended over GP. It is further recommended to take into account the missing physics in FEM to improve the estimation of the state and FoS in data assimilation, and consider whether using an unobservable output (i.e. FoS) is essential.

REFERENCES

- Ada, M., & San, B. T. (2018). Comparison of machine-learning techniques for landslide susceptibility mapping using two-level random sampling (2LRS) in Alakir catchment area, Antalya, Turkey. *Natural Hazards*, 90(1), 237–263. <https://doi.org/10.1007/s11069-017-3043-8>
- Al-Bittar, T., Soubra, A.-H., & Thajeel, J. (2018). Kriging-based reliability analysis of strip footings resting on spatially varying soils. *Journal of Geotechnical and Geoenvironmental Engineering*, 144(10), 04018071. [https://doi.org/10.1061/\(ASCE\)GT.1943-5606.000195](https://doi.org/10.1061/(ASCE)GT.1943-5606.000195)
- Chakraborty, A., & Goswami, D. (2017). Slope stability prediction using artificial neural network (ANN). *International Journal of Engineering and Computer Science*, 6(6), 21845–21848. <https://doi.org/10.18535/ijecs/v6i6.49>
- Jamalinia, E., Tehrani, F. S., Steele-Dunne, S. C., & Vardon, P. J. (2021a). A data-driven surrogate approach for the temporal stability forecasting of vegetation covered dikes. *Water*, 13(1), 107. <https://doi.org/10.3390/w13010107>
- Jamalinia, E., Tehrani, F. S., Steele-Dunne, S. C., & Vardon, P. J. (2021b). Predicting rainfall induced slope stability using random forest regression and synthetic data. *Understanding and Reducing Landslide Disaster Risk: Volume 6 Specific Topics in Landslide Science and Applications*, 223–229. https://doi.org/10.1007/978-3-030-60713-5_24
- Jamalinia, E., Vardon, P. J., & Steele-Dunne, S. C. (2020). The impact of evaporation induced cracks and precipitation on temporal slope stability. *Computers and Geotechnics*, 122, 103506. <https://doi.org/10.1016/j.compgeo.2020.103506>
- Jamalinia, E., Vardon, P. J., & Steele-Dunne, S. C. (2021). The effect of soil–vegetation–atmosphere interaction on slope stability: A numerical study. *Environmental Geotechnics*, 8(7), 430–441. <https://doi.org/10.1680/jenge.18.00201>
- Kang, F., Han, S., Salgado, R., & Li, J. (2015). System probabilistic stability analysis of soil slopes using Gaussian process regression with latin hypercube sampling. *Computers and Geotechnics*, 63, 13–25. <https://doi.org/10.1016/j.compgeo.2014.08.010>
- Mahmoodzadeh, A., Mohammadi, M., Daraei, A., Ali, H. F. H., Al-Salihi, N. K., & Omer, R. M. D. (2020). Forecasting maximum surface settlement caused by urban tunneling. *Automation in Construction*, 120, 103375. <https://doi.org/10.1016/j.autcon.2020.103375>
- Mahmoodzadeh, A., Mohammadi, M., Daraei, A., Faraj, R. H., Omer, R. M. D., & Sherwani, A. F. H. (2020). Decision-making in tunneling using artificial intelligence tools. *Tunnelling and Underground Space Technology*, 103, 103514. <https://doi.org/10.1016/j.tust.2020.103514>
- Mahmoodzadeh, A., Mohammadi, M., Ibrahim, H. H., Rashid, T. A., Aldalwie, A. H. M., Ali, H. F. H., & Daraei, A. (2021). Tunnel geomechanical parameters prediction

- using Gaussian process regression. *Machine Learning with Applications*, 3, 100020. <https://doi.org/10.1016/j.mlwa.2021.100020>
- Mentani, A., Govoni, L., Bourrier, F., & Zabatta, R. (2023). Metamodelling of the load-displacement response of offshore piles in sand. *Computers and Geotechnics*, 159, 105490. <https://doi.org/10.1016/j.compgeo.2023.105490>
- Qi, C., & Tang, X. (2018). Slope stability prediction using integrated metaheuristic and machine learning approaches: A comparative study. *Computers & Industrial Engineering*, 118, 112–122. <https://doi.org/10.1016/j.cie.2018.02.028>
- Soubra, A.-H., Al-Bittar, T., Thajeel, J., & Ahmed, A. (2019). Probabilistic analysis of strip footings resting on spatially varying soils using kriging metamodelling and importance sampling. *Computers and Geotechnics*, 114, 103107. <https://doi.org/10.1016/j.compgeo.2019.103107>
- Toe, D., Mentani, A., Govoni, L., Bourrier, F., Gottardi, G., & Lambert, S. (2018). Introducing meta-models for a more efficient hazard mitigation strategy with rock-fall protection barriers. *Rock Mechanics and Rock Engineering*, 51, 1097–1109. <https://doi.org/10.1007/s00603-017-1394-9>
- Van den Eijnden, A. P., Schweckendiek, T., & Hicks, M. A. (2022). Metamodelling for geotechnical reliability analysis with noisy and incomplete models. *Georisk: Assessment and Management of Risk for Engineered Systems and Geohazards*, 16, 518–535. <https://doi.org/10.1080/17499518.2021.1952611>
- Wang, Z. Z., Goh, S. H., & Zhang, W. (2023). Reliability-based design in spatially variable soils using deep learning: An illustration using shallow foundation. *Georisk: Assessment and Management of Risk for Engineered Systems and Geohazards*, 17(2), 423–437. <https://doi.org/10.1080/17499518.2022.2083178>
- Wei, X., Zhang, L., Yang, H.-Q., Zhang, L., & Yao, Y.-P. (2021). Machine learning for pore-water pressure time-series prediction: Application of recurrent neural networks. *Geoscience Frontiers*, 12(1), 453–467. <https://doi.org/10.1016/j.gsf.2020.04.011>

5

CONCLUSION AND FUTURE WORK

5.1. CONCLUSION

The overall idea of this research was to find an improved estimation of slope stability system by using monitoring data more systematically. It is imperative to predict an accurate FoS of slope systems, allowing stakeholders to protect their assets and to undertake remedial measures in good time when needed.

When there are changes in loading, i.e. slope heightening, or changes in water load, the displacement response can be measured. It was hypothesised that this displacement, which can be measured using geodetic techniques, both in situ and with remote sensing, can be related to and used to improve estimates of the factor of safety of a slope. The factor of safety itself cannot be measured which gives challenges in terms of model training and validation.

In this research, FEM models including hydro-mechanical (temporal) processes are used to investigate the ability of ensemble methods for data assimilation to estimate and improve estimations of the FoS. These ensemble-based techniques have been applied on a field study of an open pit mine remediation, where a newly constructed slope was formed in order to form a boundary to a lake, and the lake was then filled. The slope (partially) failed during filling. The performance of data assimilation with different constitutive models and data assimilation schemes has been investigated.

Following a reasonably successful, yet computationally intensive, data assimilation process, a Gaussian process-based surrogate model has been trained and tested, and shown to achieve significantly faster estimations of the FoS. A validation process using real data was also carried out, with limited success. Here, the conclusions are presented for each of the research questions from Chapter 1.

Research question 1: How can the measurements be used in numerical models for the stability of slope? What are the effects of the different constitutive models in measurement assimilation?

A FEM model of slope stability has been integrated with an ensemble-based data assimilation scheme, i.e. the Ensemble Kalman filter. This approach was used to estimate the key material parameters, state (displacement) and factor of safety of a slope. The effect of two different constitutive models on the factor of safety was studied, via a synthetic twin experiment. The standard and simple Mohr-Coulomb (MC) model and the more sophisticated, yet less commonly used, Hardening Soil (HS) model were tested. The approach using the HS model was able to estimate the factor of safety with a narrow posterior distribution, starting from a different prior distribution of material parameters, including those not encompassing the actual parameters. The results suggest that constitutive models which include a smooth transition between elastic and plastic zones, are more effective in data assimilation schemes than those in which the relation between stiffness and strength parameters is less well represented. When choosing a constitutive model that captures these relations, the results of this study suggested that the use of data assimilation techniques for slope-reliability estimates offers the opportunity to improve slope-reliability estimates with relatively limited stress perturbations. Therefore, the results of Chapter 2 suggested that using the HS model is more generally applicable than the MC model when considering data assimilation.

Research question 2: What kind of data assimilation scheme can be used in the slope stability analysis to estimate the parameter and FoS?

There are three well-established data assimilation methods, e.g., the ensemble Kalman filter (EnKF), ensemble smoother (ES) and ensemble smoother with multiple data assimilation (ESMDA), which have been successfully used in different fields. An approach of using a commercial FEM software integrated with different data assimilation schemes to estimate the parameter, state and FoS was developed. The performance of these data schemes were tested by comparing the results of FoS with a synthetic truth of FoS and the computation time. The results of a synthetic twin experiment showed that EnKF estimated an FoS that is close to the true FoS with a small standard deviation. ESMDA, when using four iterative assimilation steps, was also able to estimate a FoS close to the truth, yet had a higher standard deviation, whereas it performed much worse when only using two iterative assimilation steps. ES provided a physically consistent estimate with a low computational time. Though the estimate is seen to have a slight bias when compared to the true factor of safety. The (theoretical) computation time required by the ES is the smallest, followed by ESMDA with two iterative assimilation steps, ESMDA with four assimilation steps, and EnKF. Due to some limitations in the forward model i.e., the commercial software which was not designed for data assimilation, ESMDA needed relatively more computation time than the EnKF and ES, which offers an opportunity for software designers to consider data assimilation requirements in their software design.

Research question 3: How can we validate the data assimilation scheme and surrogate model on a case study?

In the previous research questions, the data assimilation schemes were investigated and verified based on synthetic measurements. ES was selected as the data assimilation scheme due to its provision of a physically consistent estimate with a low computational time. This case study represented an open pit mine in Cottbus, Germany. The LIDAR measurements of the vertical displacements were assimilated into a finite element method (FEM) model. Model parameters, displacement ensemble and factor of safety (FoS) were estimated from this analysis. The posterior estimation of FoS were compared with slope failure observed in the field. The data assimilation results provided better results when comparing the ground truth of slope, however it was clear that not all physical processes were included in the model. As the data assimilation approach developed involves multiple FEM analyses it is computationally expensive and therefore developing a real-time assessment system is likely to be impractical. To make the computations faster, two GP surrogate models were used to estimate the FoS. These GP models were trained and tested based on the prior and posterior ensemble of displacements and FoS and then were attempted to be validated with the original case study measurements to estimate the FoS. Due to the persisting mismatch between the model and the measured data due to the identified missing physical processes, the on-ground measurements had a different nature than the training and testing data. In fact, due to the extrapolative prediction disabilities of machine learning models, the GP models could not estimate realistic values of FOS. Therefore, it was concluded that a model used to train a surrogate model must not miss physical processes which impact the measured data. However, data assimilation methods which utilise imperfect models were shown to be able to be

used more successfully. It also highlighted the difficulty in using surrogate modelling to reproduce an unobservable factor (i.e., the FoS) where an intermediate modelling step is needed.

5.2. RECOMMENDATIONS FOR THE FUTURE STUDIES

To further build on the methodologies developed in this work, the following can be directions for future research.

Spatial variability in slope domain with HS model parameters: In the current work, the slope domain of the problem was considered homogeneous which simplifies the problem. Further validation of the data assimilation scheme is needed by considering the spatial variability in the HS model parameter. This aspect will pose computation challenges as each parameter varies for each Gauss point in the model.

Automatic slope stability assessment: In this study, a single slope stability section was tested for data assimilation, with analysis built and triggered manually. Remote devices, such as InSAR, are able to provide measurements every 3-4 days. A platform can be built which integrates InSAR estimates with an FEM model to estimate the parameters, state and FoS for any given slope automatically when new data is available. Automated, this approach would allow for a more comprehensive assessment of infrastructure and identification of potential problems.

Surrogate model efficiency: In this study, two GP models were built based on limited synthetic data and a preliminary investigation has been presented. There is a need to do a more rigorous study regarding this topic. Furthermore, the training and testing should have the same nature as the validation data.

Missing physics of numerical model and data assimilation: In Chapter 4, ES has been implemented with a FEM model on a realistic case study. It was clear that certain processes, specifically those related to meteorological variations, were not included, which made reproducing all of the observed processes difficult. However, ES was reasonably successful in producing estimates of material parameters and the FoS. Extending this investigation to explore under what conditions data assimilation schemes can identify missing physics in the model or when more detailed physics is needed will be invaluable. This investigation can also be extended to identify the missing physics represented in our observations by using the data assimilation.

Leveraging data assimilation for application in industry: In this study, we demonstrate that data assimilation can be valuable in enhancing predictive capabilities, taking into account the findings and conclusions in this thesis. We recommend that stakeholders incorporate data assimilation techniques in their practical projects to take advantage of more extensive data collection that is now common. This approach will support real-time design and execution in geotechnical projects.

A

APPENDIX RELATED TO CHAPTER 3

A.1. SENSITIVITY OF THE DISPLACEMENT ESTIMATES TO THE DATA ASSIMILATION SETUP

A sensitivity analysis is conducted to study the influence of number of measurements, measurement error and ensemble size on the numerical data assimilation setup to the displacement estimates. In order to evaluate the final results, the normalised root mean square error (NRMSE) is calculated for the horizontal nodal displacement in the entire model domain. Considering that the root mean square error $RMSE$ of horizontal nodal displacement (in meters) is given by:

$$RMSE = \sqrt{\frac{1}{N_{u_x}} \sum_{i=1}^{N_{u_x}} (u_{x_i}^t - u_{x_i}^e)^2}. \quad (A.1)$$

The NRMSE is given by:

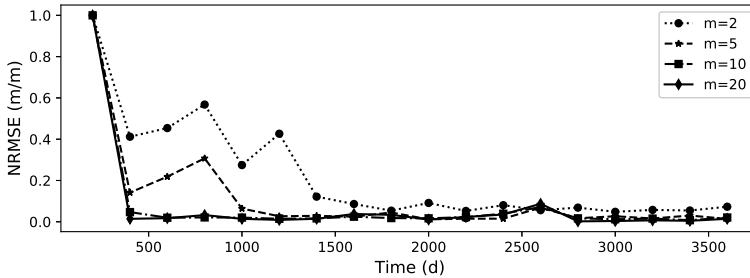
$$NRMSE = \frac{RMSE}{RMSE_i} \quad (A.2)$$

where N_{u_x} is the total number of unknown horizontal displacements in the slope, *i.e.*, the number of nodes in the model, $u_{x_i}^t$ is the true horizontal nodal displacement at node i and $u_{x_i}^e$ is the estimated horizontal nodal displacement at this node. The normalised root mean square error (NRMSE) is the ratio between the RMSE and its value for the prior RMSE estimate. The normalisation facilitates the comparison of the resulting deformations of different magnitudes. The lower the NRMSE, the closer the result is to the true displacement. It should be kept in mind that the expected value of the difference between $u_{x_i}^t - u_{x_i}^e$ should in the ideal case be equal to the measurement error. In this section, the sensitivity analysis for the close-to-failure case is presented, *i.e.*, the case where the prior ensemble of parameters have been selected such, that the slope is in a condition close to failure. Note that while studying the sensitivity of one factor of the data assimilation setup, the other factors are kept constant.

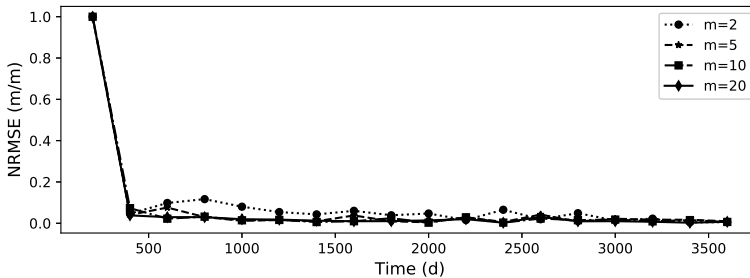
A.1.1. SENSITIVITY TO THE NUMBER OF MEASUREMENTS

In order to choose the required number of measurements in data assimilation scheme for the model comparison, several cases with different number of measurements are selected. Fig. A.1 shows the NRMSE for different number of measurements (m) for the MC and the HS model. All measurement points are located on the sloping face starting from point A towards C (see Fig. 2.5). A set of $m = 2, 5, 10$ and 20 measurements is selected to study the sensitivity of the horizontal displacement estimate to the number of measurements. Fig. 2.5 illustrates the location of the measurements for the number of measurements $m=10$. The NRMSE for all nodal points in the mesh geometry is plotted against the time, and is seen to generally decrease with time, meaning that after each assimilation step, the resulting deformation estimate is closer to the truth.

It can be seen from Fig. A.1a that the NRMSE for the MC case converges more slowly towards the expected value for the NRMSE when $m = 2$ and $m = 5$. Some fluctuations in the NRMSE values are observed with this number of measurements. However, in the case of $m = 10$ and $m = 20$, the solution quickly approaches the expected value of the NRMSE, with the majority of the improvement occurring within the first data assimilation steps. In case of the HS model, the NRMSE of the estimated horizontal displacement does not fluctuate (see Fig. A.1b). The NRMSE reaches its expected value even with a relatively low number of measurements ($m = 2$ or 5). It can be seen from Fig. A.1 that $m \geq 10$ appears to be an effective choice for the number of measurements for both models. Because of this, a value of $m = 10$ was used in Section 2.4 of this study.



(a)



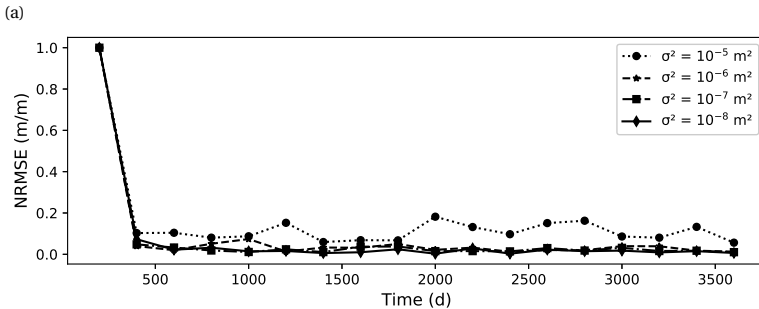
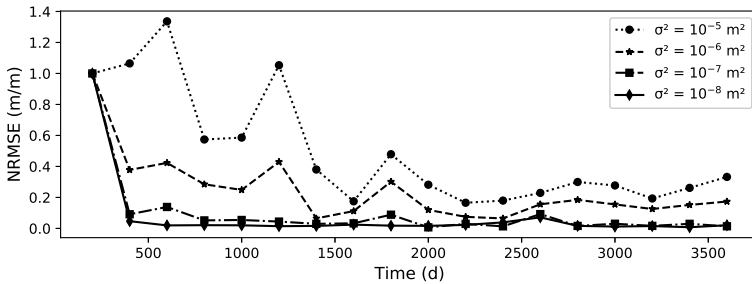
(b)

Figure A.1: RMSE estimation of the horizontal nodal displacement for different number of measurements for the (a) MC and (b) HS material models.

A.1.2. SENSITIVITY TO THE MEASUREMENT ERROR

In order to study the effect of the measurement error, several experiments are performed with different measurement error variance. Fig. A.2 shows the NRMSE of horizontal nodal displacement resulting from different choices of the measurement error variance ϵ . In case of the MC model (see Fig. A.2a), it can be seen that the when the error variance is 10^{-5} m^2 , the NRMSE fluctuates, but does not converges towards the expected value of the NRMSE, which should be for each case equal to the value of ϵ chosen for that case. For error variance of 10^{-6} m^2 , the NRMSE still fluctuates. For error variances less than 10^{-6} m^2 , the solution is seen to quickly approach its expected value.

In case of the HS model (see Fig. A.2b), the NRMSE fluctuates when the error variance is 10^{-5} m^2 , but with a significantly lower level than for the MC model. When the error variance is less than 10^{-6} m^2 , a satisfactory solution is obtained. For both models, the horizontal displacement approximates the true horizontal displacement within the assumed error margin when the error is less than 10^{-7} m^2 . In a realistic case, measurements of deformations at the slope would be available from geotechnical devices (inclinometer, laser sensor, extensometer) or geodetic measurements (levelling, InSAR or laser). With current geodetic/geotechnical measurement techniques (e.g. Abellán et al., 2009; Hou et al., 2005; Lovas et al., 2008) it is realistic to measure at an accuracy of $\approx 1 \text{ mm}$ (equivalent to an error variance of 10^{-7} m^2), therefore a value of 10^{-7} m^2 measurement error is assumed in Section 2.4 of this study.



(a)

(b)

Figure A.2: RMSE estimation of the horizontal nodal displacement for different choices of the measurement error variance for the (a) MC and (b) HS material models.

A.1.3. ENSEMBLE SIZE

Several cases with different ensemble members (N_e) are used to study the influence of different ensemble sizes on the estimate of the horizontal nodal displacement in the mesh of the synthetic slope. Fig. A.3 shows the NRMSE resulting from different ensemble sizes. In case of the MC model (Fig. A.3a), the NRMSE reduces to around 10% of the prior RMSE and then oscillates when the number of ensemble members is less than 50. In case of the HS model (Fig. A.3b), the NRMSE converges towards the expected value of the NRMSE with ensemble members, $N_e \geq 30$. For this reason, an ensemble size of $N_e = 50$ is selected in Section 2.4 of this study.

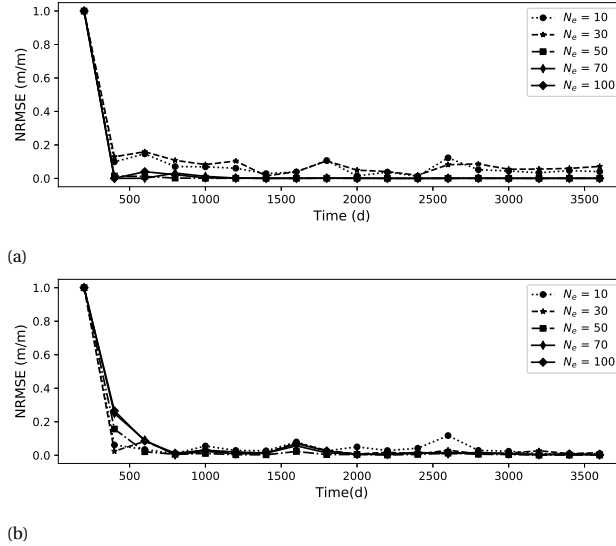


Figure A.3: RMSE estimation of the horizontal nodal displacement for different ensemble size for (a) MC and (b) HS material models.

B

APPENDIX FOR CHAPTER 4

The algorithms for the different data assimilation schemes are presented in this appendix.

Algorithm 1 Ensemble Kalman Filter (EnKF)

Input: $\mu_{phi}^o, \sigma_{phi}^o, \mu_e^o, \sigma_e^o, \sigma_{obs}^2, Dw, c, \mathbf{D}_{truth}, G$

Output: \mathbf{Z}^a, \mathbf{F}

- 1: Initialisation
 - 2: Read input and define variables
 - 3: Initialise required vector and matrices
 - 4: $\mathbf{e}^o = \mathcal{N}(\mu_e^o, \sigma_e^o)$ ▷ prior E_{50}^{ref} sampling
 - 5: $\mathbf{p}^o = \mathcal{N}(\mu_{phi}^o, \sigma_{phi}^o)$ ▷ prior ϕ' sampling
 - 6: **while** $t \leq t_{assim}$ **do**
 - 7: Read water level time series $Dw(t)$
 - 8: **while** $i \leq N_e$ **do** ▷ loop over ensembles
 - 9: Instructions to set up realisation i
 - 10: $\mathbf{x} = \text{hm}(\mathbf{e}^t(i), \mathbf{p}^t(i), Dw, p)$ ▷ HM analysis and extract \mathbf{x}
 - 11: $f = \text{sa}(\text{hm}(\mathbf{e}^t(i), \mathbf{p}^t(i), Dw, p)$ ▷ FoS analysis
 - 12: $\mathbf{f}(i) = f$ ▷ save f in vector \mathbf{f}
 - 13: $\mathbf{X}_t^f[:, i] = \mathbf{x}$ ▷ save \mathbf{x} in matrix
 - 14: $\mathbf{Z}_t^f = (\mathbf{X}_t^f, \mathbf{e}^t, \mathbf{p}^t)$
 - 15: $\mathbf{C}_{zz}^e = \text{cov}(\mathbf{Z}_t^f)$
 - 16: $\mathbf{d}_t^l = \mathbf{d}_t + \epsilon_t^l, l = 1, 2, \dots, N_e$
 - 17: $\mathbf{Z}_t^a = \mathbf{Z}_t^f + \mathbf{C}_{zz}^e \mathbf{G}^T (\mathbf{G} \mathbf{C}_{zz}^e \mathbf{G}^T + \mathbf{C}_{dd})^{-1} (\mathbf{D}_t - \mathbf{G} \mathbf{Z}_t^f)$
-

Algorithm 2 Ensemble smoother (ES)**Input:** $\mu_{phi}^o, \sigma_{phi}^o, \mu_e^o, \sigma_e^o, \sigma_{obs}^2, Dw, c, \mathbf{D}_{truth}, G$ **Output:** $\tilde{\mathbf{Z}}^a$

- 1: Initialisation
- 2: Read input and define variables
- 3: Initialise required vector and matrices
- 4: $\mathbf{e}^o = \mathcal{N}(\mu_e^o, \sigma_e^o)$ ▷ prior E_{50}^{ref} sampling
- 5: $\mathbf{p}^o = \mathcal{N}(\mu_{phi}^o, \sigma_{phi}^o)$ ▷ prior ϕ' sampling
- 6: $\boldsymbol{\theta}^o = (\mathbf{e}^o, \mathbf{p}^o)^T$ ▷ prior parameter matrix
- 7: **while** $i \leq N_e$ **do** ▷ loop over ensembles
- 8: **while** $t \leq t_{assim}$ **do** ▷ loop over timesteps
- 9: Read water level time series $Dw(t)$
- 10: Setup for initial stress state
- 11: $\mathbf{x} = \text{hm}(\mathbf{e}^o(i), \mathbf{p}^o(i), Dw, c)$ ▷ HM analysis and extract \mathbf{x}
- 12: $f = \text{sa}(\text{hm}(\mathbf{e}^o(i), \mathbf{p}^o(i), Dw, c))$ ▷ FoS analysis
- 13: $\mathbf{A}_i^f[:, t] = \mathbf{x}$ ▷ save \mathbf{x} in matrix
- 14: $f(t) = f$ ▷ save f in vector \mathbf{f}
- 15: $\mathbf{Z}_t^f = (\mathbf{X}_t^f, \boldsymbol{\theta}^o)^T$ ▷ develop \mathbf{Z}_t^f for all time steps
- 16: $\tilde{\mathbf{Z}} = (\mathbf{Z}_1^f, \mathbf{Z}_2^f, \dots, \mathbf{Z}_{t_{assim}}^f)^T$ ▷ stacking all forecast-parameter matrices
- 17: $\tilde{\mathbf{C}}_{zz}^e = \text{cov}(\tilde{\mathbf{Z}})$ ▷ estimate the spatial-temporal covariance matrix
- 18: $\mathbf{d}_t^l = \mathbf{d}_t + \epsilon_t^l, l = 1, 2, \dots, N_e$
- 19: $\mathbf{D}_t = (\mathbf{d}_t^1, \mathbf{d}_t^2, \dots, \mathbf{d}_t^{N_e})$ ▷ develop \mathbf{D}_t for all time steps
- 20: $\tilde{\mathbf{D}} = (\mathbf{D}_1, \mathbf{D}_2, \dots, \mathbf{D}_{t_{assim}})^T$ ▷ stacking all perturbed observations matrices
- 21: $\tilde{\mathbf{C}}_{dd} = \sigma_{obs}^2 \mathbf{I}$
- 22: Read $\tilde{\mathbf{G}}$ from file
- 23: $\tilde{\mathbf{Z}}^a = \tilde{\mathbf{Z}} + \tilde{\mathbf{C}}_{zz}^e \tilde{\mathbf{G}}^T (\tilde{\mathbf{G}} \tilde{\mathbf{C}}_{zz}^e \tilde{\mathbf{G}}^T + \tilde{\mathbf{C}}_{dd})^{-1} (\tilde{\mathbf{D}} - \tilde{\mathbf{G}} \tilde{\mathbf{Z}})$ ▷ extract estimated parameters from $\tilde{\mathbf{Z}}^a$

Algorithm 3 Ensemble smoother with multiple data assimilation (ESMDA)**Input:** $\mu_{phi}^o, \sigma_{phi}^o, \mu_e^o, \sigma_e^o, \sigma_{obs}^2, Dw, c, \mathbf{D}_{truth}, \mathbf{G}, \alpha$ **Output:** $\tilde{\mathbf{Z}}^a$

- 1: Initialisation
 - 2: Read input and define variables
 - 3: Initialise required vector and matrices
 - 4: $\mathbf{e}^o = \mathcal{N}(\mu_e^o, \sigma_e^o)$ ▷ prior E_{50}^{ref} sampling
 - 5: $\mathbf{p}^o = \mathcal{N}(\mu_{phi}^o, \sigma_{phi}^o)$ ▷ prior ϕ' sampling
 - 6: $\boldsymbol{\theta}^o = (\mathbf{e}^o, \mathbf{p}^o)^T$ ▷ prior parameter matrix
 - 7: Select the α vector
 - 8: **while** $k \leq \text{len}(\alpha)$: **do** ▷ loop over α
 - 9: **while** $i \leq N_e$ **do** ▷ loop over ensembles
 - 10: **while** $t \leq t_{assim}$ **do** ▷ loop over timesteps
 - 11: Read water level time series $Dw(t)$ ▷ loop over timesteps
 - 12: Setup for initial stress state
 - 13: $\mathbf{x} = \text{hm}(\mathbf{e}^k(i), \mathbf{p}^k(i), Dw, c)$ ▷ HM analysis and extract \mathbf{x}
 - 14: $f = \text{sa}(\text{hm}(\mathbf{e}^k(i), \mathbf{p}^k(i), Dw, c))$ ▷ FoS analysis
 - 15: $\mathbf{A}_i^f[:, t] = \mathbf{x}$ ▷ save \mathbf{x} in matrix
 - 16: $\mathbf{f}(t) = f$ ▷ save f in vector \mathbf{f}
 - 17: $\mathbf{Z}_t^f = (\mathbf{X}_t^f, \boldsymbol{\theta}^k)^T$ ▷ develop \mathbf{Z}_t^f for all time steps
 - 18: $\tilde{\mathbf{Z}} = (\mathbf{Z}_1^f, \mathbf{Z}_2^f, \dots, \mathbf{Z}_{t_{assim}}^f)^T$ ▷ stacking all forecast-parameter matrices
 - 19: $\tilde{\mathbf{C}}_{zz}^e = \text{cov}(\tilde{\mathbf{Z}})$ ▷ estimate the spatial-temporal covariance matrix
 - 20: $\mathbf{d}_t^l = \mathbf{d}_t + \sqrt{\alpha(k)} \mathbf{e}_t^l, l = 1, 2, \dots, N_e$
 - 21: $\mathbf{D}_t = (\mathbf{d}_t^1, \mathbf{d}_t^2, \dots, \mathbf{d}_t^{N_e})$ ▷ Develop \mathbf{D}_t for all time steps
 - 22: $\tilde{\mathbf{D}} = (\mathbf{D}_1, \mathbf{D}_2, \dots, \mathbf{D}_{t_{assim}})^T$ ▷ stacking all perturbed measurements matrices
 - 23: $\tilde{\mathbf{C}}_{dd} = \sigma_{obs}^2 \mathbf{I}$
 - 24: Read $\tilde{\mathbf{G}}$ from file
 - 25: $\tilde{\mathbf{Z}}^a = \tilde{\mathbf{Z}} + \tilde{\mathbf{C}}_{zz}^e \tilde{\mathbf{G}}^T (\tilde{\mathbf{G}} \tilde{\mathbf{C}}_{zz}^e \tilde{\mathbf{G}}^T + \alpha(k) \tilde{\mathbf{C}}_{dd})^{-1} (\tilde{\mathbf{D}} - \tilde{\mathbf{G}} \tilde{\mathbf{Z}})$ ▷ extract estimated parameters
- from $\tilde{\mathbf{Z}}^a$

CURRICULUM VITÆ

Muhammad MOHSAN

06-03-1990 Born in Toba Tek Singh, Pakistan

EDUCATION

- 2018–2023 PhD candidate in Reservoir Engineering
Faculty of Civil Engineering and Geoscience
Delft University of Technology, Delft, The Netherlands
- 2016–2018 Master of Science in Geotechnical Engineering
Department of Civil Engineering
The University of Tokyo, Japan
- 2009–2013 Bachelor of Science in Civil Engineering
Department of Civil Engineering
University of Engineering & Technology (UET), Lahore, Pakistan

EMPLOYEMENT

- 2023–2024 Research Engineer & Software quality assurance
Bentley Systems, Delft, The Netherlands
- 2018–2023 PhD Researcher
Faculty of Civil Engineering and Geoscience
Delft University of Technology, Delft, The Netherlands
- 2014–2016 Lecturer
Department of Civil Engineering
MNS-UET, Multan, Pakistan

LIST OF PUBLICATIONS

JOURNAL PAPERS

3. **Mohsan, M.**, Vardon, P. J., & Vossepoel, F. C. (2024). *A case study of the Cottbus open pit mine: Use of data assimilation and surrogate modelling for slope stability analysis.* (to be submitted)
2. **Mohsan, M.**, Vossepoel, F. C & Vardon, P. J., . (2023). *On the use of different data assimilation schemes in a fully coupled hydro-mechanical slope stability* ,[Georisk: Assessment and Management of Risk for Engineered Systems and Geohazards](#), 18(1), 121–137.
1. **Mohsan, M.**, Vardon, P. J., & Vossepoel, F. C. (2021). *On the use of different constitutive models in data assimilation for slope stability* , [Computers and Geotechnics](#), 138, 104332.

CONFERENCE AND PROCEEDING PAPERS

3. **Mohsan, M.**, Vardon, P. J., & Vossepoel, F. C. (2022). *Options for the implementations of data assimilation for geotechnics.* In [International Association for Computer Methods and Advances in Geomechanics \(IACMAG\)](#), Proceedings of the 16th Int. Conference of IACMAG, Torino, Italy.
2. **Mohsan, M.**, Vardon, P. J., & Vossepoel, F. C. (2021). *FEM-EnKF integration to evaluate the impact of constitutive models for reliable factor of safety prediction.* In [Nederlands Aardwetenschappelijk Congres \(NAC\)](#), Utrecht, Netherlands.
1. **Mohsan, M.**, Vardon, P. J., & Vossepoel, F. C. (2021). *Implementation of data assimilation scheme in a geo-mechanical slope stability model.* In [Nederlands Aardwetenschappelijk Congres \(NAC\)](#), Utrecht, Netherlands.